

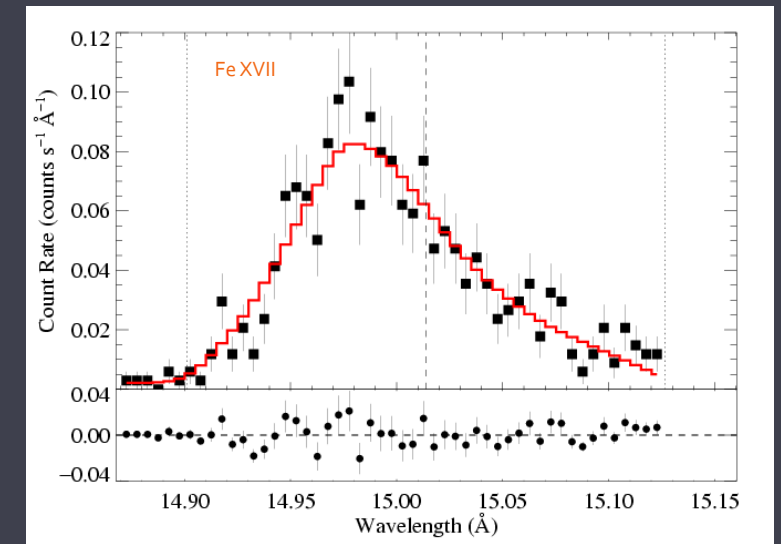
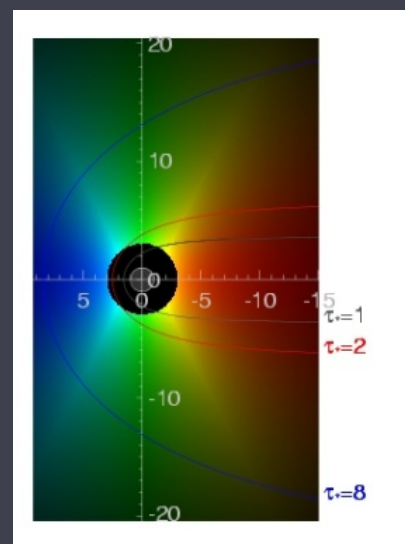
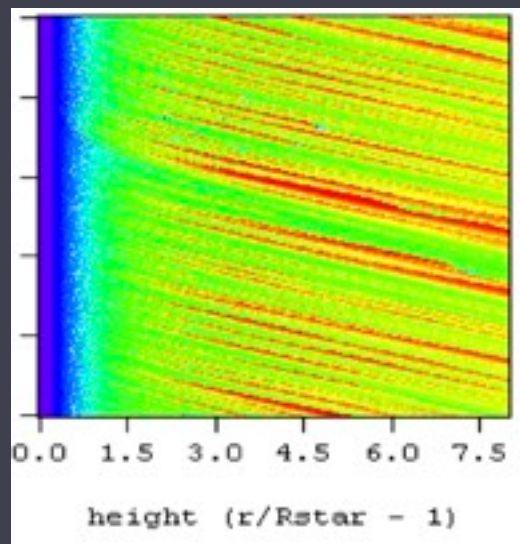
X-ray Spectroscopy of Massive Stars: Constraints on Stellar Wind Mass-Loss Rates and Shock Physics

David Cohen
Swarthmore College

with Jon Sundqvist & Stan Owocki (U. Delaware), Maurice Leutenegger (GSFC),
Marc Gagné & Véronique Petit (West Chester University), Asif ud-Doula (Penn St.),
Alex Fullerton (STScI),

and

Emma Wollman (Swarthmore '09; Caltech), Erin Martell (Swarthmore '09; U. Chicago),
James MacArthur (Swarthmore '11; Sandia National Laboratory)



cool stars

vs.

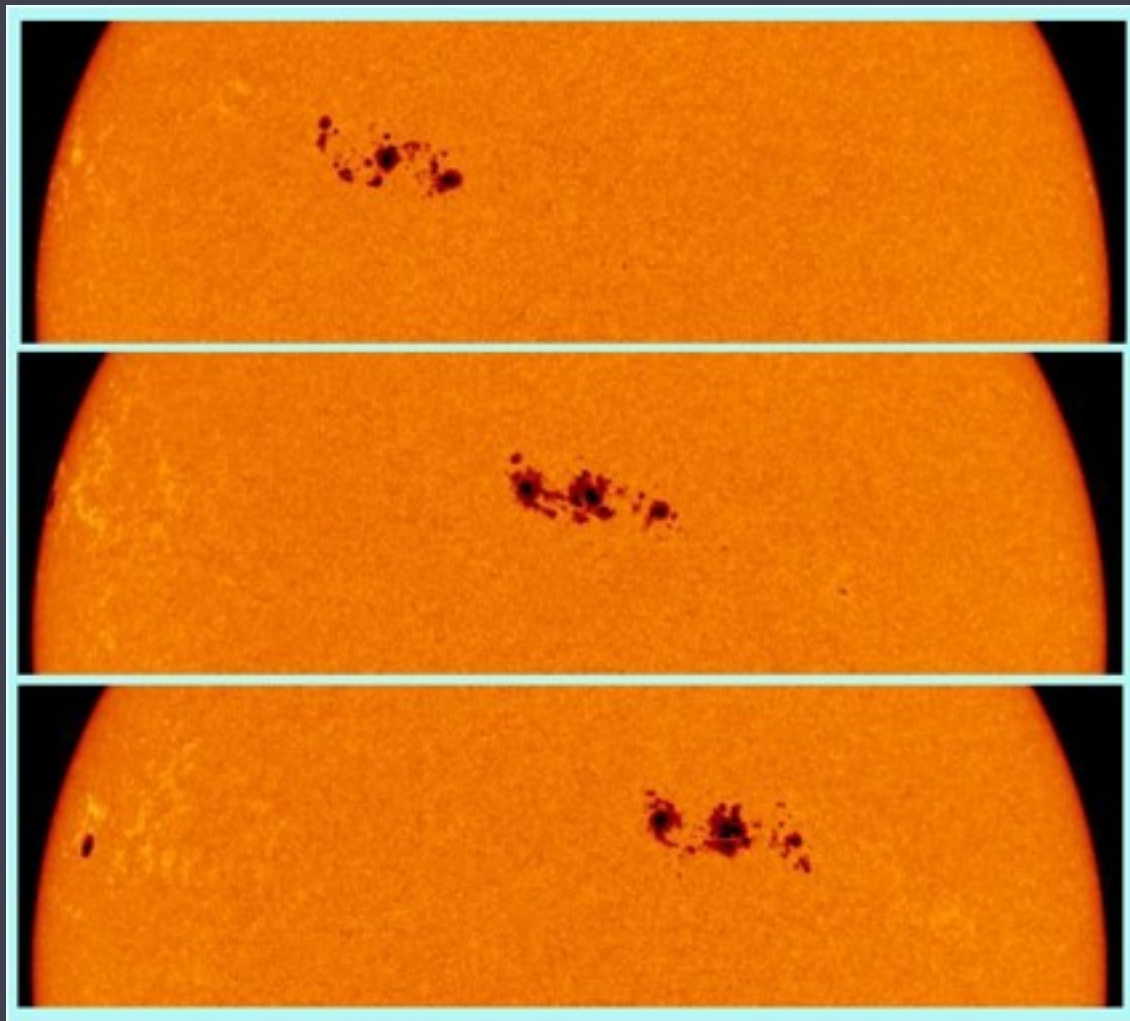
hot stars



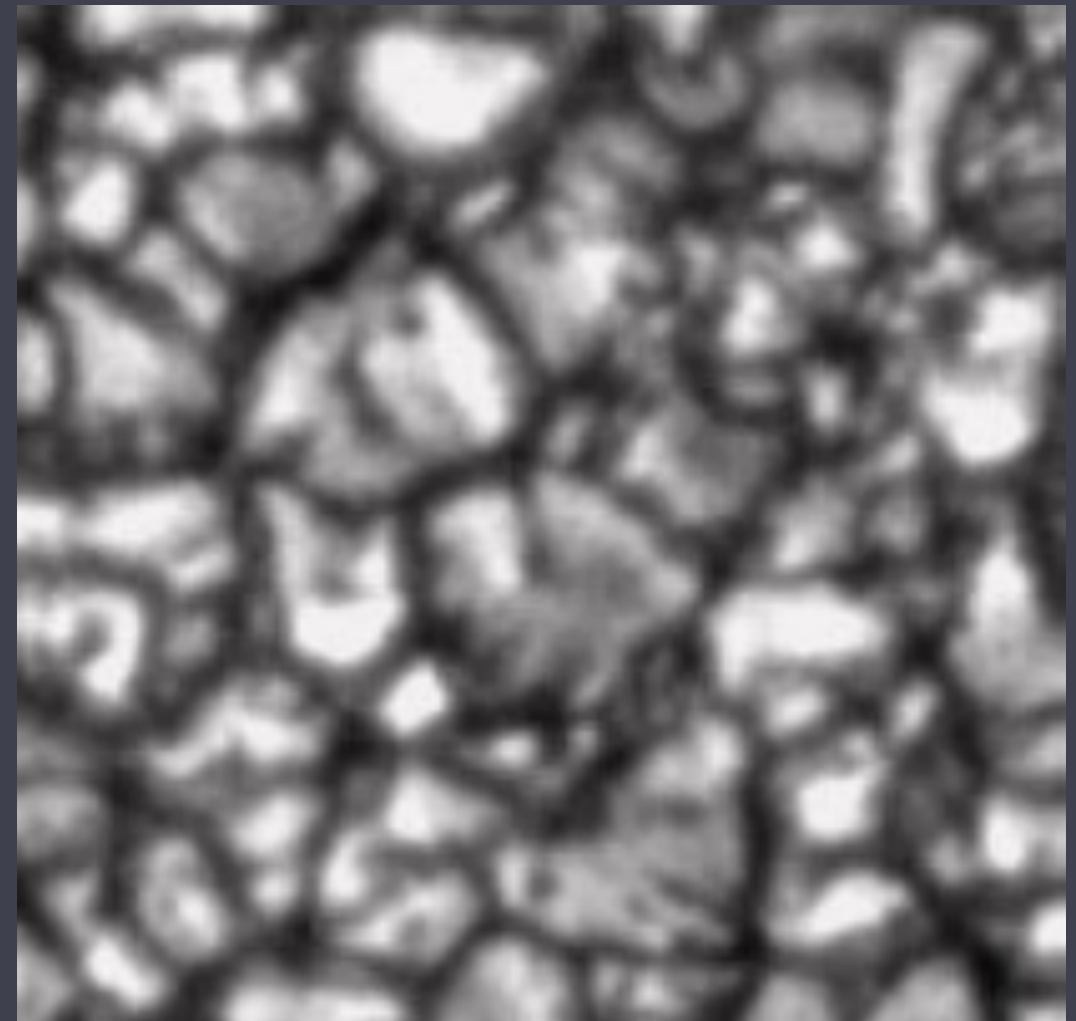
starfish, *in situ*, at the Monterey (California) Aquarium

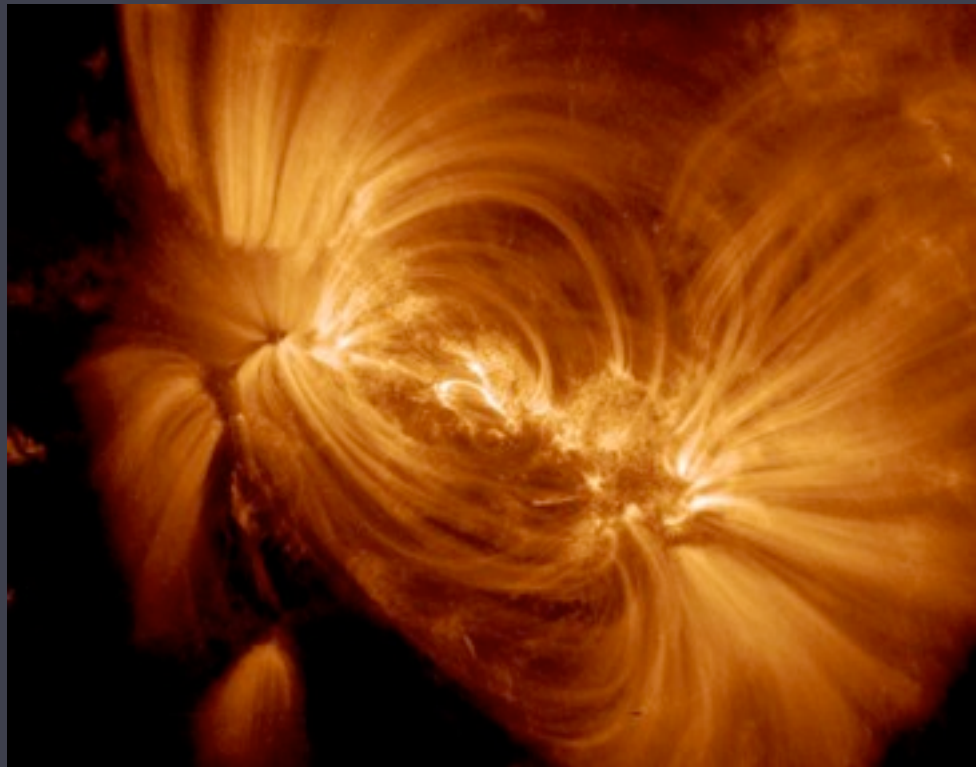
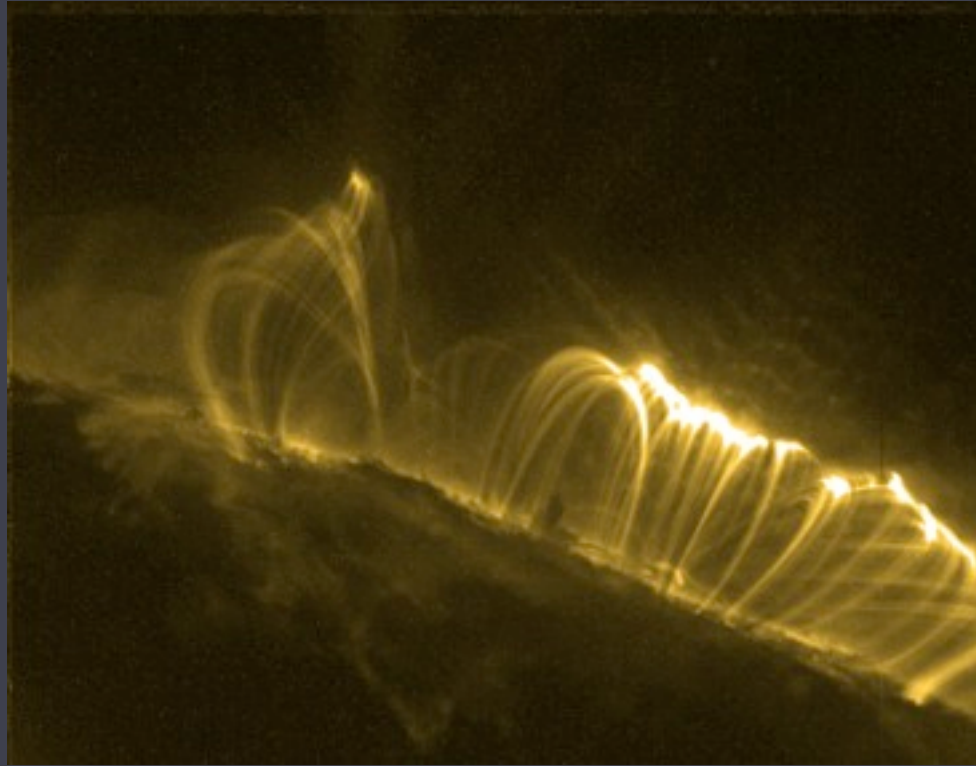
The Sun's X-ray emission is associated with its magnetic dynamo (rotation + convection are key ingredients)

rotation



convection





NASA:TRACE

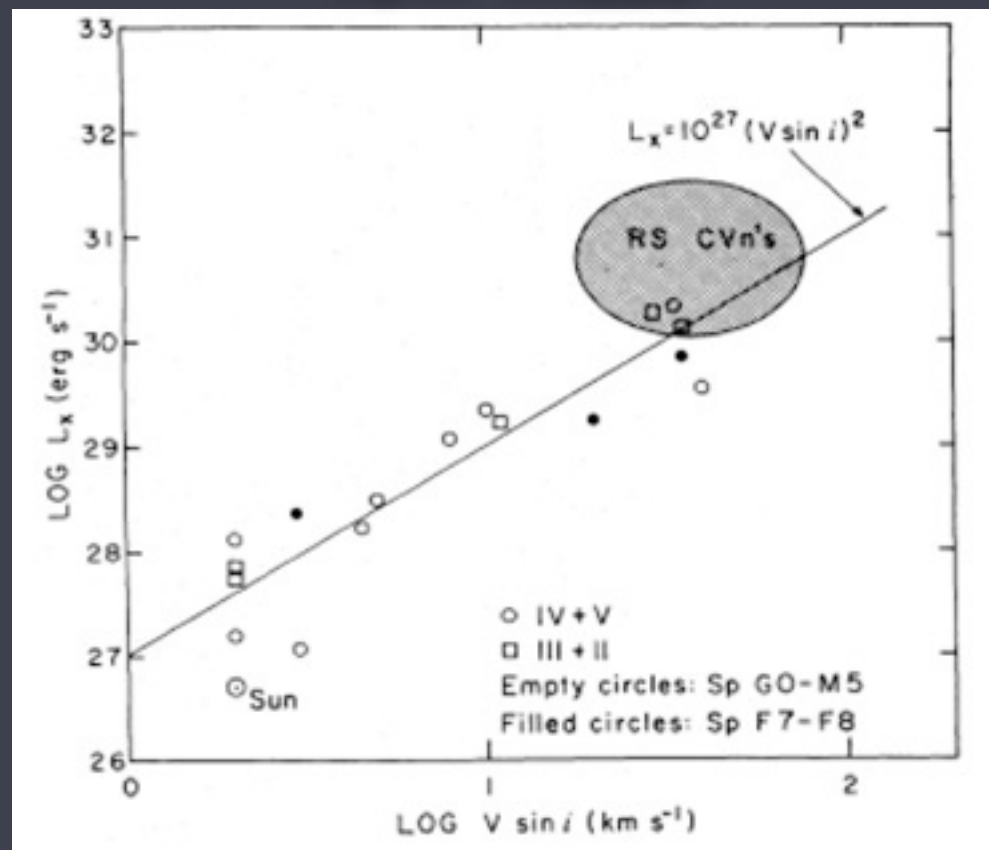
Massive stars have some *other* X-ray production mechanism



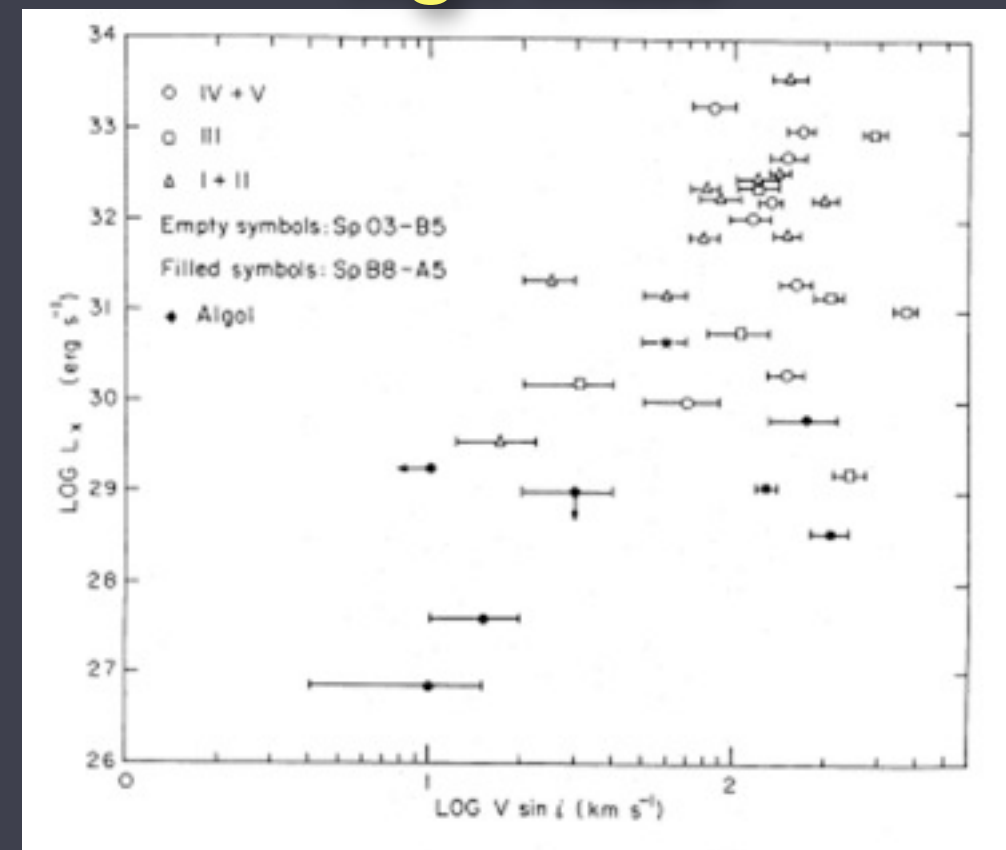
Most massive stars do *not* have magnetic fields (theoretically understood as due to lack of convection)

No observed correlation between rotation and X-ray luminosity

low mass



high mass



Basic properties of massive stars - O stars

mass $\sim 50 M_{\text{sun}}$

luminosity $\sim 10^6 L_{\text{sun}}$

surface temperature $\sim 45,000 \text{ K}$



discovery of massive star X-ray emission in 1970s

THE ASTROPHYSICAL JOURNAL, 234:L51-54, 1979 November 15
© 1979. The American Astronomical Society. All rights reserved. Printed in U.S.A.

DISCOVERY OF AN X-RAY STAR ASSOCIATION IN VI CYGNI (CYG OB2)

F. R. HARNDEN, JR., G. BRANDUARDI, M. ELVIS,¹ P. GORENSTEIN, J. GRINDLAY,
J. P. PYE,¹ R. ROSNER, K. TOPKA, AND G. S. VAIANA²

Harvard-Smithsonian Center for Astrophysics, Cambridge, Massachusetts

Received 1979 June 26; accepted 1979 July 26

ABSTRACT

A group of six X-ray sources located within $0^{\circ}.4$ of Cygnus X-3 has been discovered with the *Einstein* Observatory. These sources have been positively identified and five of them correspond to stars in the heavily obscured OB association VI Cygni. The optical counterparts include four of the most luminous O stars within the field of view and a B5 supergiant. These sources are found to have typical X-ray luminosities L_x (0.2–4.0 keV) $\sim 5 \times 10^{33}$ ergs s⁻¹, with temperatures $T \sim 10^{6.8}$ K and hydrogen column densities $N_H \sim 10^{22}$ cm⁻², and therefore comprise a new class of low-luminosity galactic X-ray sources associated with early-type stars.

○ Stars are the brightest X-ray sources in young clusters

In addition to the X-ray and UV radiation from ○ stars

Prodigious matter, momentum, and kinetic energy input into the cluster environment via their **stellar winds**



Tr 14 in Carina: *Chandra*

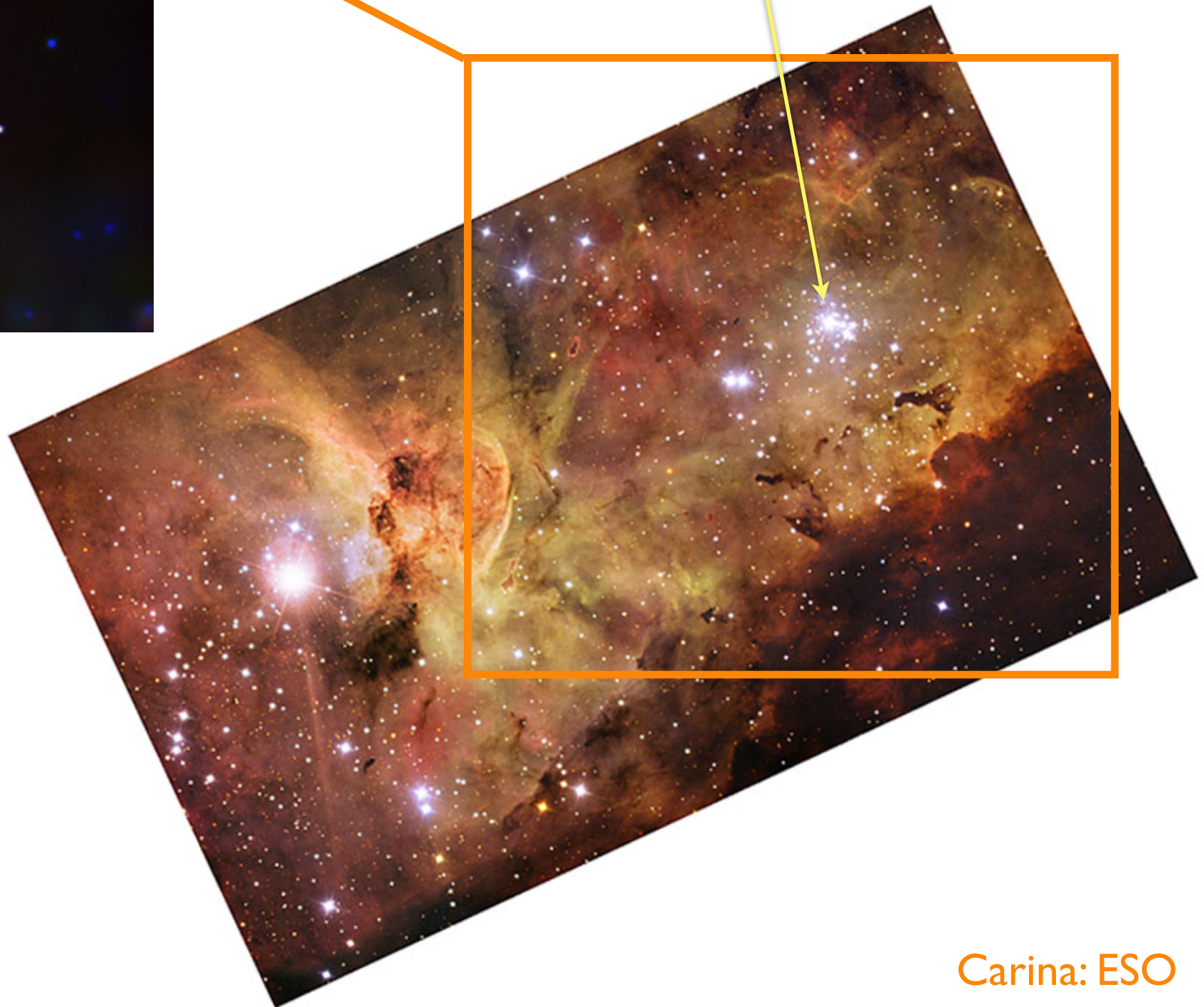
These winds are the site and energy source of the X-ray emission

The Carina Complex

HD 93129A (O2If*)



Tr 14 in Carina: *Chandra*



Carina: ESO

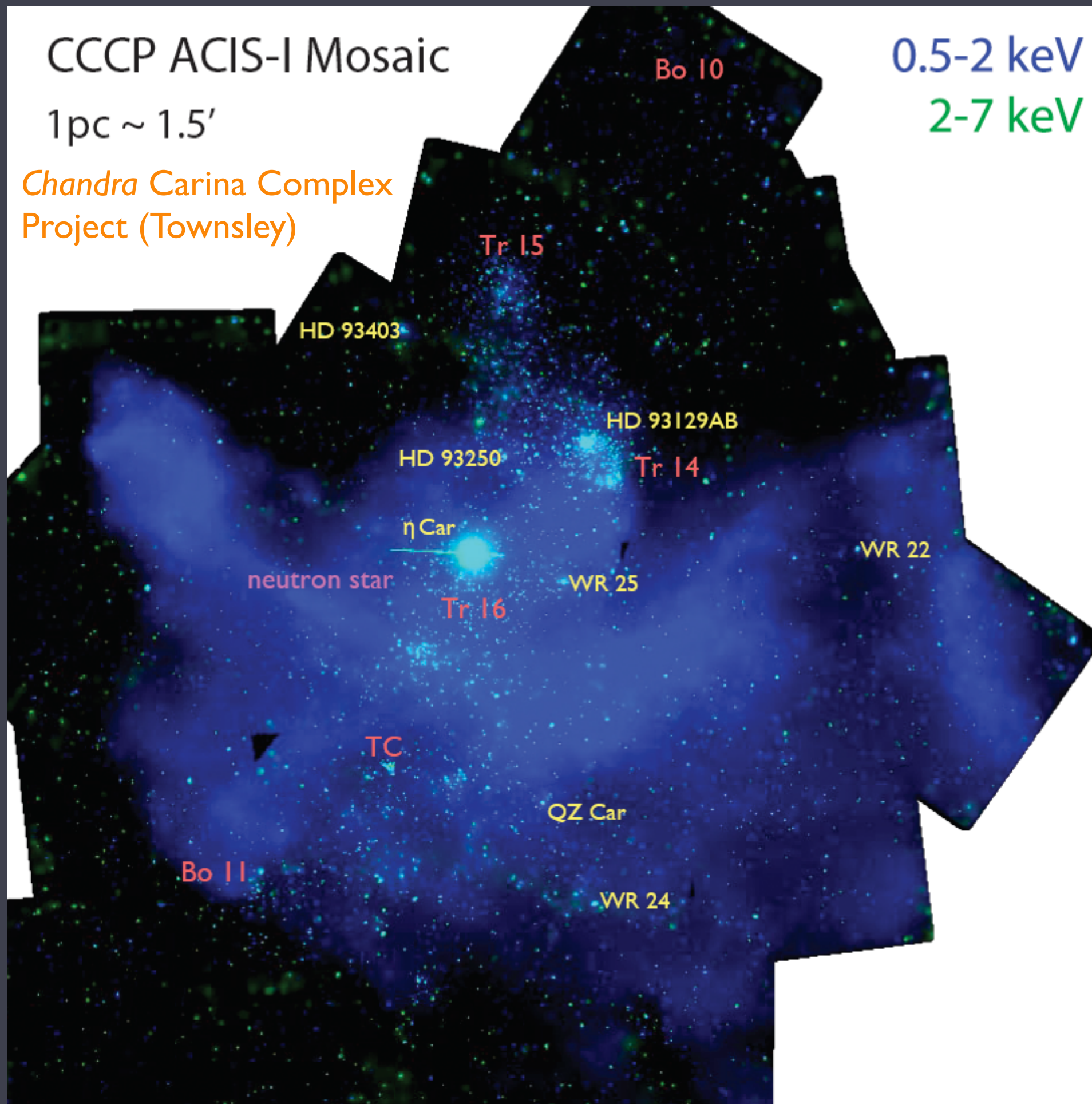
CCCP ACIS-I Mosaic

1 pc ~ 1.5'

Chandra Carina Complex
Project (Townsend)

0.5-2 keV

2-7 keV





wind-blown bubble around a massive star



NGC 6888 Crescent Nebula - Tony Hallas

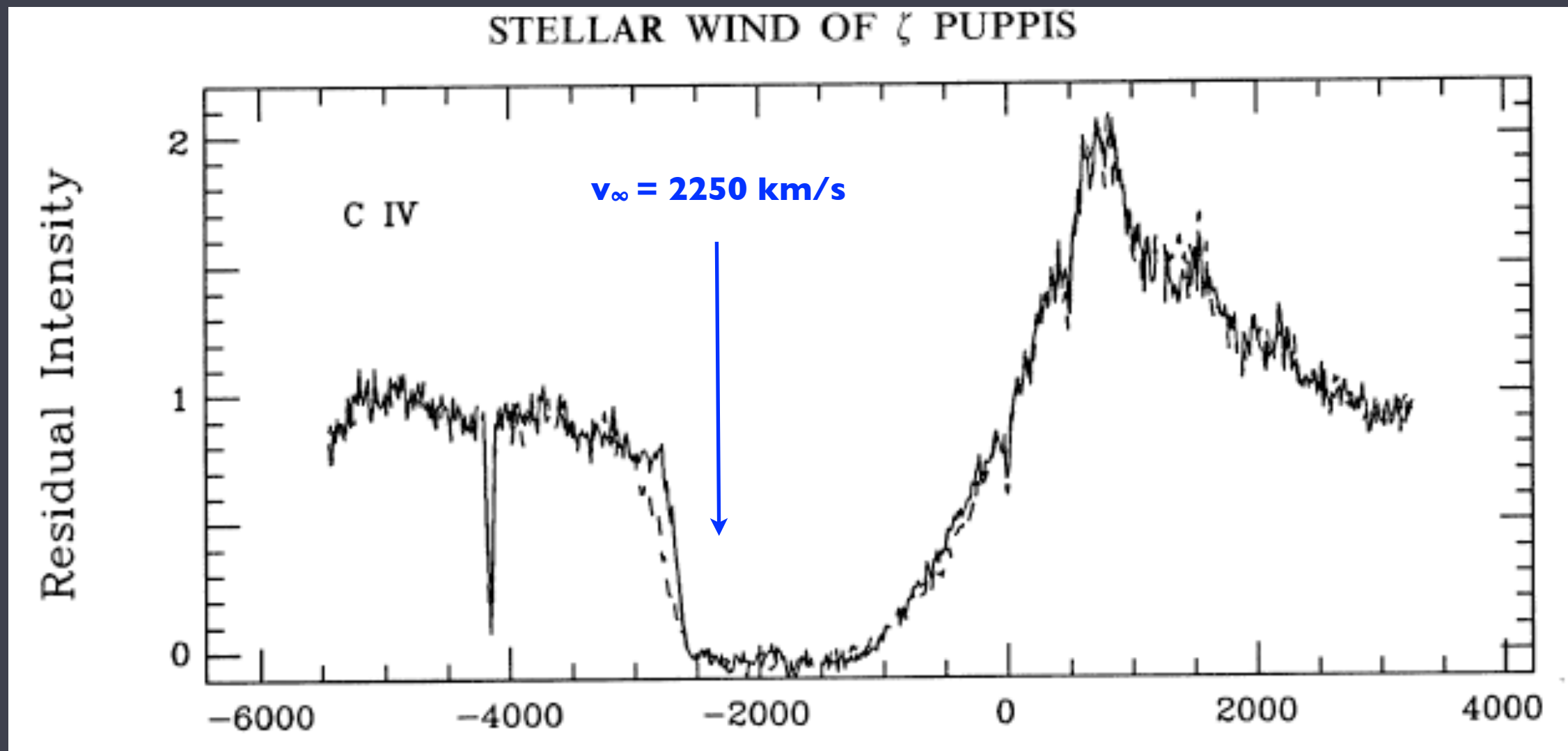
In general, X-ray imaging of massive stars is not useful

...use spectroscopy as a proxy for imaging

Radiation-driven O star winds

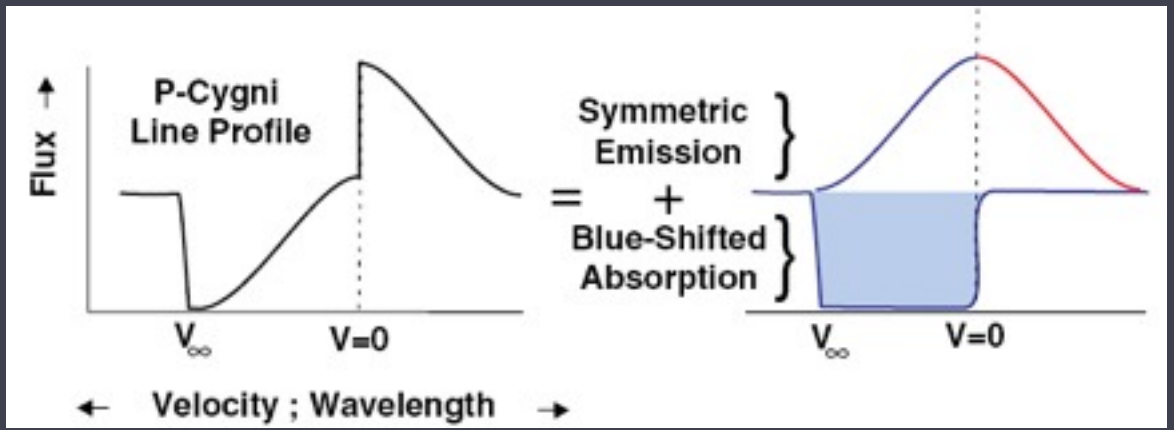
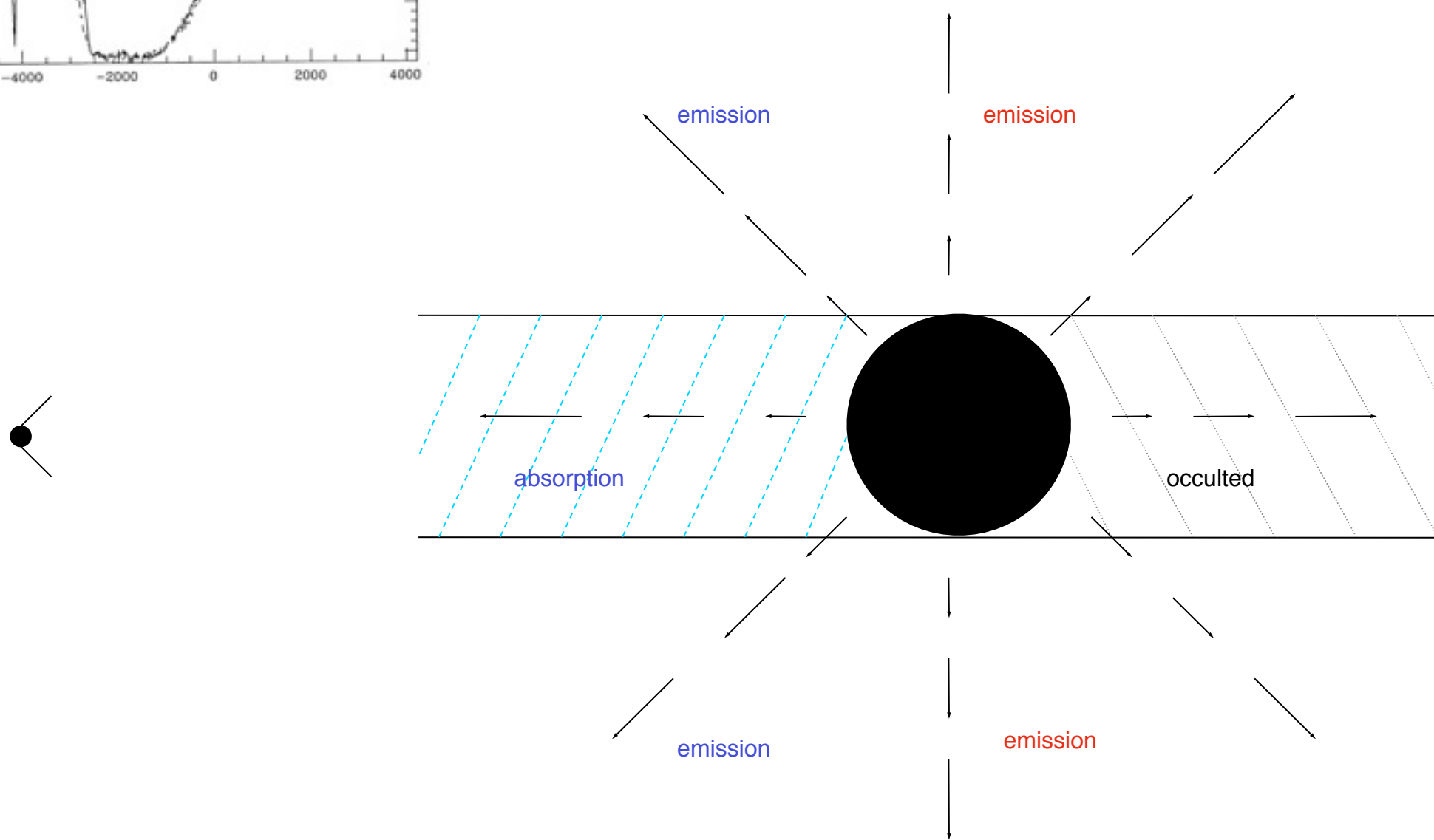
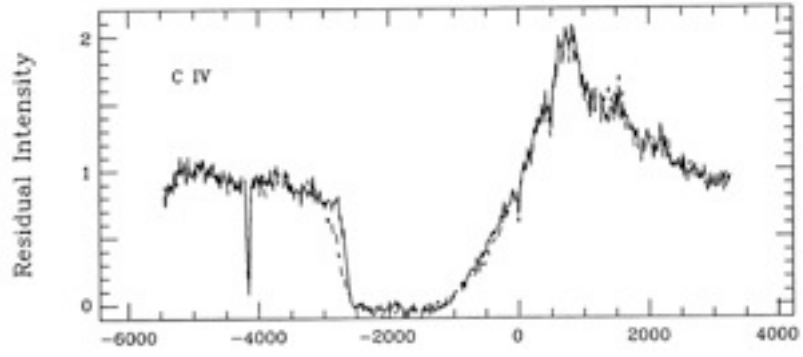
ζ Pup (O4 supergiant): $\dot{M} \sim \text{few } 10^{-6} M_{\text{sun}}/\text{yr}$

UV spectrum: C IV 1548, 1551 Å



Velocity (km/s)

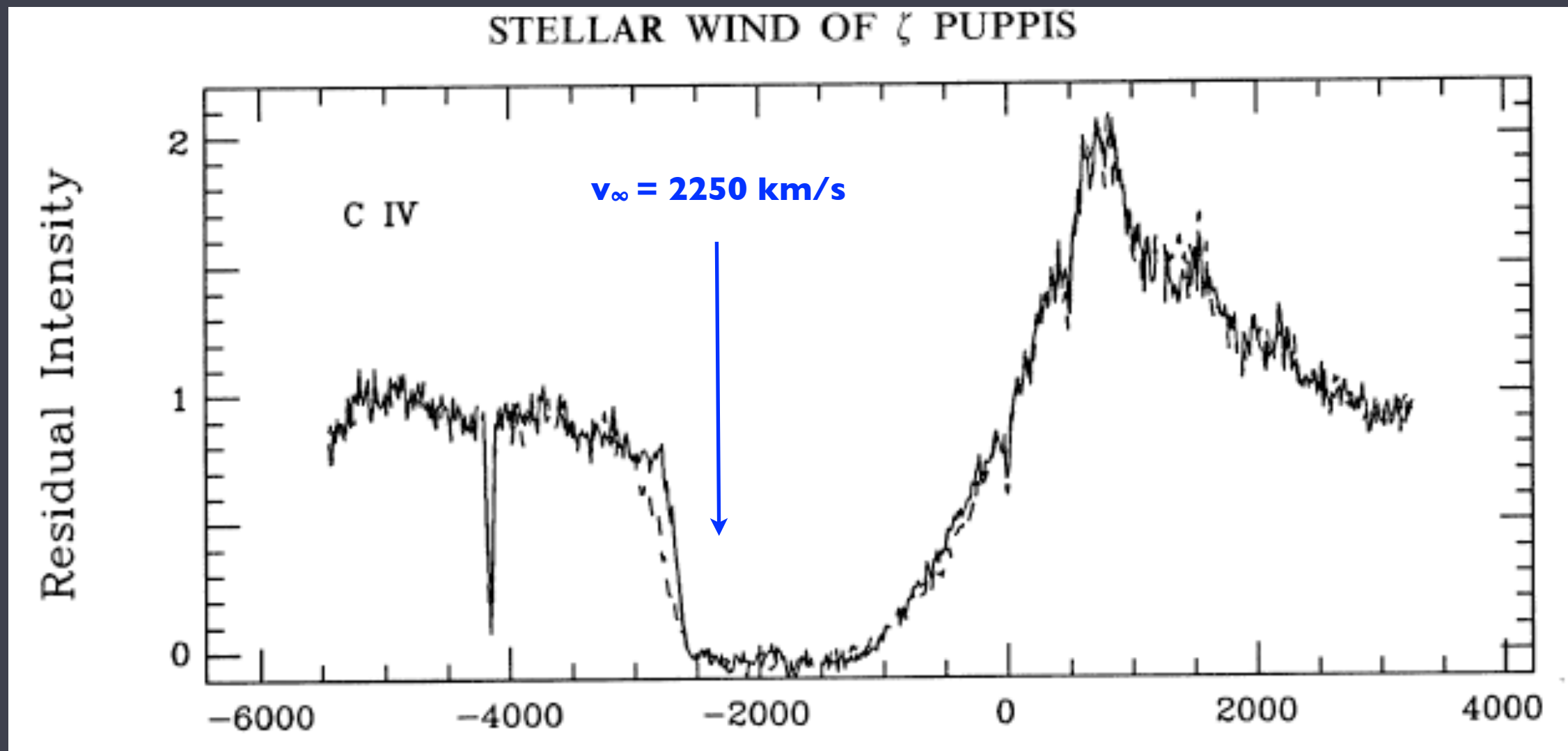
STELLAR WIND OF ζ PUPPIS



Radiation-driven O star winds

ζ Pup (O4 supergiant): $\dot{M} \sim \text{few } 10^{-6} M_{\text{sun}}/\text{yr}$

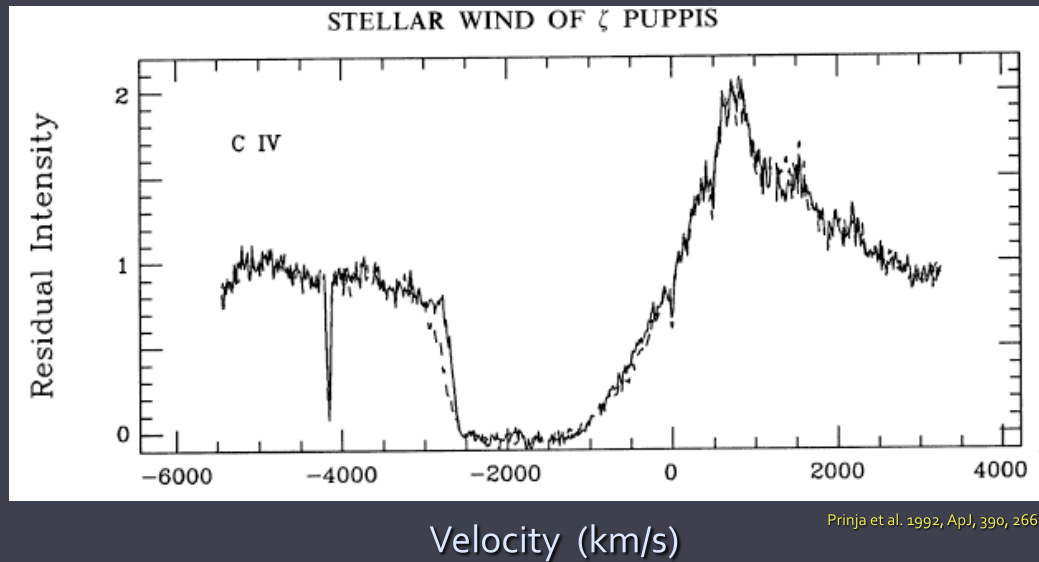
UV spectrum: C IV 1548, 1551 Å



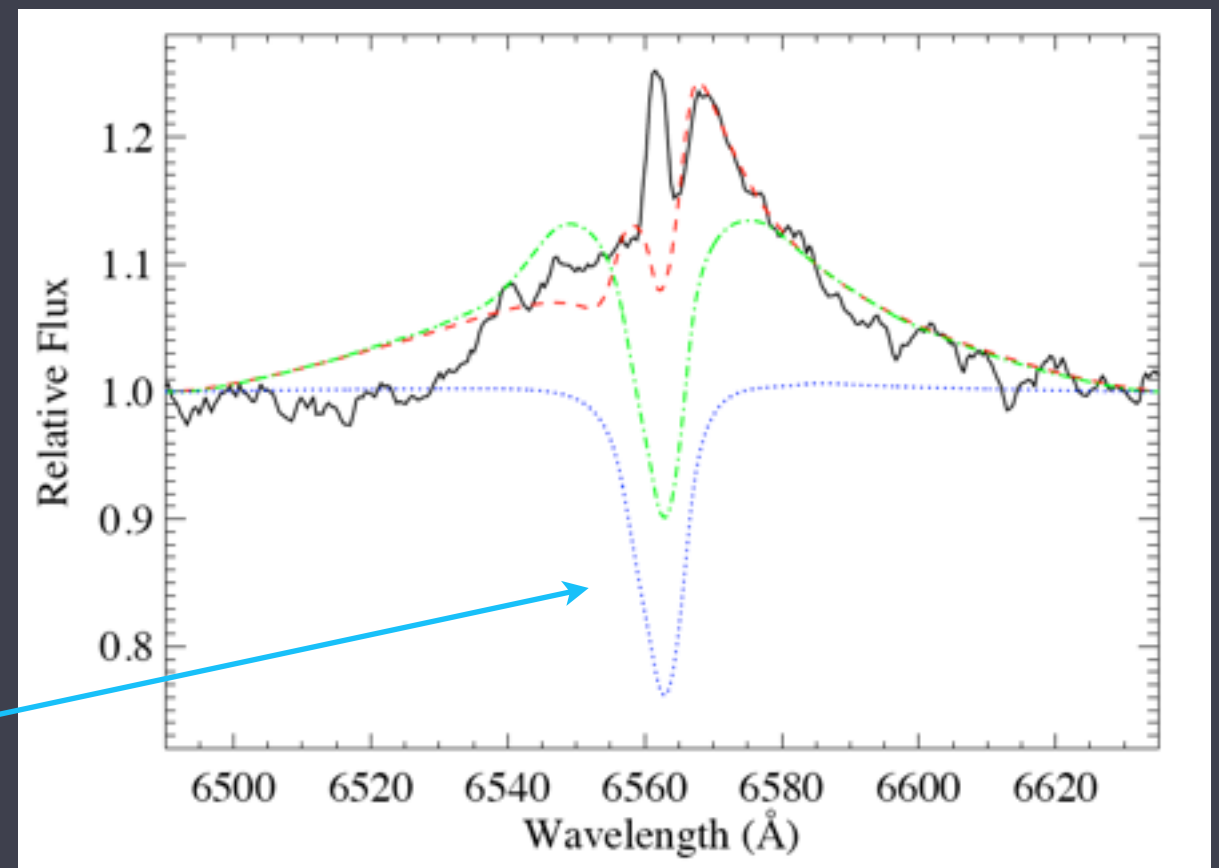
Velocity (km/s)

Wind mass-loss rates (\dot{M}) can be inferred from the strength of the absorption component

but, more reliable are emission lines such as hydrogen Balmer- α



photosphere only,
no wind



Radiation-driven winds of massive stars

L/c = momentum in the (mostly UV) radiation from the stellar surface $< \dot{M}v_{\infty}$ (wind momentum)

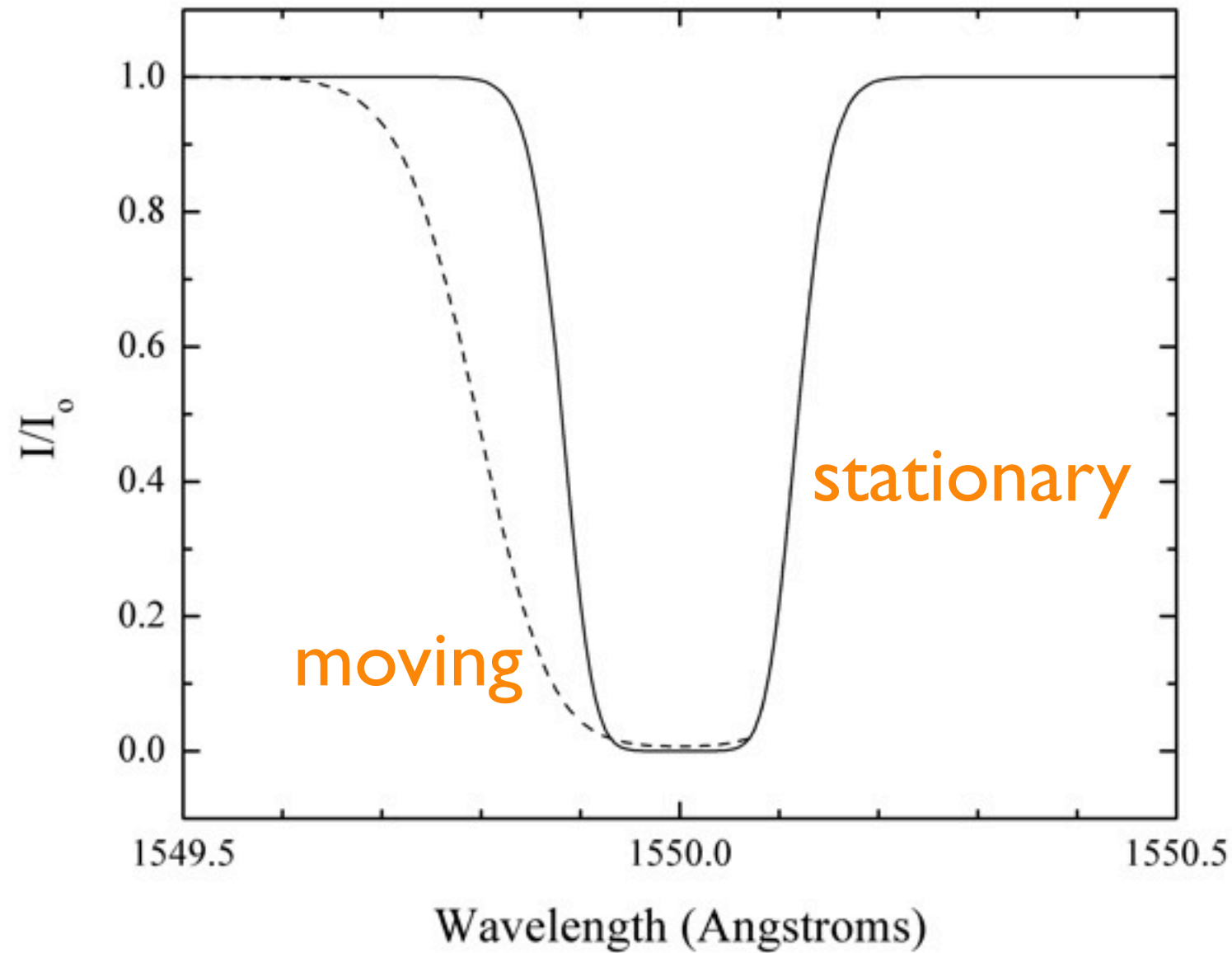
radiation couples to the matter in the wind via resonance line scattering

$\dot{M} \sim 10^{-6} M_{\text{sun}}/\text{yr}$ (10^8 times the Sun's value)

kinetic power in the wind = $1/2 \dot{M}v_{\infty}^2$ ($\sim 10^{-3} L_{\text{bol}}$)

Doppler desaturation is key to line-driven winds

line opacity increases in a moving medium



The wind kinetic power is typically 10^4 times larger than the observed L_x

some process - which doesn't have to be very efficient - converts a small fraction of this kinetic power to heat

the observed X-rays are the thermal radiation from this hot stellar wind plasma

The line-deshadowing instability (LDI)

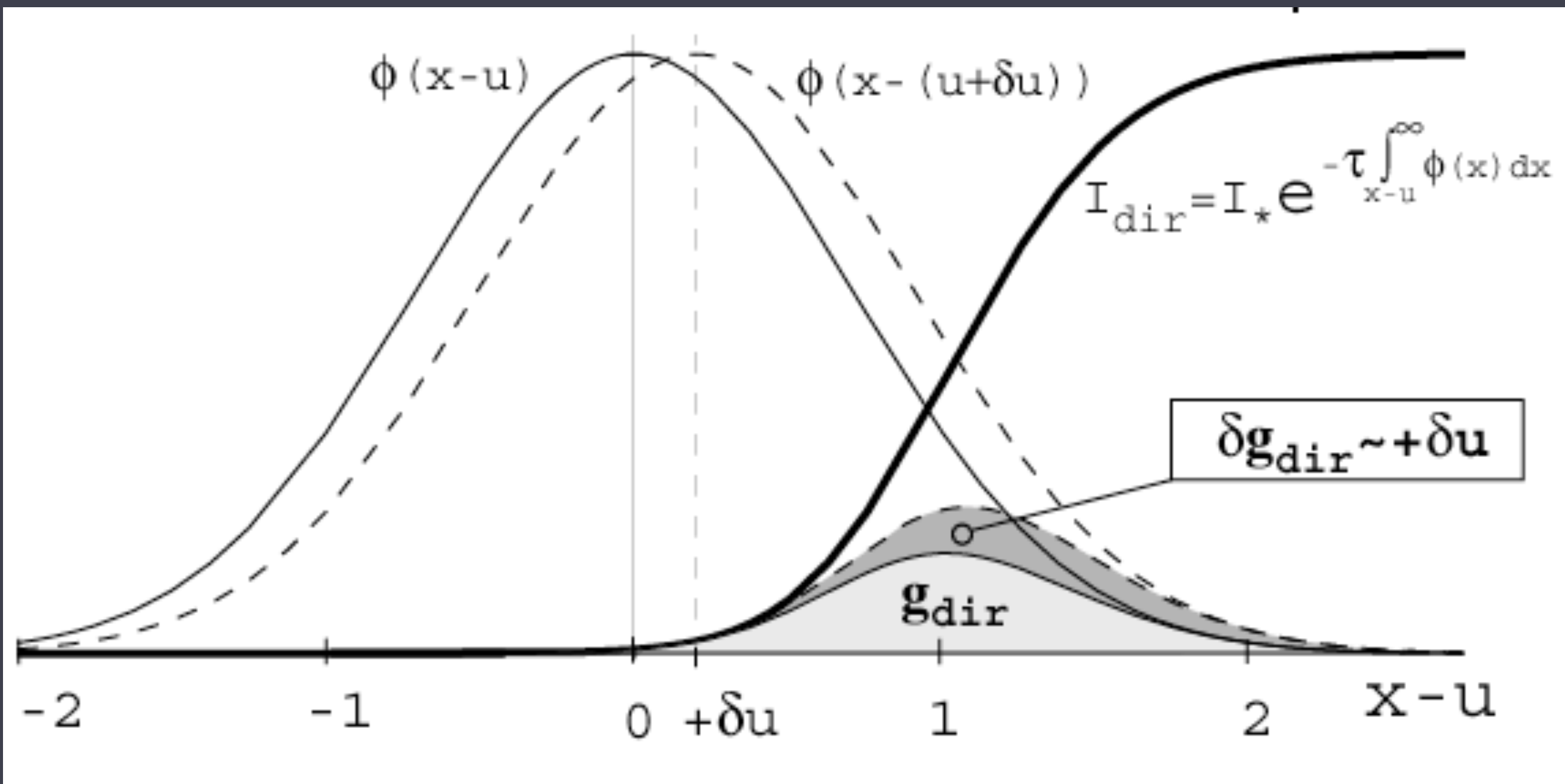
causes fast, rarefied wind plasma to slam into slower, denser wind plasma

the resulting shocks heat the plasma

general result from shock theory:

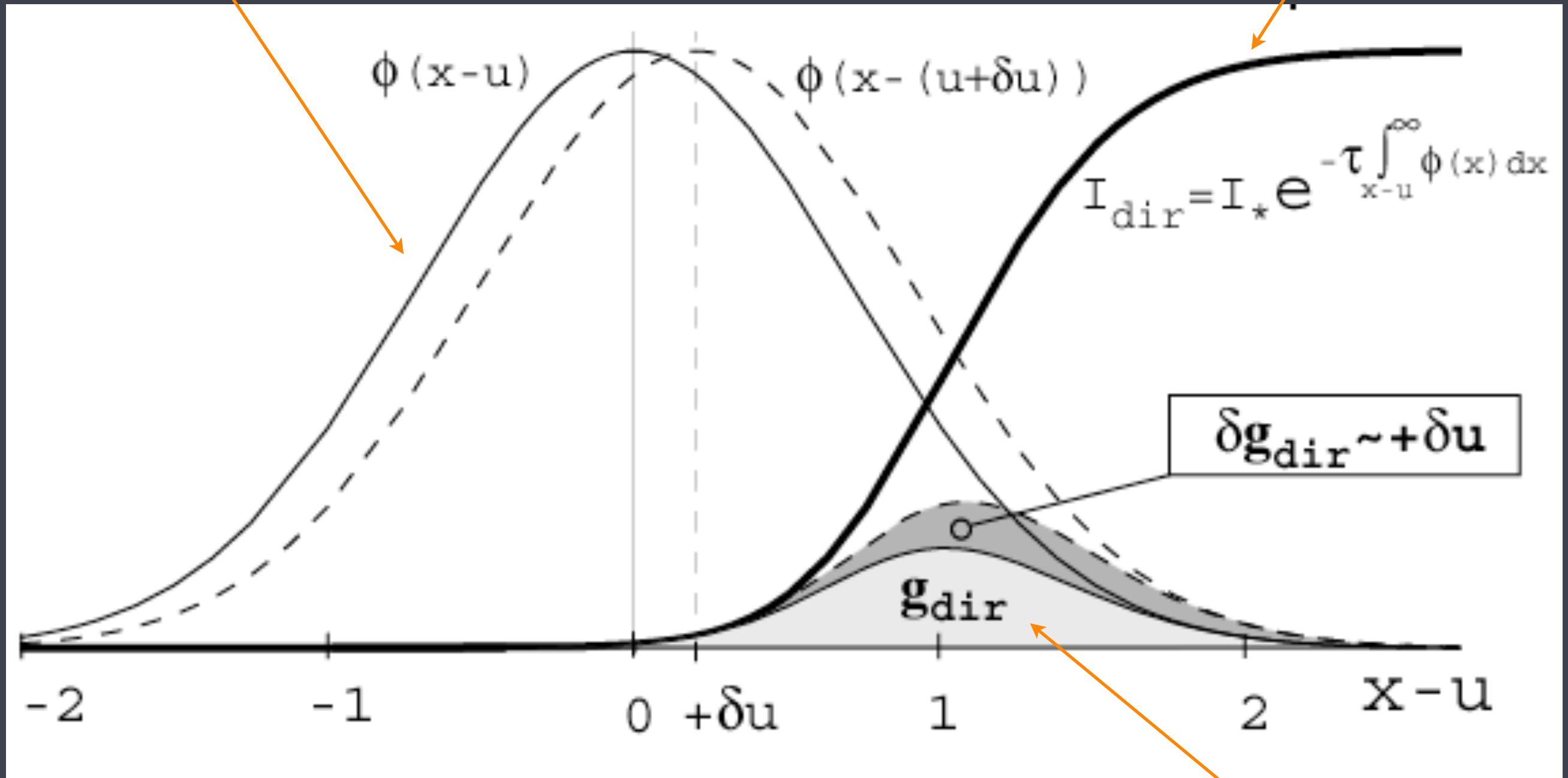
$$T \sim 10^6 (\Delta v_{\text{shock}} / 300 \text{ km/s})^2$$

the LDI was first proposed by Milne in the 1920's



line profile

photospheric radiation

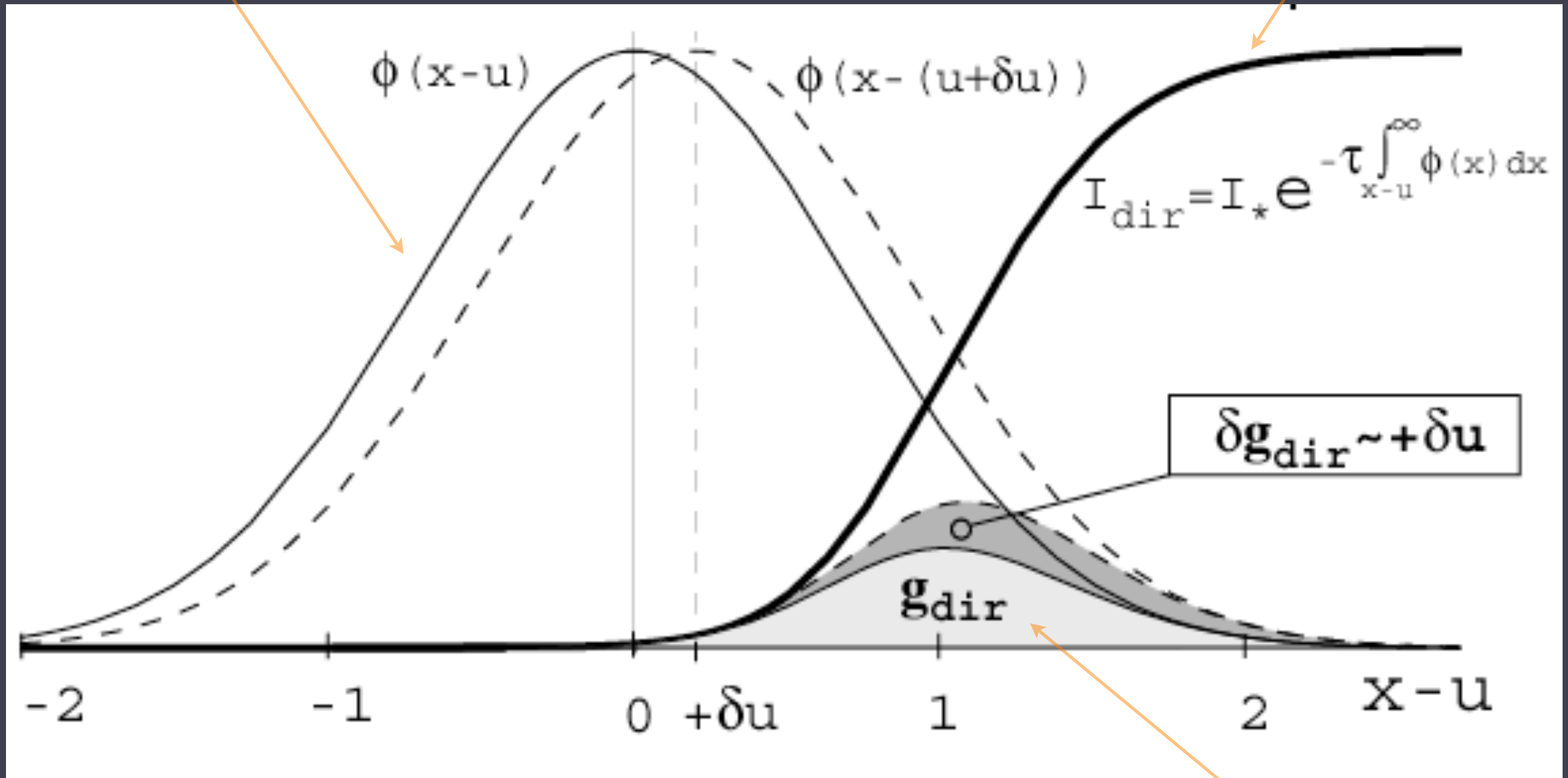


frequency

radiation force

positive velocity perturbation
line profile

photospheric radiation

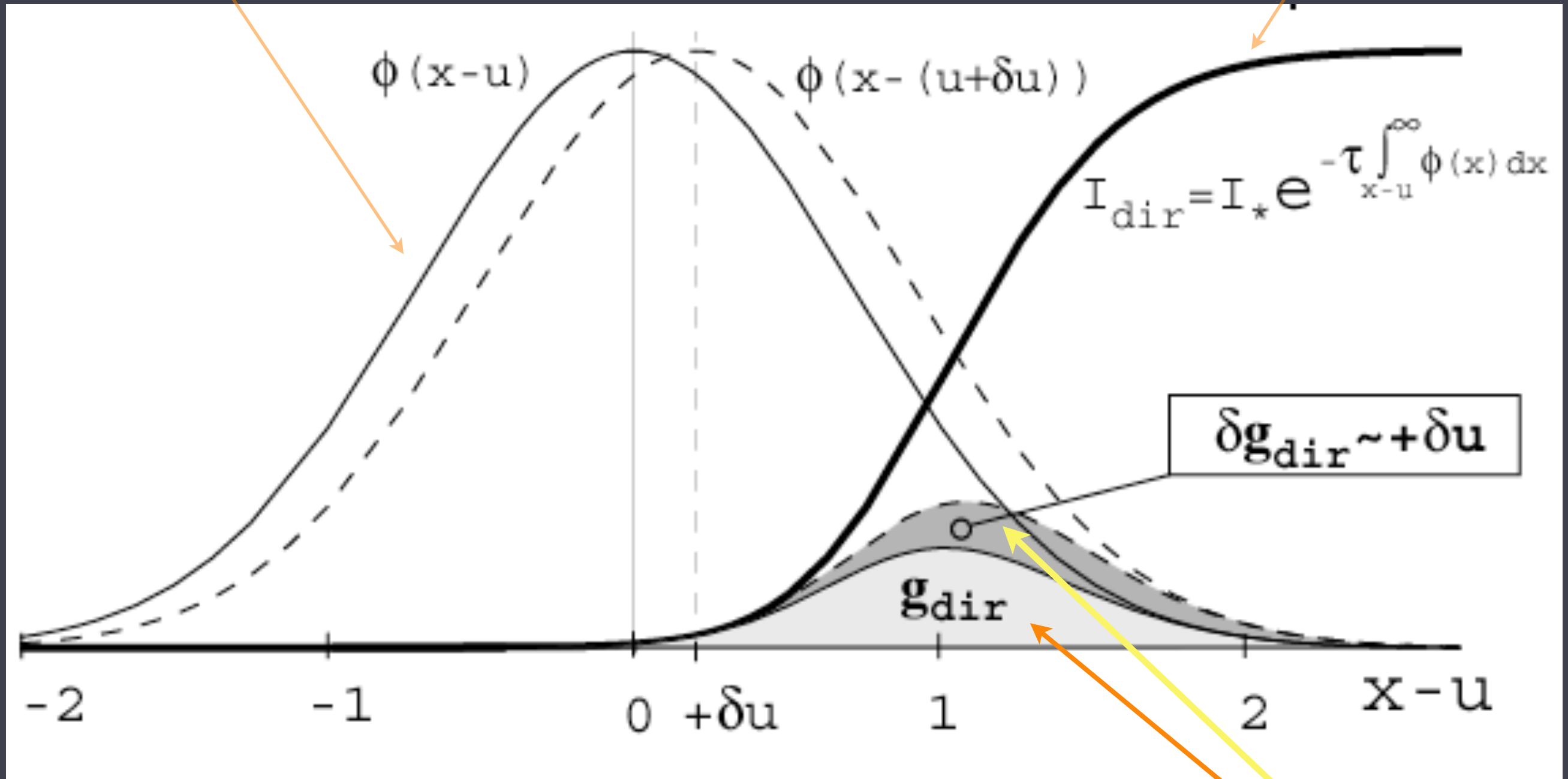


frequency

radiation force

positive velocity perturbation
line profile

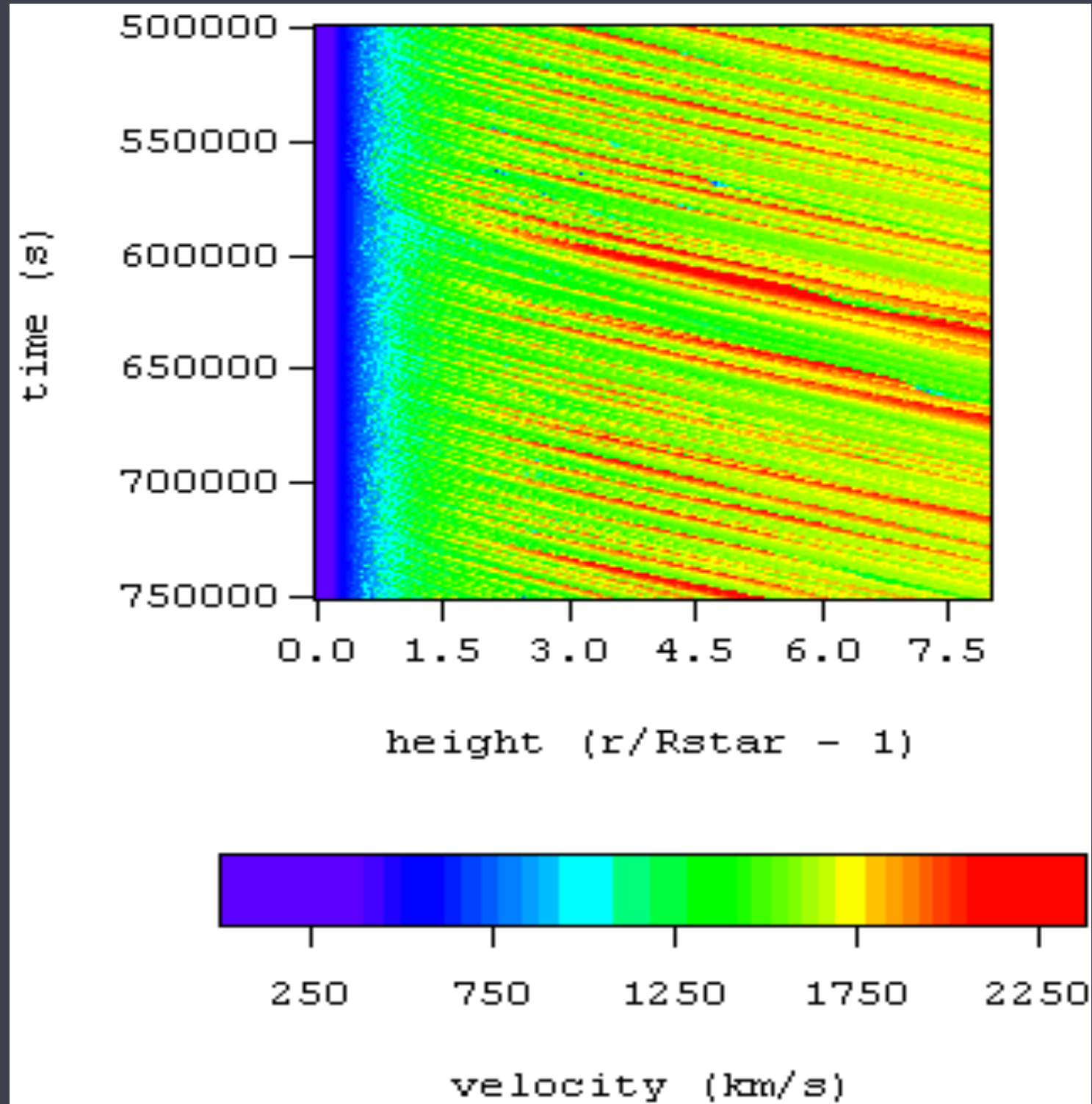
photospheric radiation



frequency

radiation force
increases

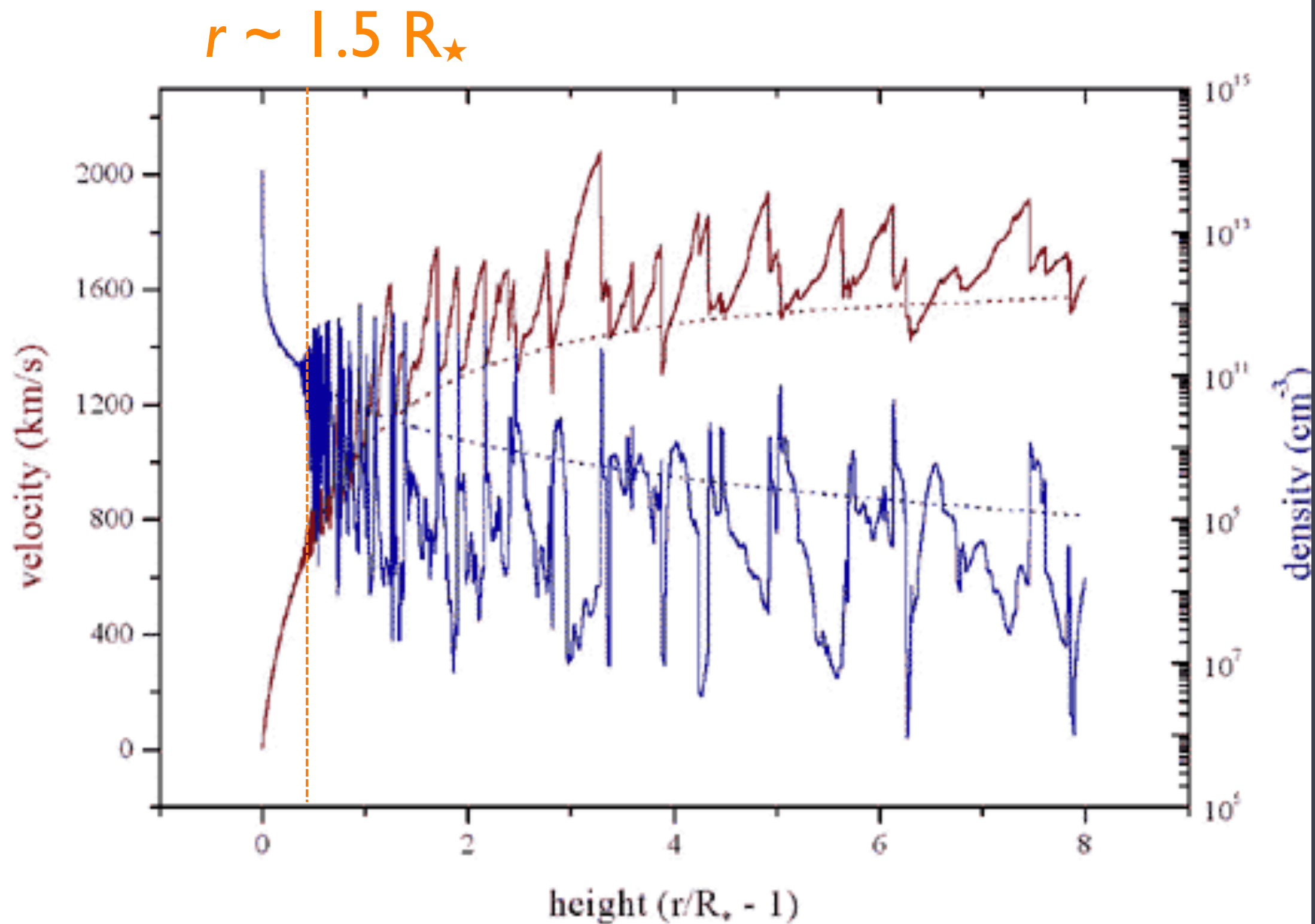
Numerical simulations of the line-deshadowing instability (LDI)



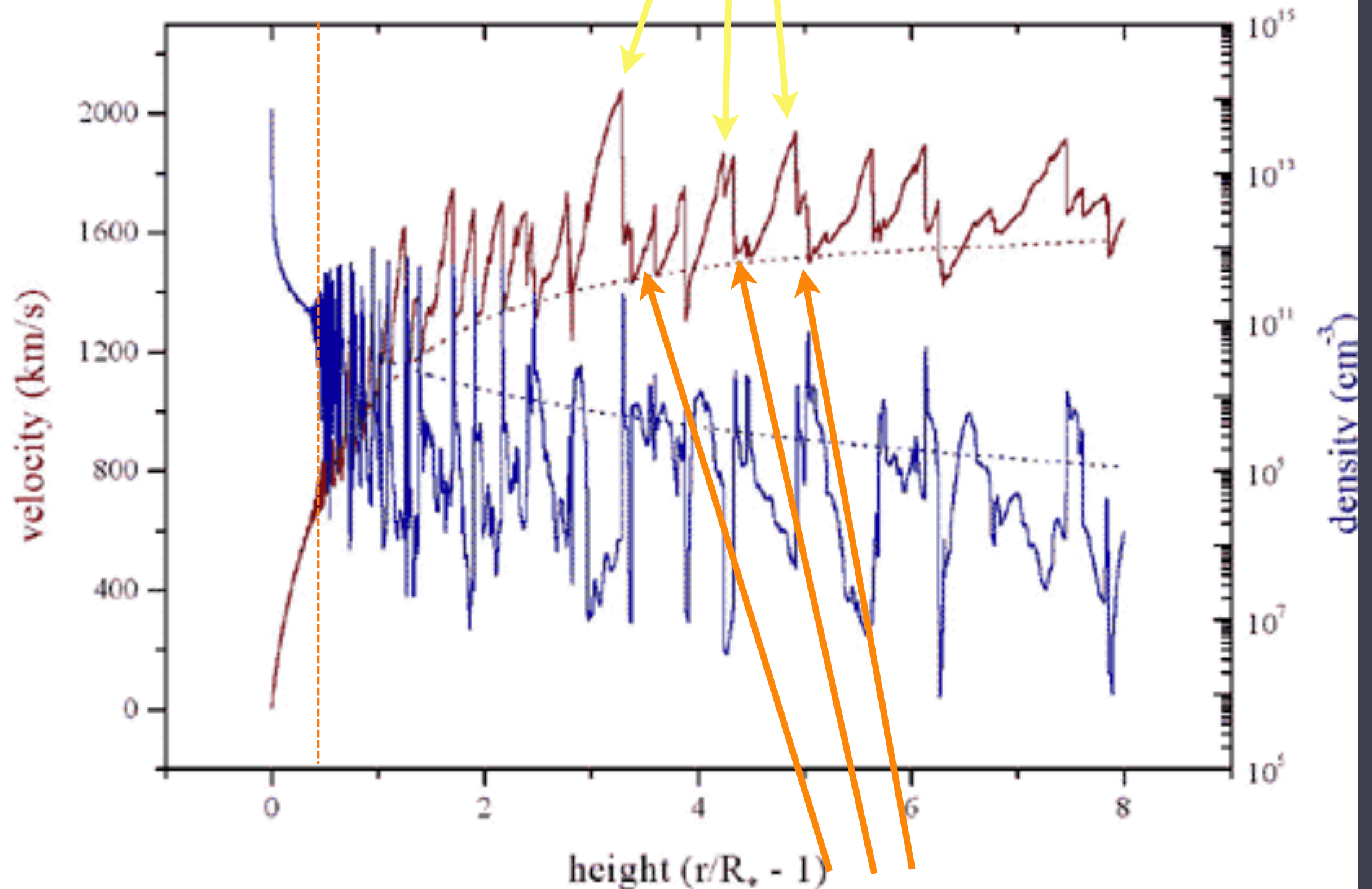
Owocki, Cooper, Cohen 1999

shock jump **velocities** \sim few 100 km/s

Numerous shock structures distributed above $r \sim 1.5 R_{\star}$

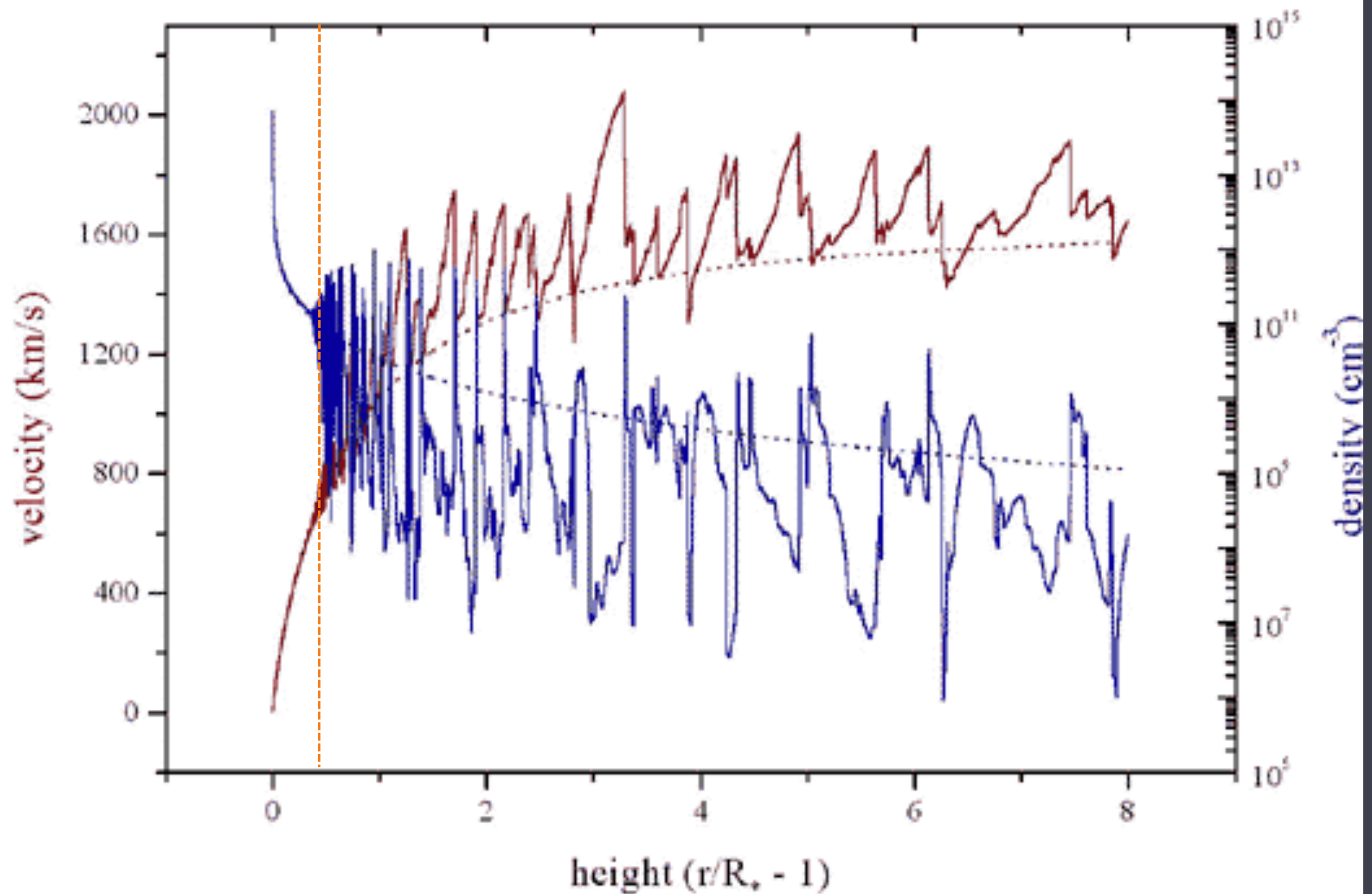


$V_{\text{shock}} \sim 300 \text{ km/s} : T \sim 10^6 \text{ K}$

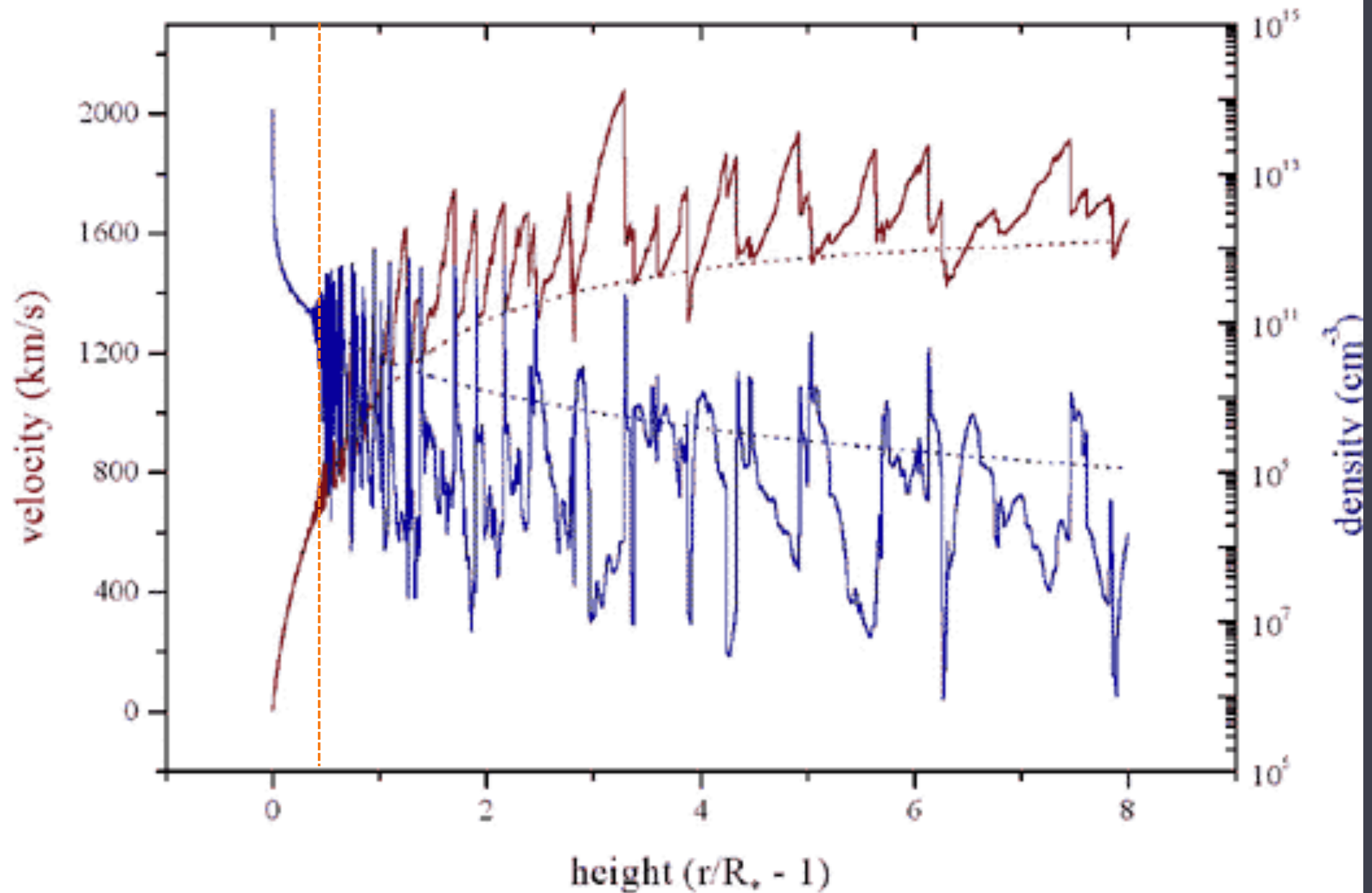


shocked wind plasma is decelerated back down to the local CAK wind velocity

Shocked plasma is moving at $v \sim 1000$ km/s

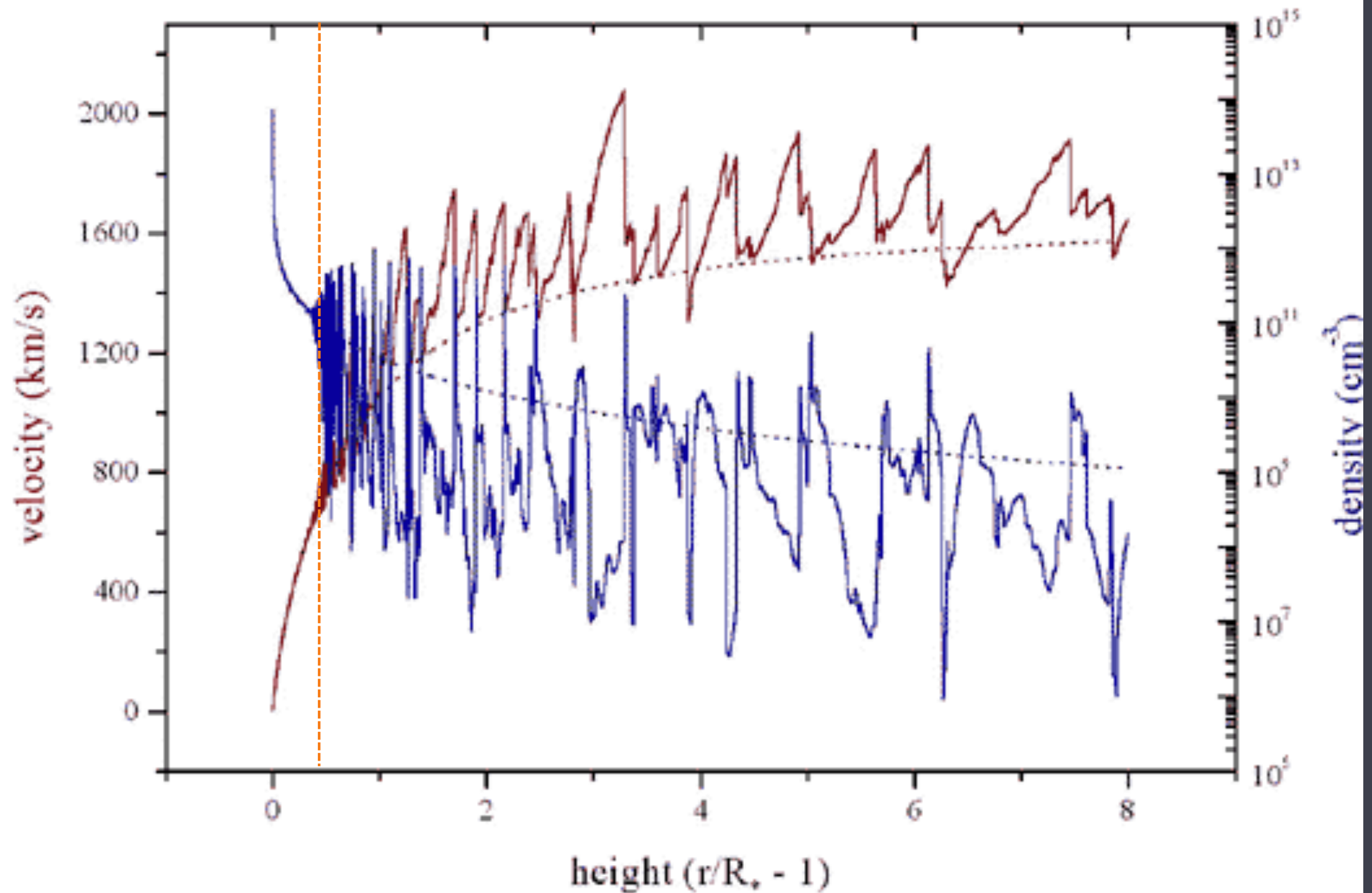


X-ray emission lines should be **Doppler broadened**

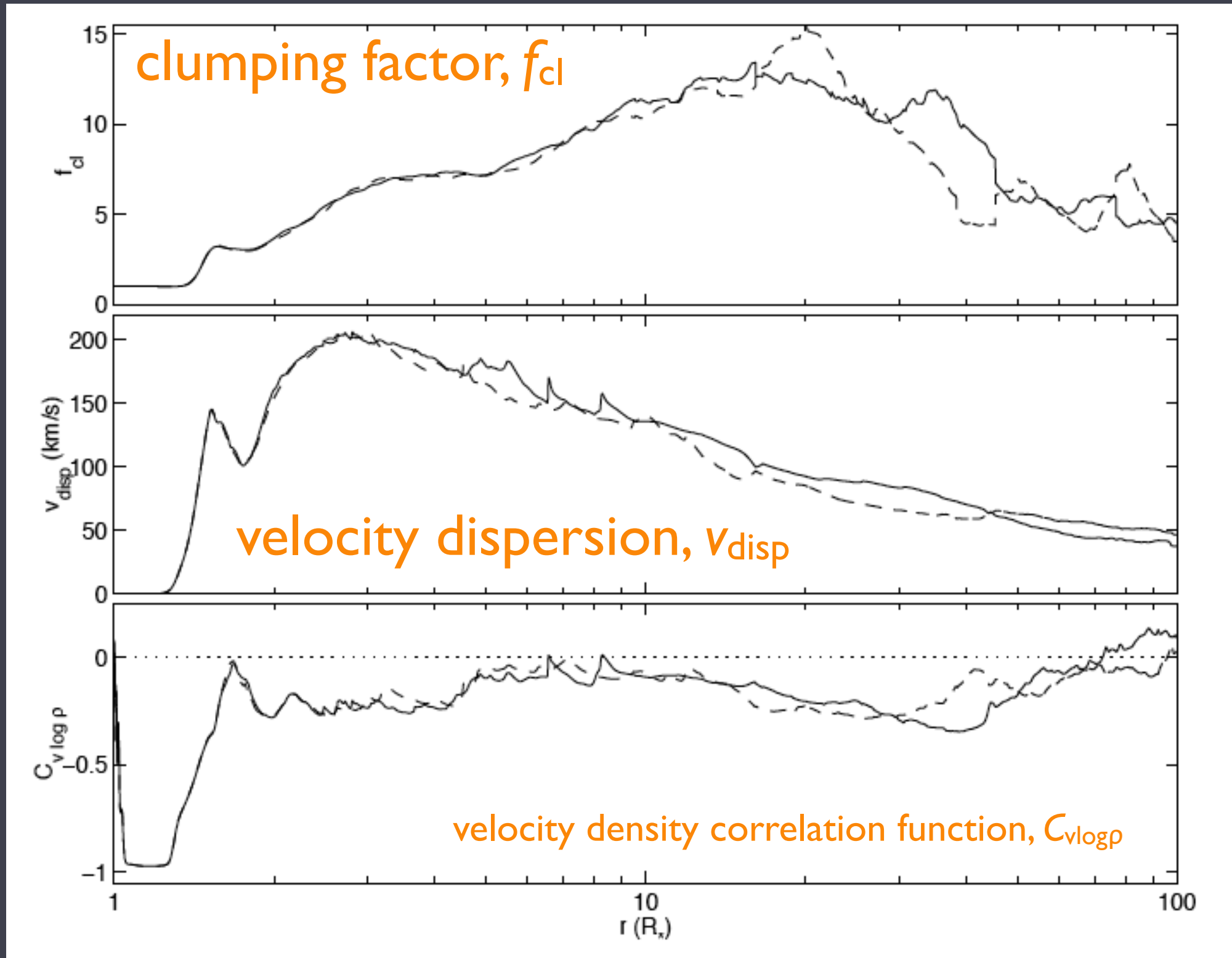


Less than 1% of the wind is emitting X-rays

>99% of the wind is cold and X-ray absorbing



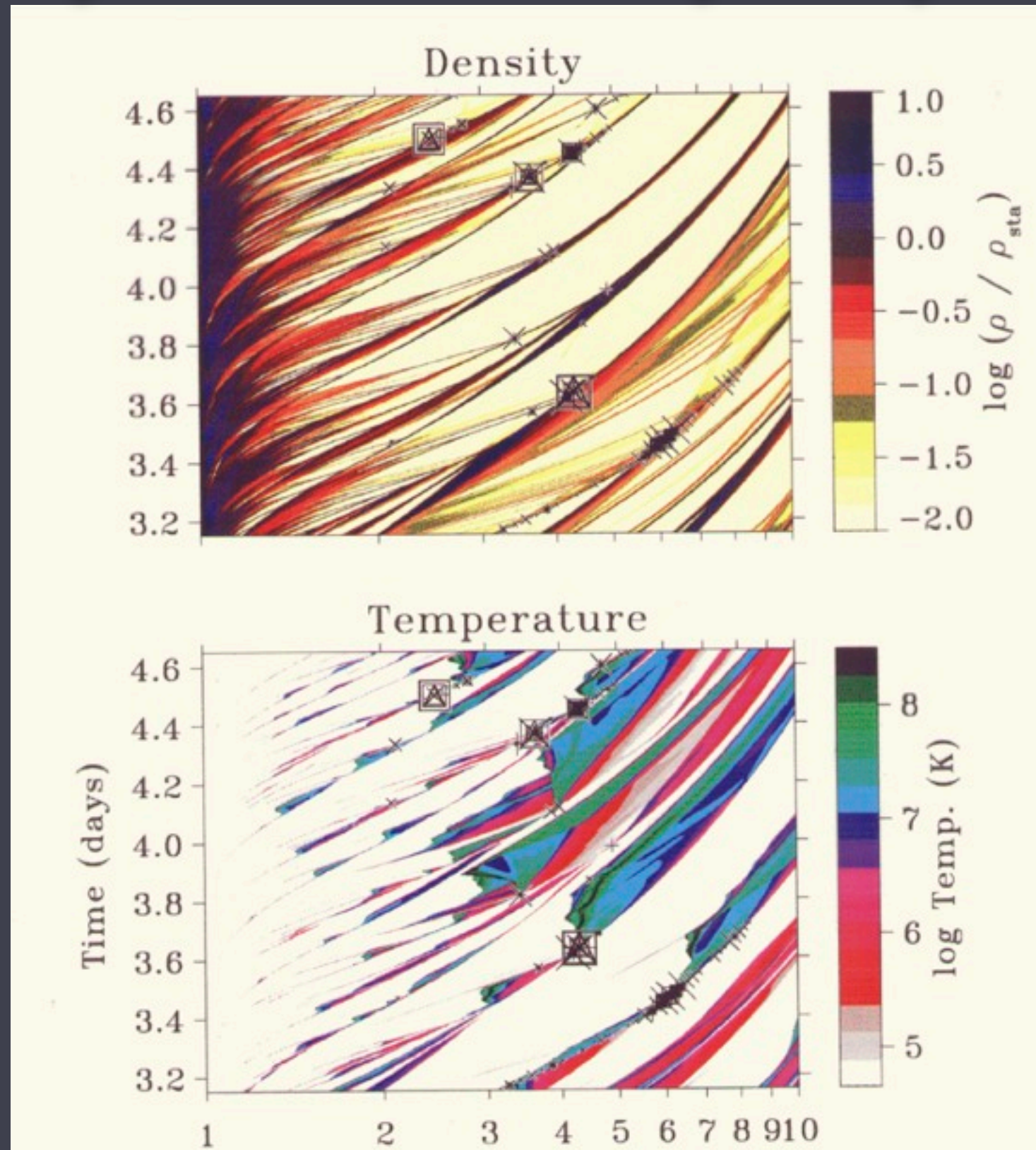
Statistics (time-average quantities) from I-D simulations



The instability in these simulations is not seeded

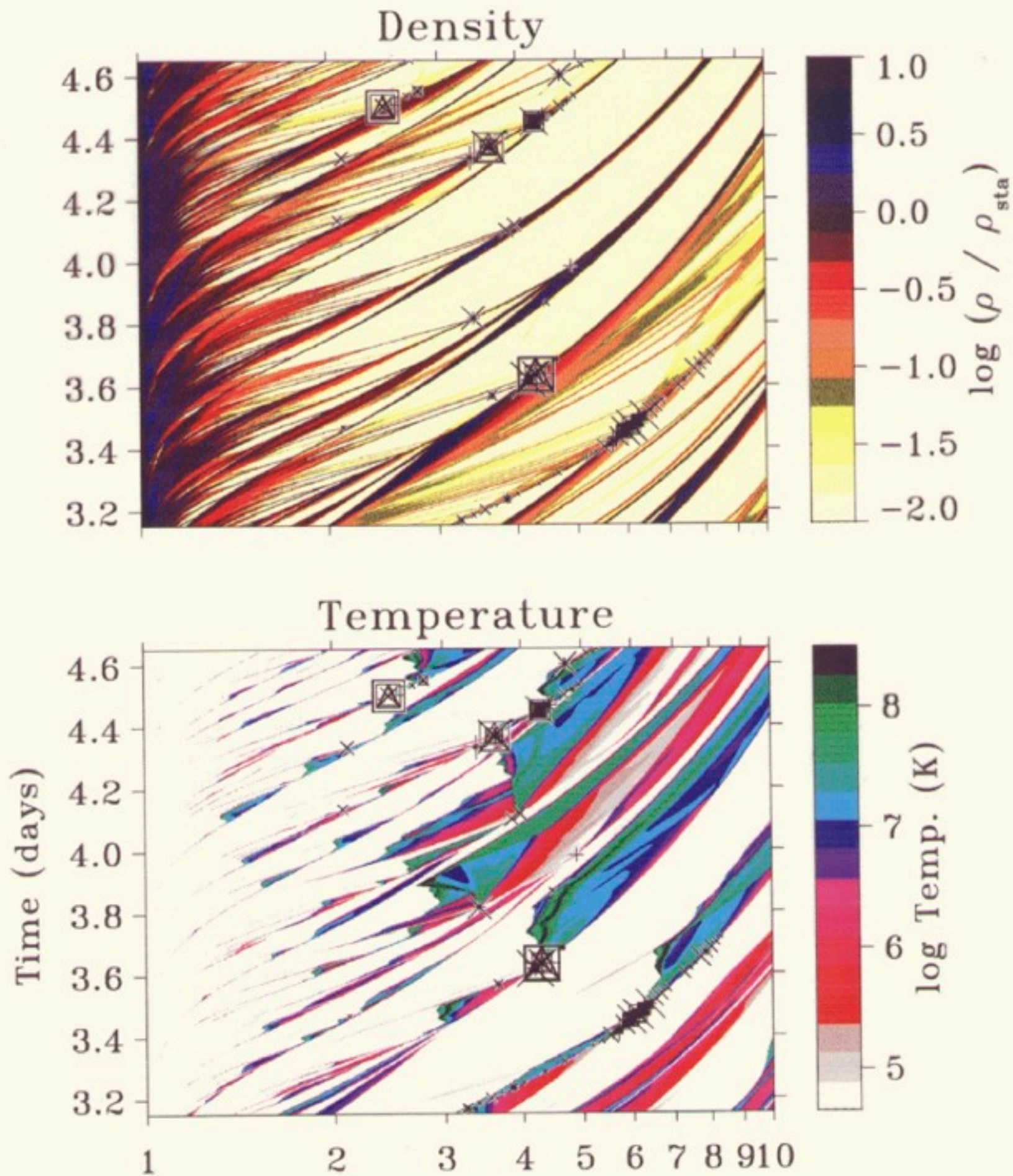
the predicted X-ray flux is too low

sound waves or turbulence at the wind base seeds the instability and leads to clump-clump collisions



Feldmeier et al. 1997

time ↑



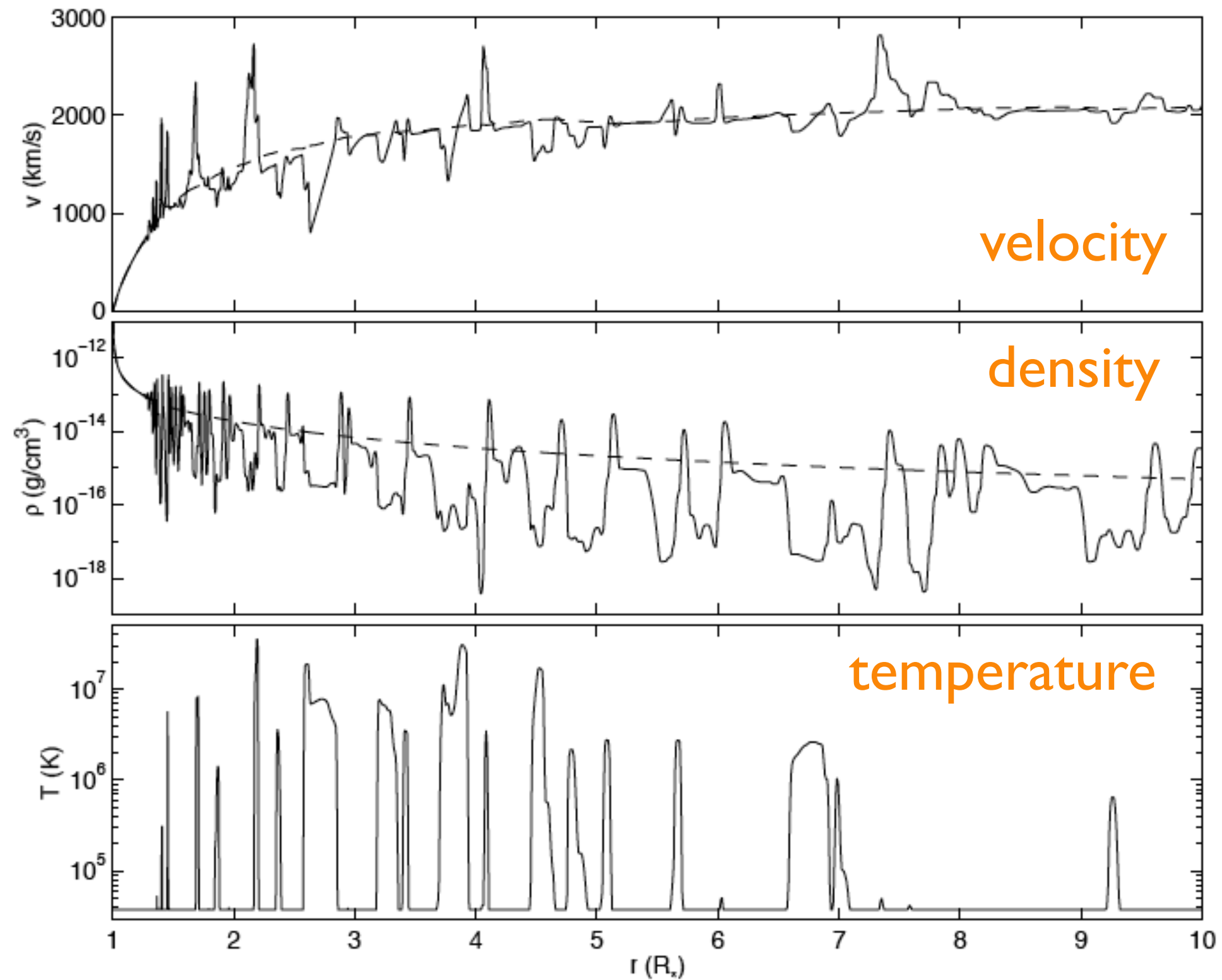
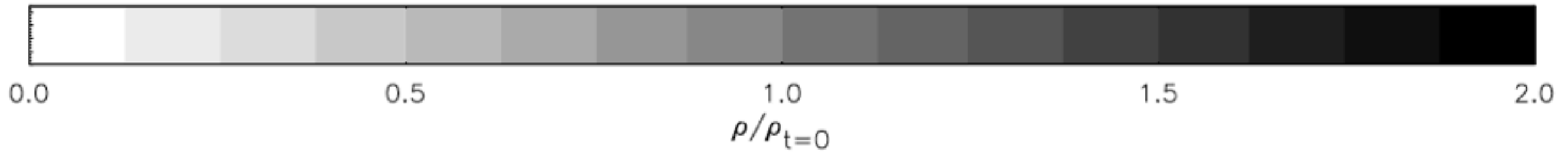
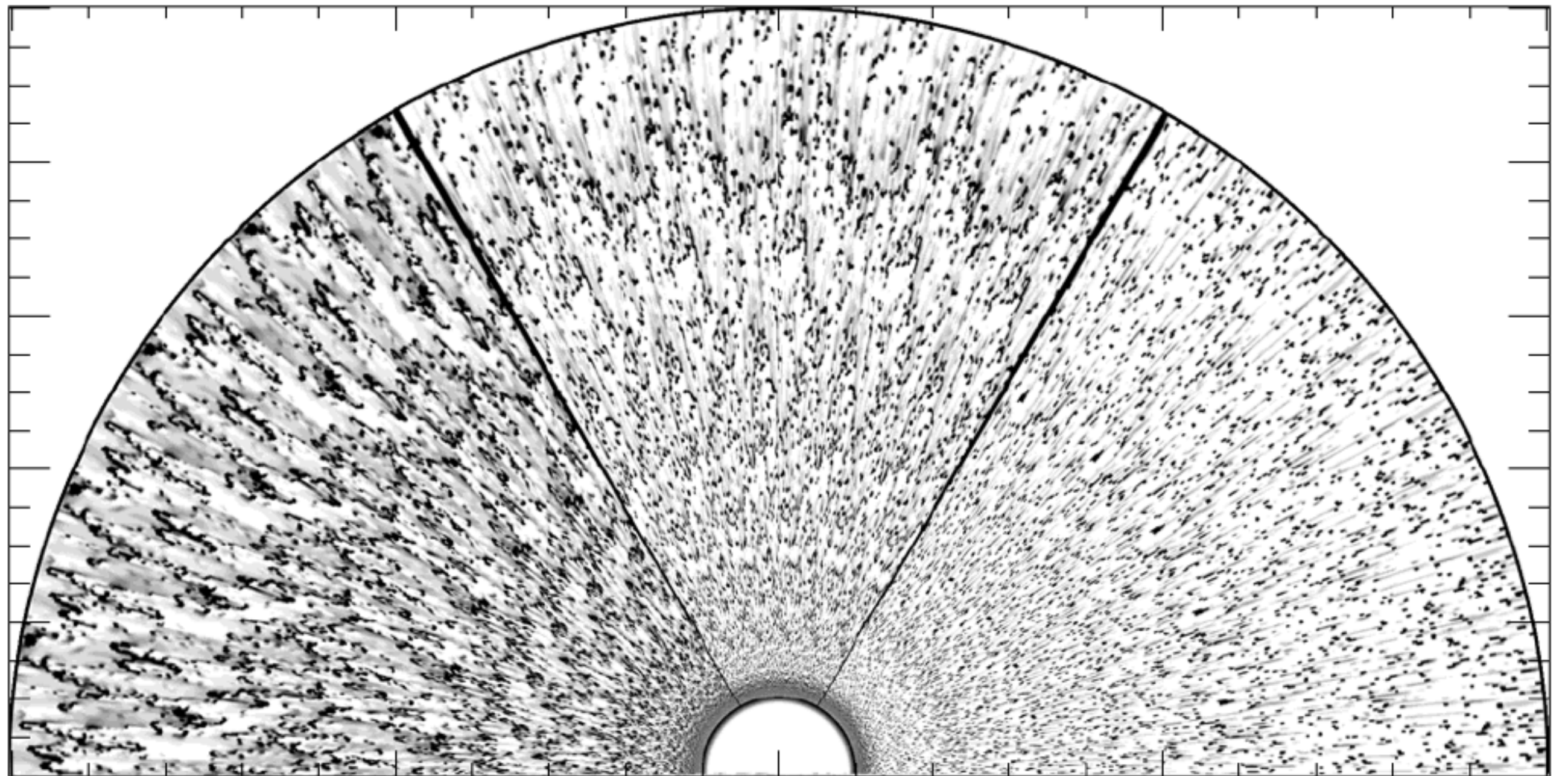


Fig. 8. Snapshot of the inner wind at 2.0 Msec after the start of the simulation, for the model with $\kappa_{\text{max}} = 10^{-2} \kappa_0$. The dashed line in the upper panels represents time-averaged values.

I-D is a severe limitation

lack of observed time variability suggests
numerous (> 100) individual post-shock cooling
volumes in the wind

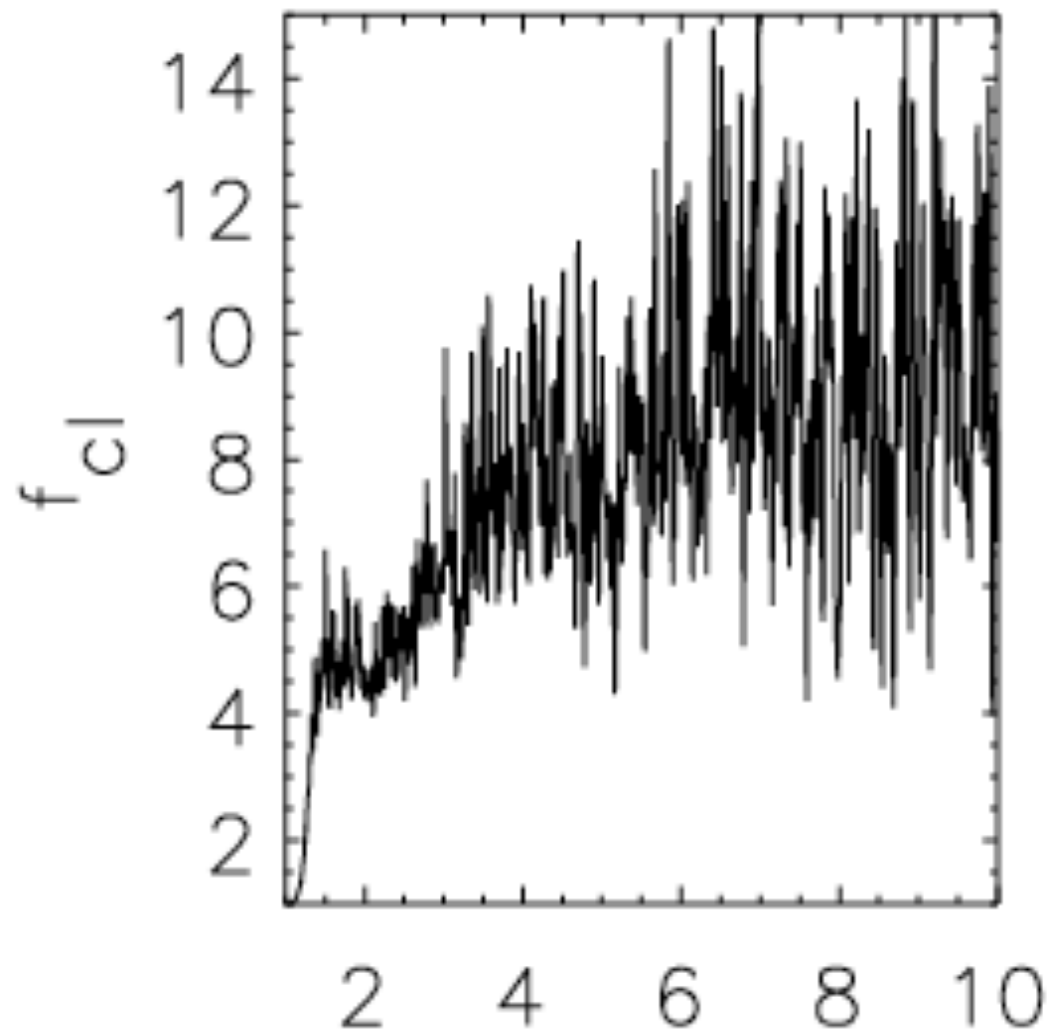
2-D simulations



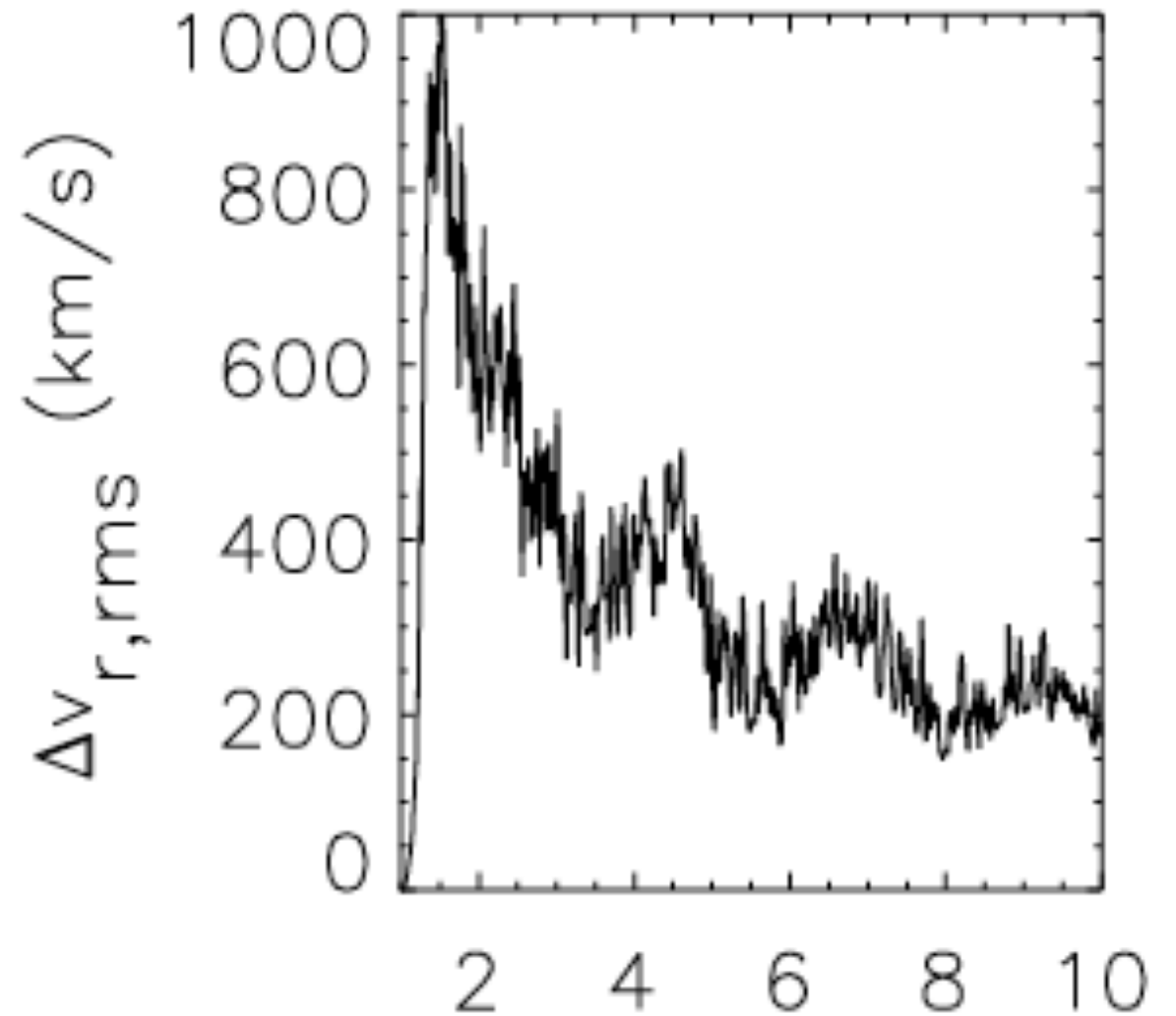
Statistics (time-average quantities) from 2-D simulations

clumping factor, f_{cl}

velocity dispersion, v_{rms}



height (R_{\star})



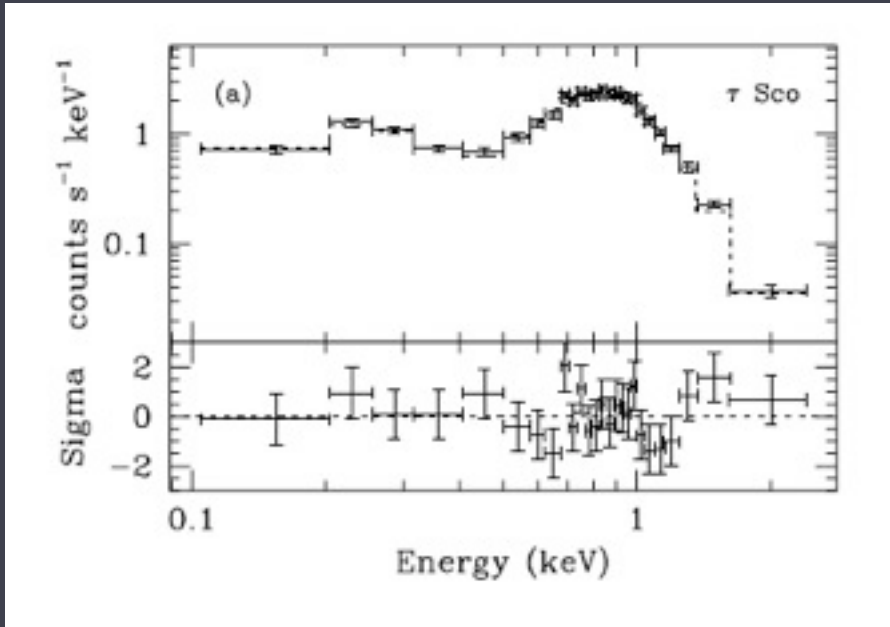
height (R_{\star})

Summary of hydro simulation results

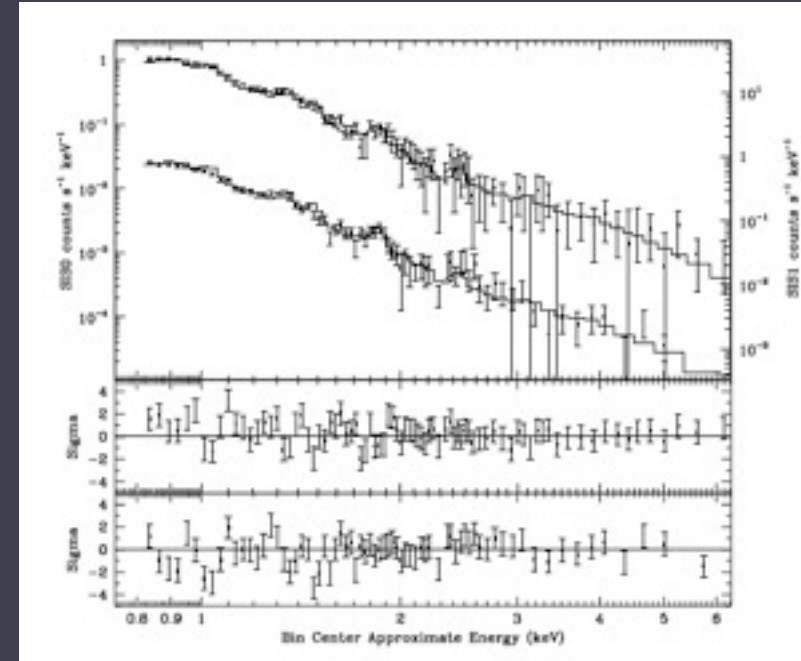
- line-deshadowing instability is robust
- seeding the instability with sound waves or turbulence at the base leads to clump-clump collisions & enhanced X-ray production
- small-scale clumping, with over-density of $f_{cl} \sim 10$
- shocks start producing hot plasma above $r \sim 1.5 R_{\star}$
thus the X-ray emitting plasma is at high velocity

now for some X-ray data...

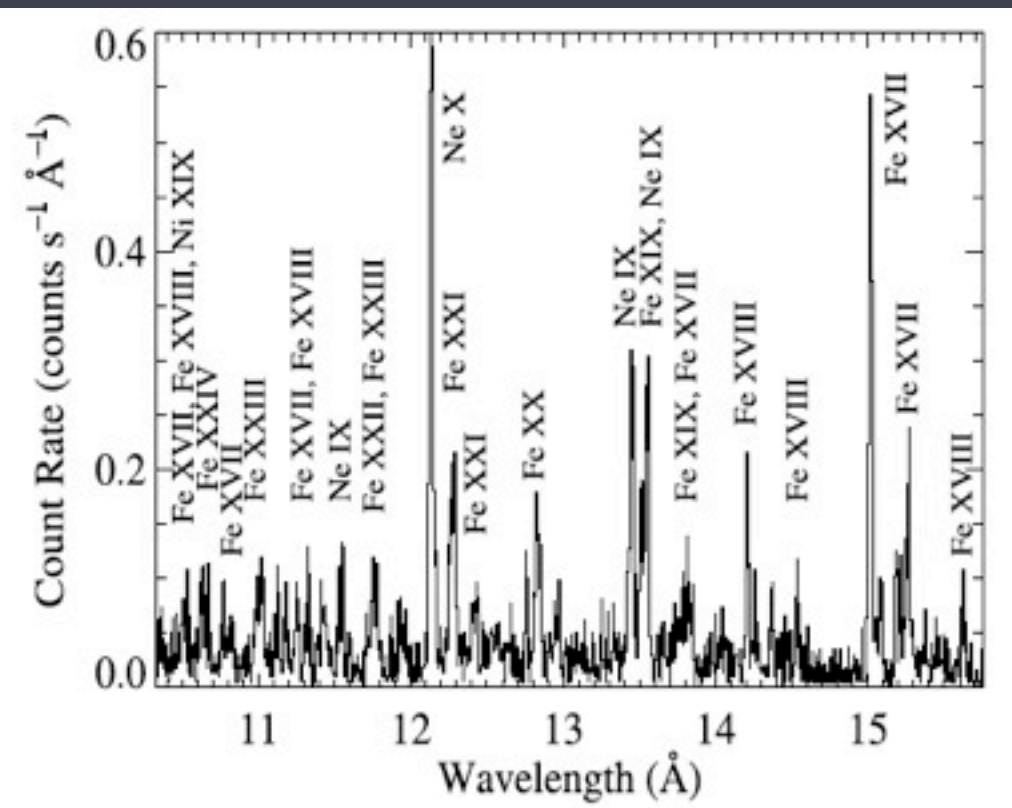
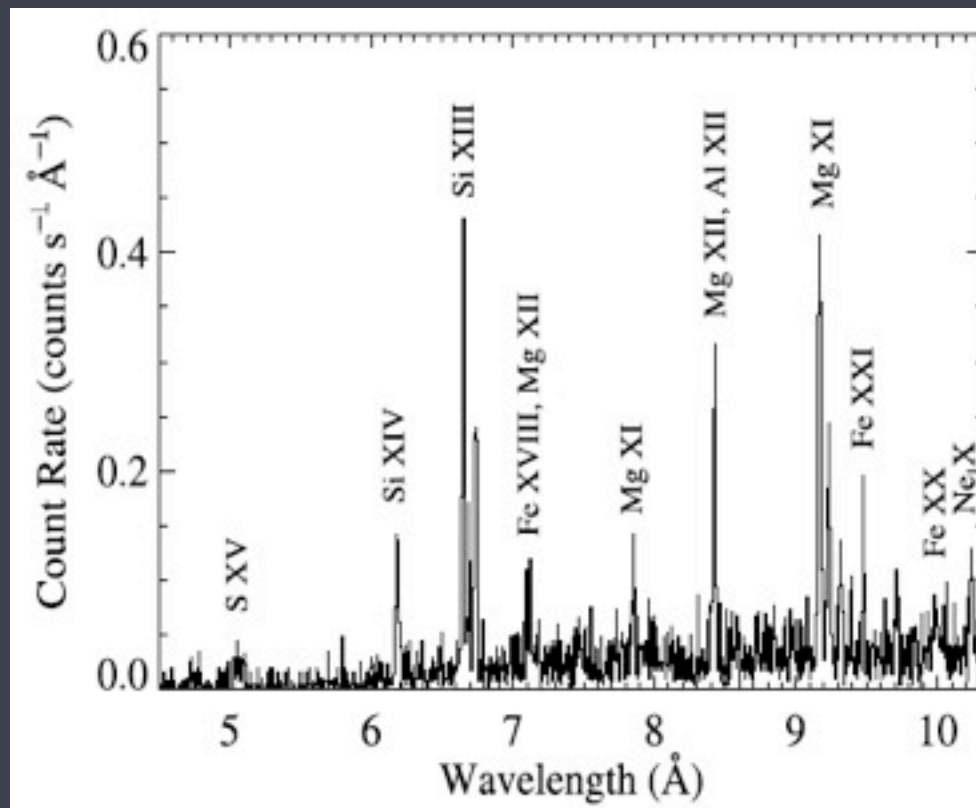
ROSAT 1991



ASCA 1994



Chandra 2001



Chandra

small effective area (poor sensitivity)
but very low background and very
well calibrated



X-ray imaging? > 0.5 arc sec, at best (100s of AU)
spectroscopy ($R < 1000$ corresp. > 300 km/s)

response to photons with $h\nu \sim 0.5$ keV up
to a few keV
(corresp. $\sim 5\text{\AA}$ to 24\AA)

X-ray Spectral Formation

Thermal emission

Equilibrium

Optically thin

X-ray Spectral Formation

like the solar corona

low density

Thermal emission

Equilibrium

Optically thin

collisions up, spontaneous down;
nearly all bound electrons in the
ground state;

“coronal approximation”
⇒ emission line dominated

X-ray Spectral Formation

like the solar corona

low density

Thermal emission

Equilibrium

Optically thin

steady-state; Maxwellian, $T_i = T_e$;
ionization: collisional from ground
state = recombination

X-ray Spectral Formation

like the solar corona

low density

Thermal emission

Equilibrium

Optically thin

some strong lines may show optical depth effects (2nd order effect on spectra);
But, cold wind component can be optically thick to X-rays produced in the hot component

X-ray Spectral Formation

plasma with $T > 10^6$ K radiates X-rays ($h\nu > 100$ eV)

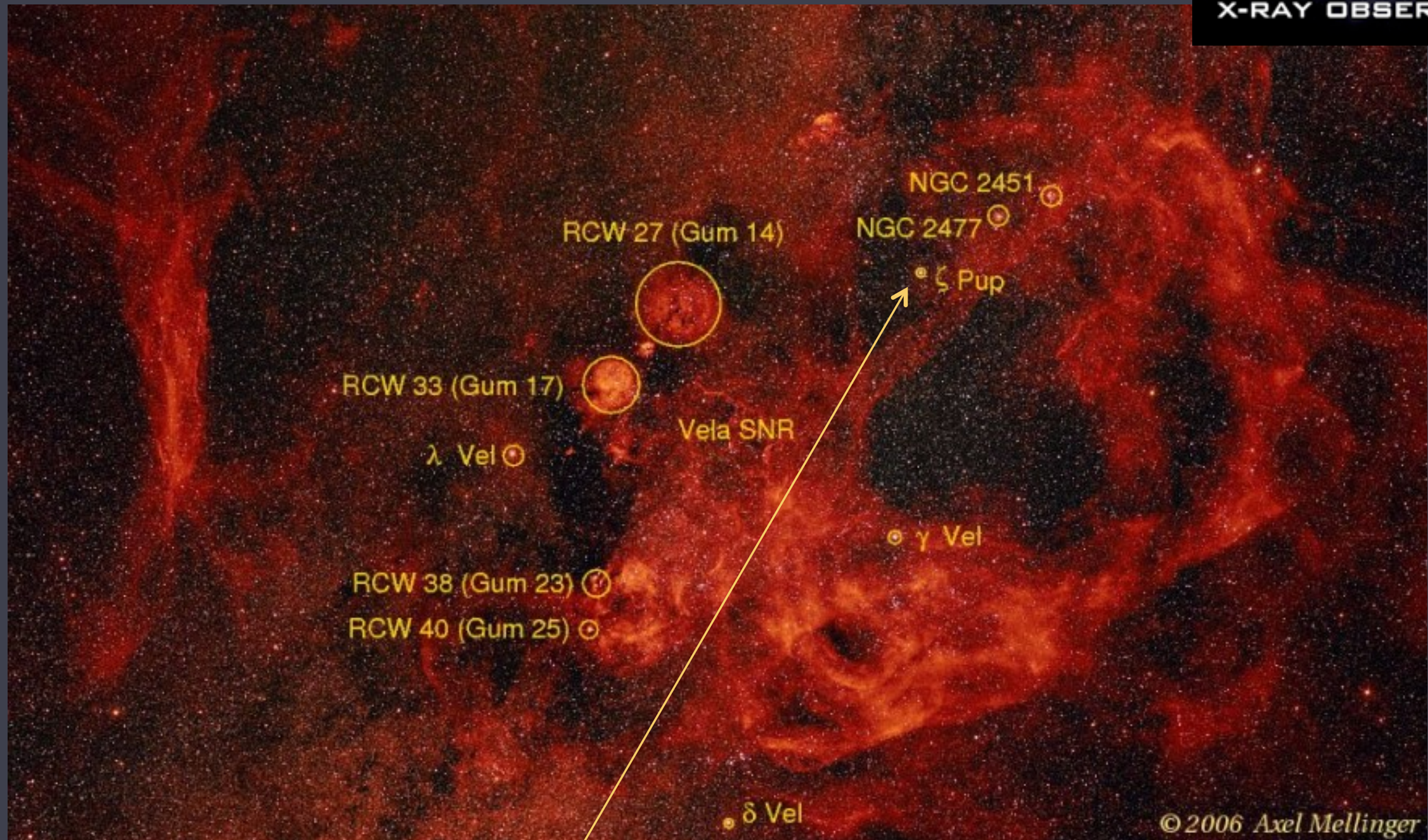
shocks heat plasma to $T \sim 10^6$ K

if $\Delta V_{\text{shock}} \sim 300$ km/s

and $T \sim (\Delta V_{\text{shock}})^2$

Chandra grating spectroscopy ($R < 1000$)

ζ Pup (O4 If)



© 2006 Axel Mellinger

cool stars

vs.

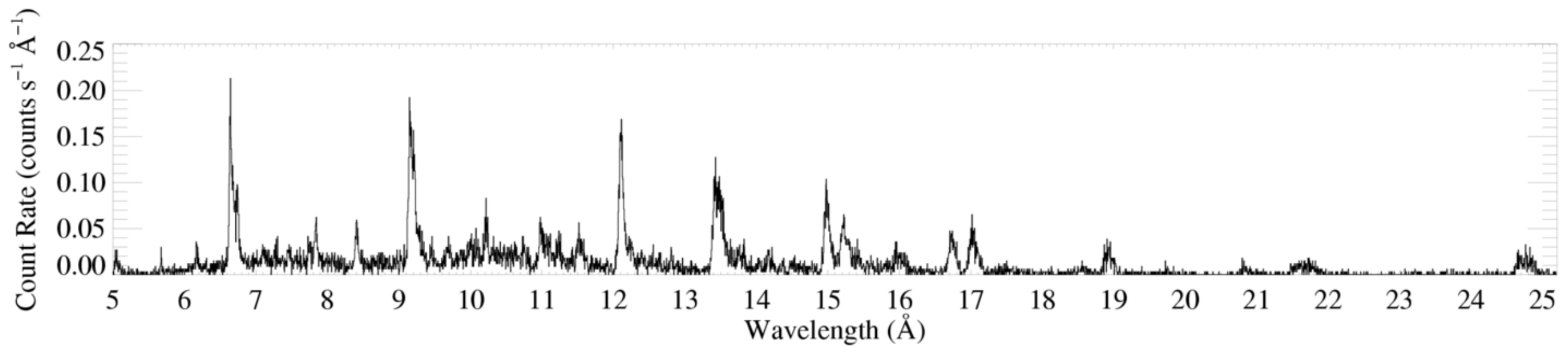
hot stars



starfish, *in situ*, at the Monterey (California) Aquarium

Chandra grating (HETGS/MEG) spectra

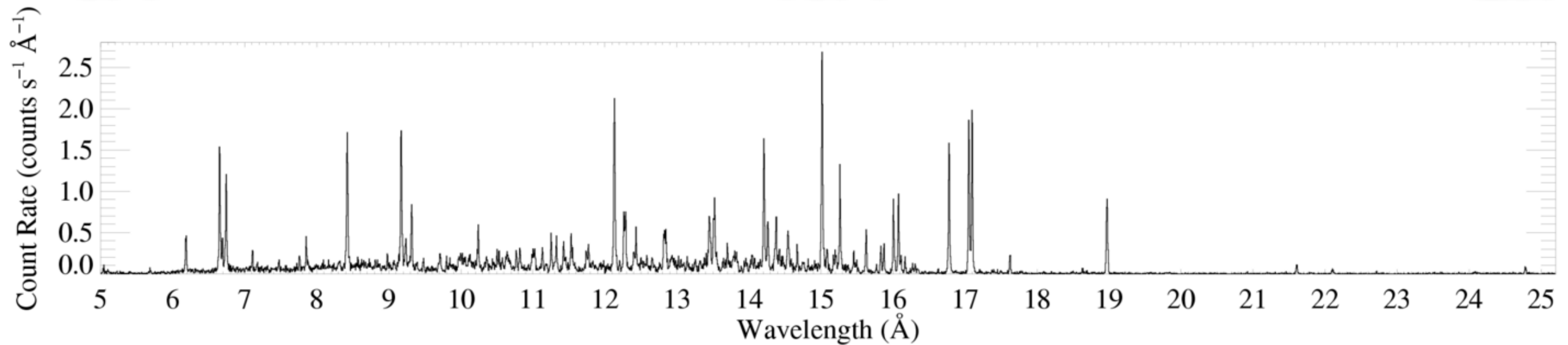
ζ Pup (O4 If)



5Å

15Å

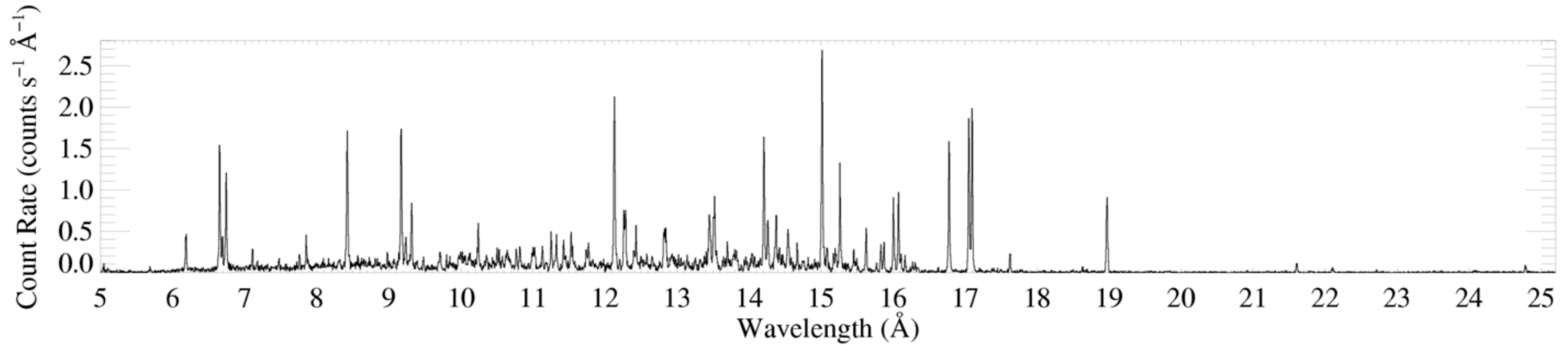
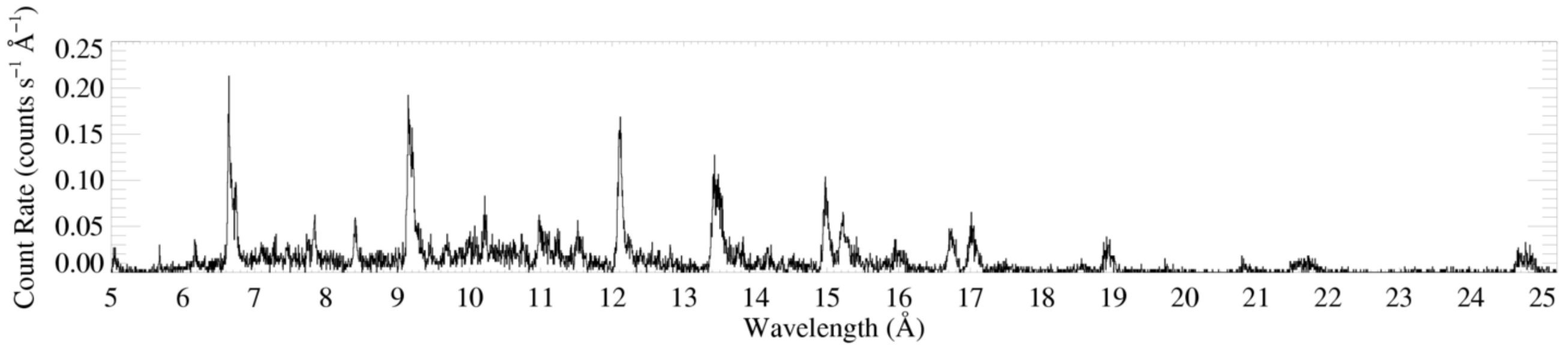
25Å



Capella (G5 III)

emission lines + bremsstrahlung + recombination

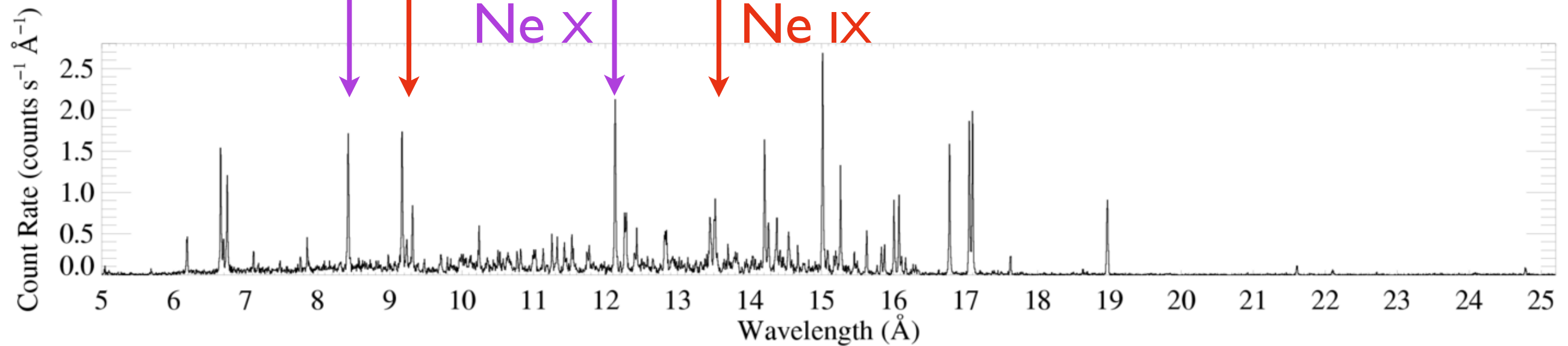
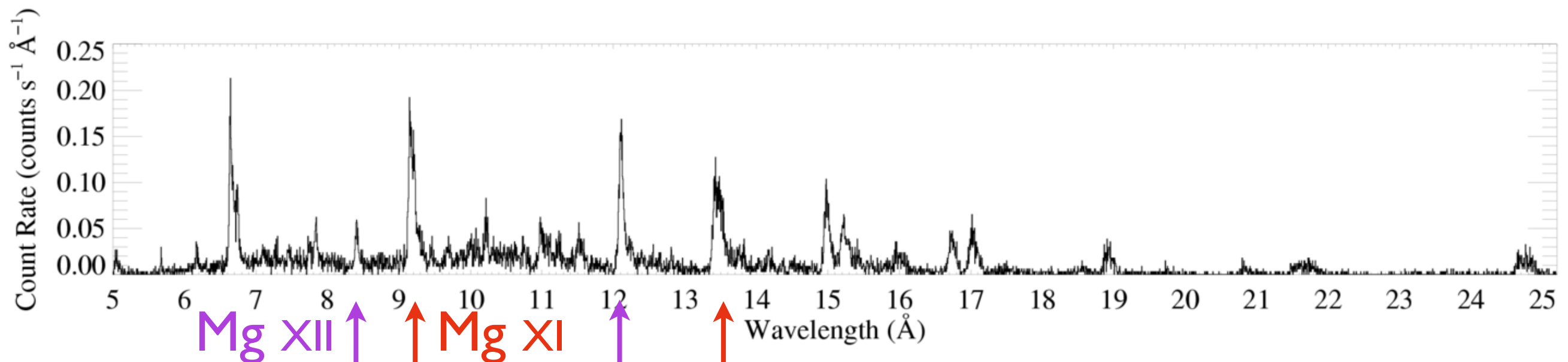
ζ Pup (O4 If)



Capella (G5 III)

Chandra grating (HETGS/MEG) spectra

ζ Pup (O4 If)

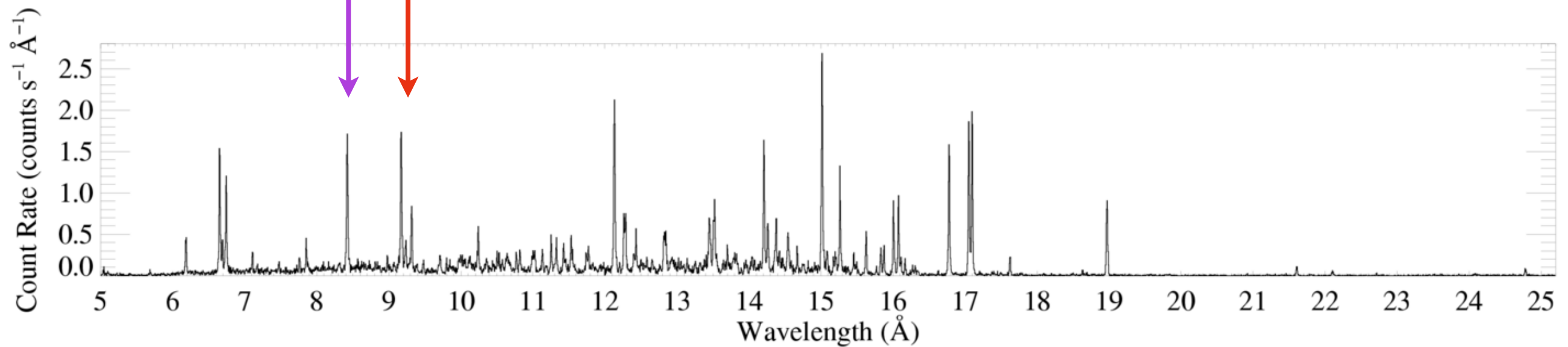
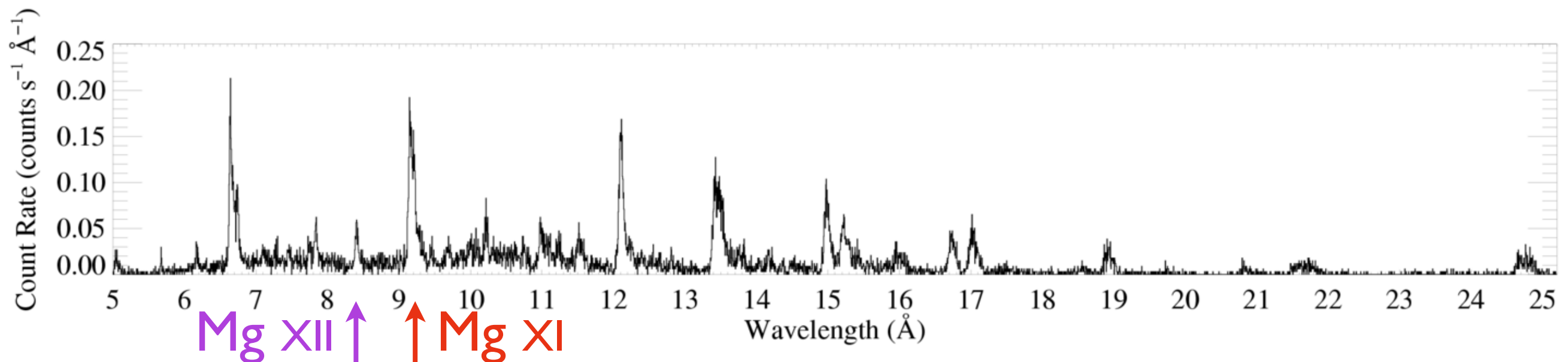


Capella (G5 III)

typical temperatures $T \sim \text{few } 10^6 \text{ K}$

(late-type stellar coronae tend to be hotter)

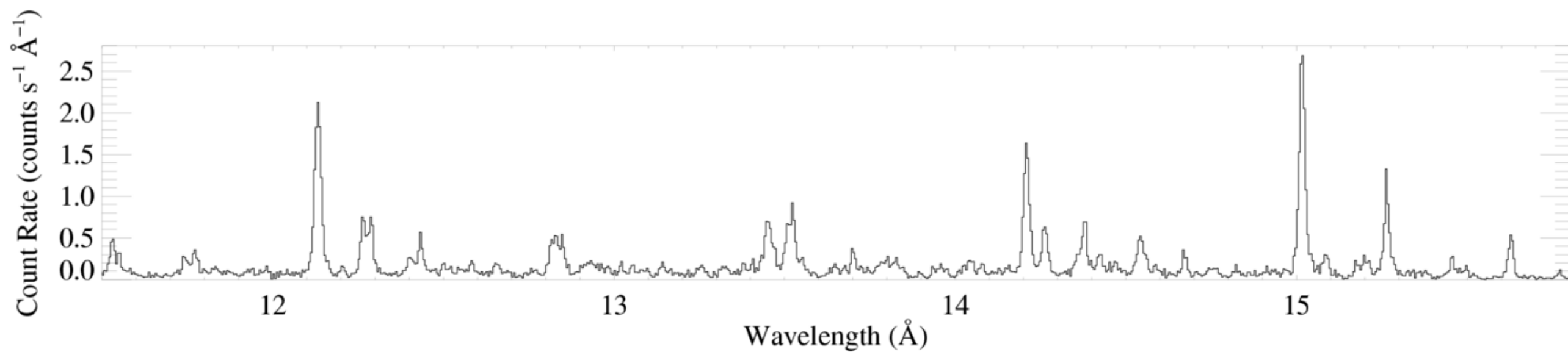
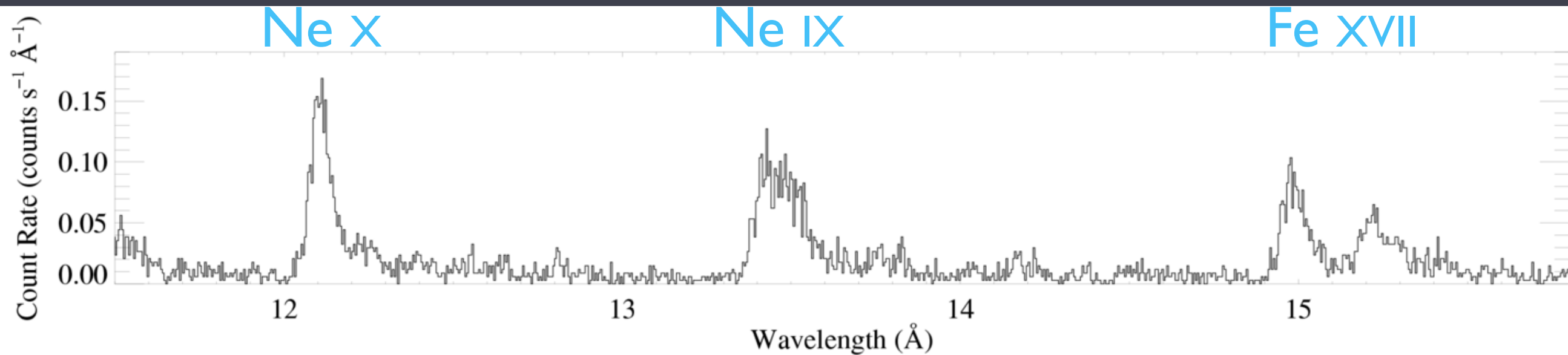
ζ Pup (O4 If)



Capella (G5 III)

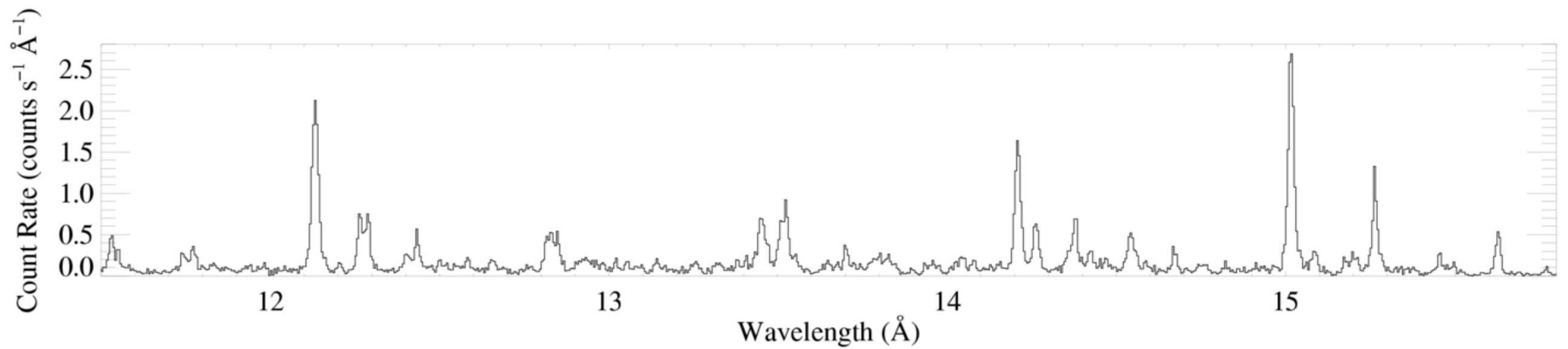
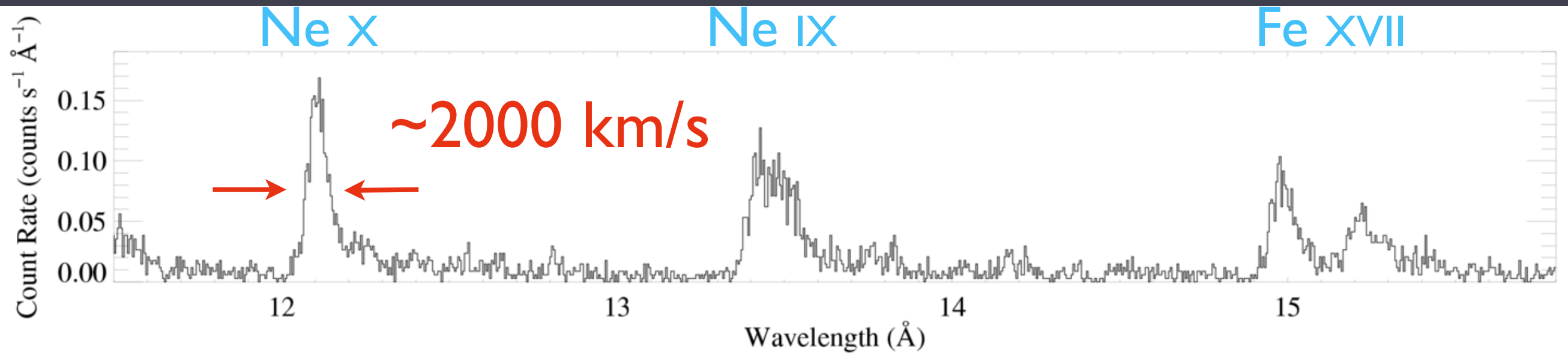
Zoom in

ζ Pup (O4 If)



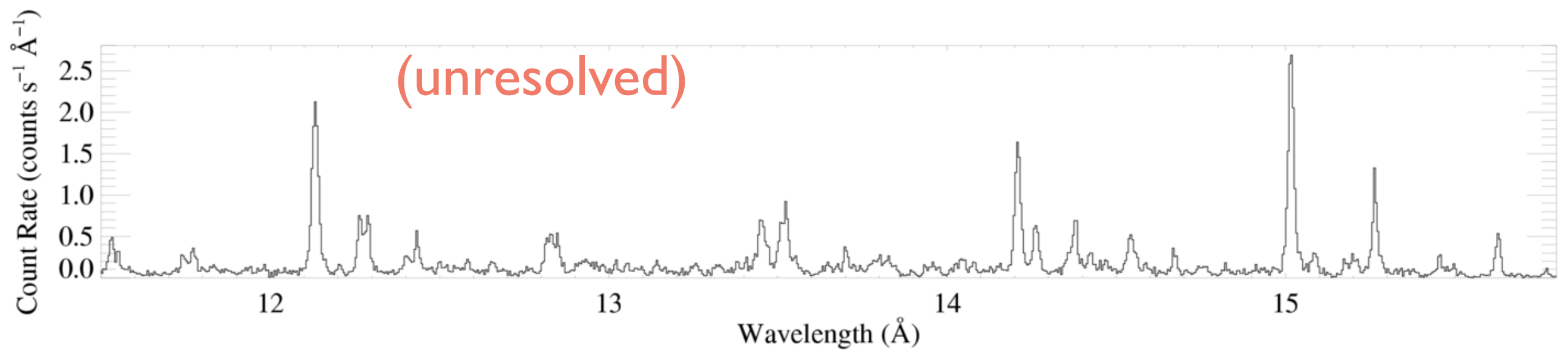
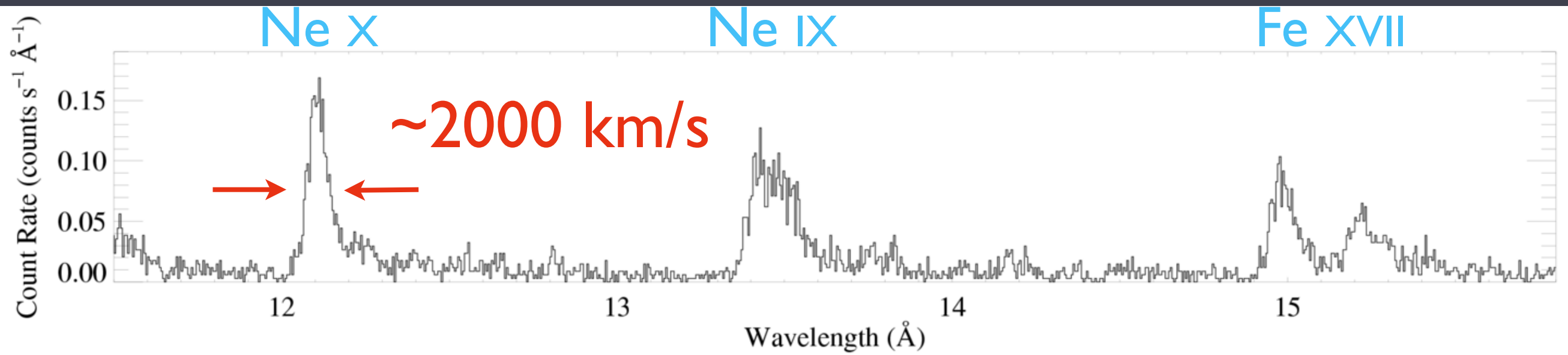
Capella (G5 III)

ζ Pup (O4 If)



Capella (G5 III)

ζ Pup (O4 If)



Capella (G5 III)

cool stars: narrow lines =
magnetically confined
coronal plasma

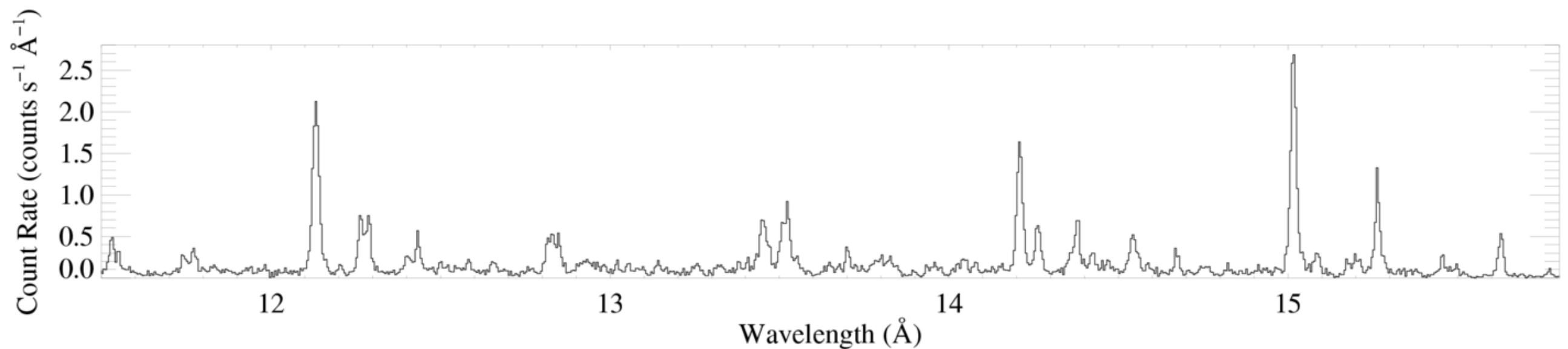
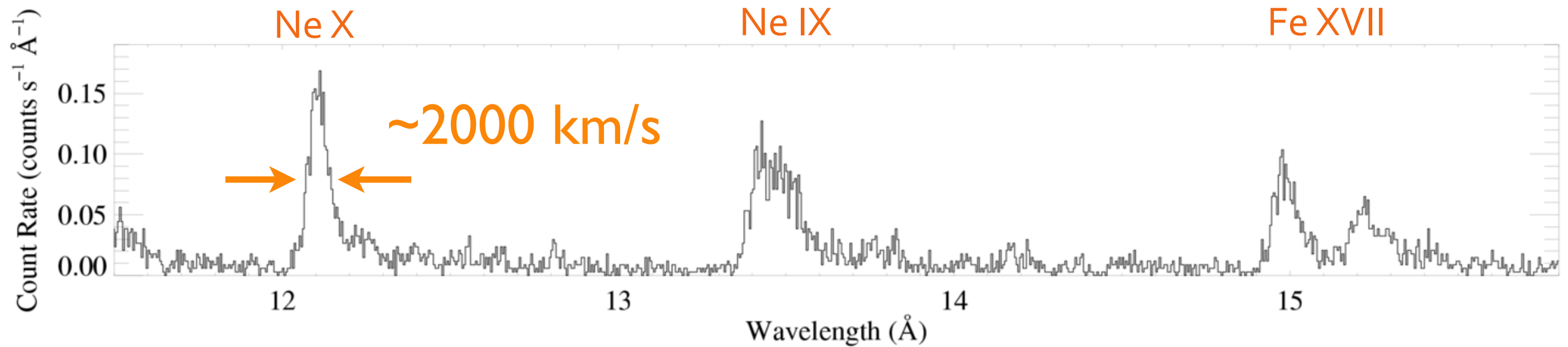
hot stars: broad lines =
outflowing, shock-heated
wind plasma



○ supergiant X-ray emission lines are **broad**

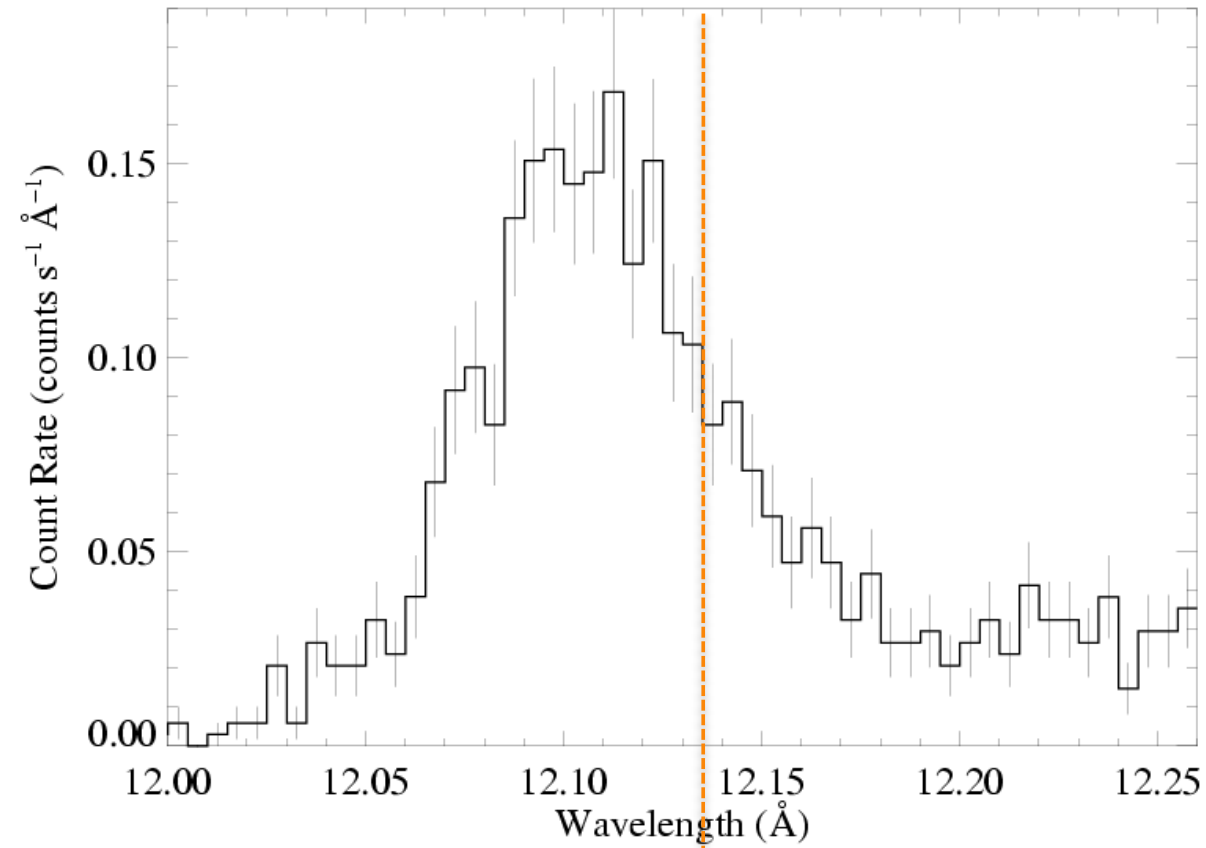
Chandra grating spectrum

ζ Pup (O4If)

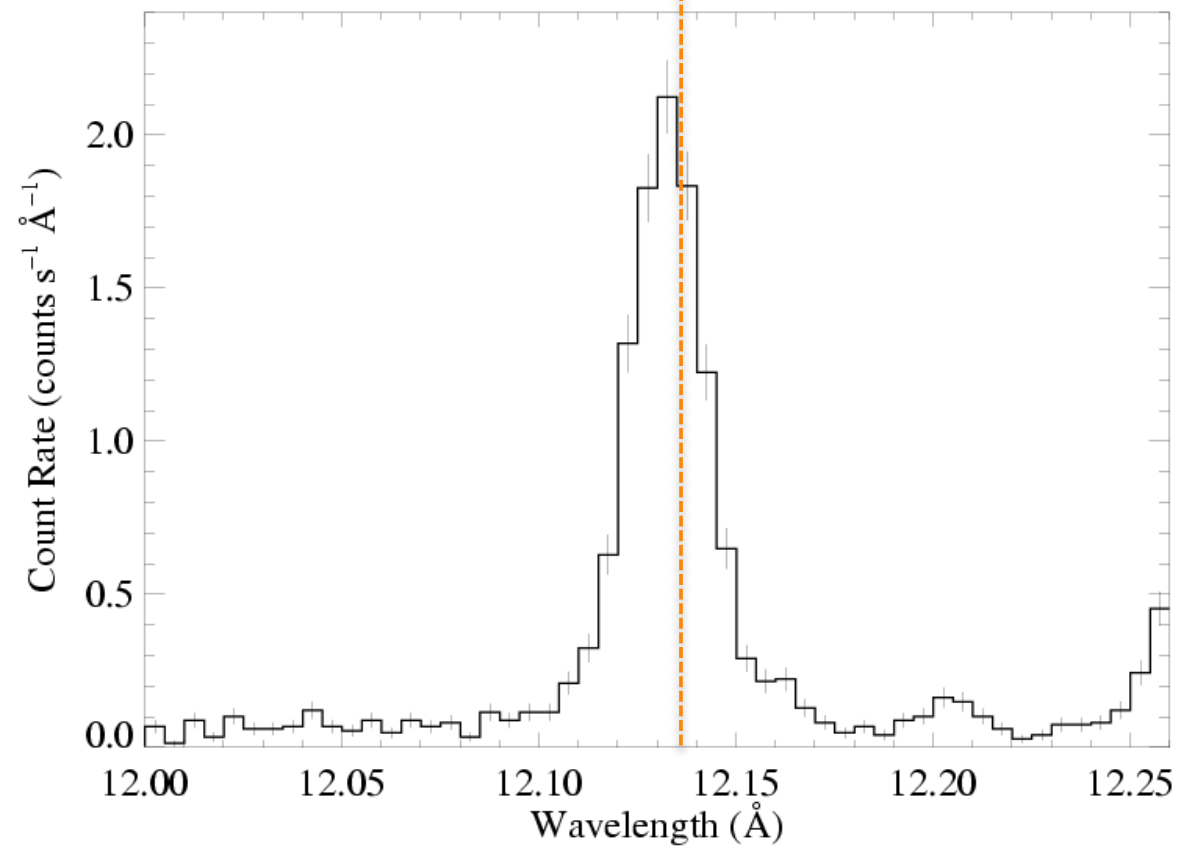


Capella: G star for comparison (narrow lines)

lines are
asymmetric

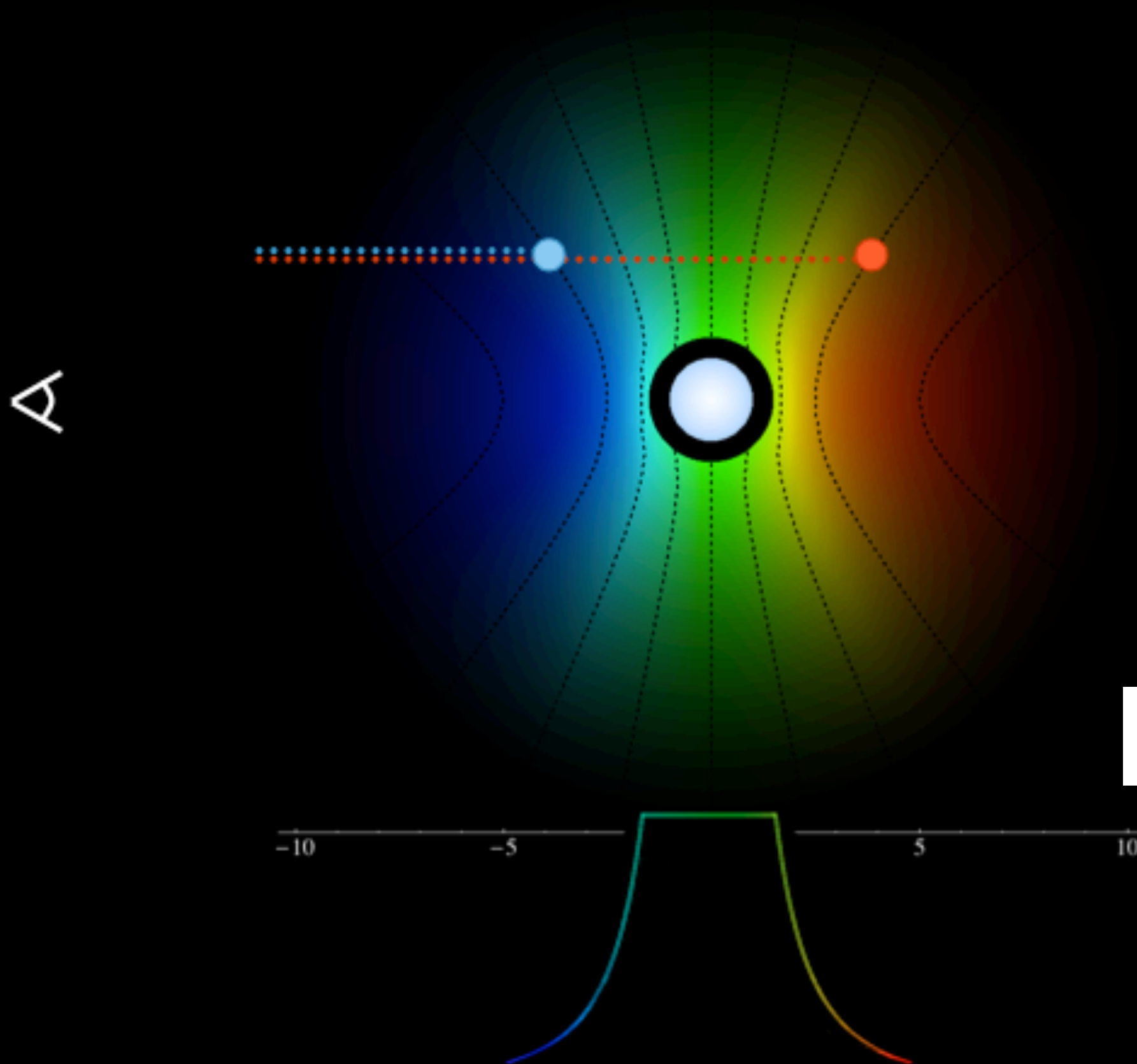


ζ Pup (O4If)

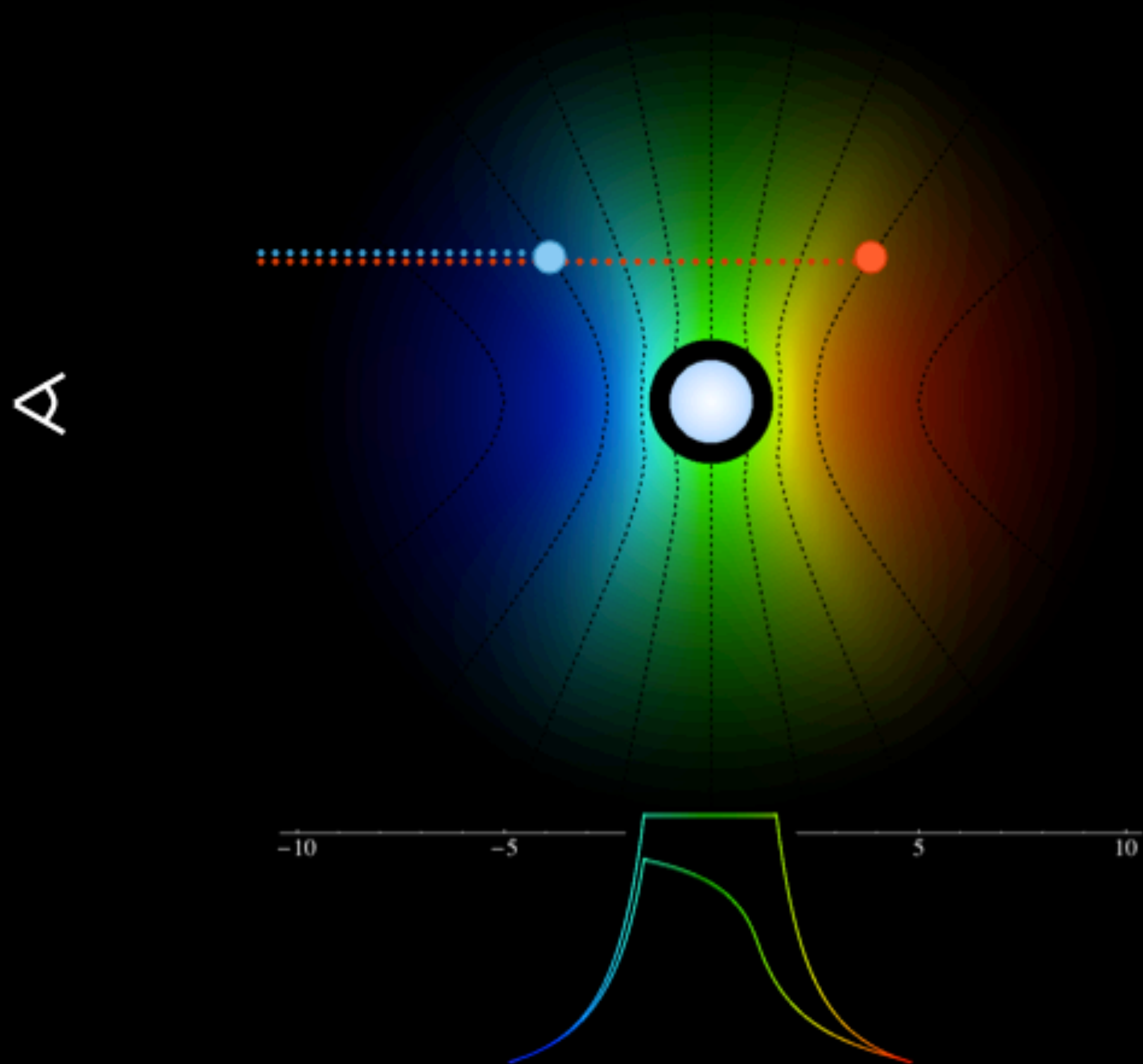


Capella (G5 III)

Line Asymmetry



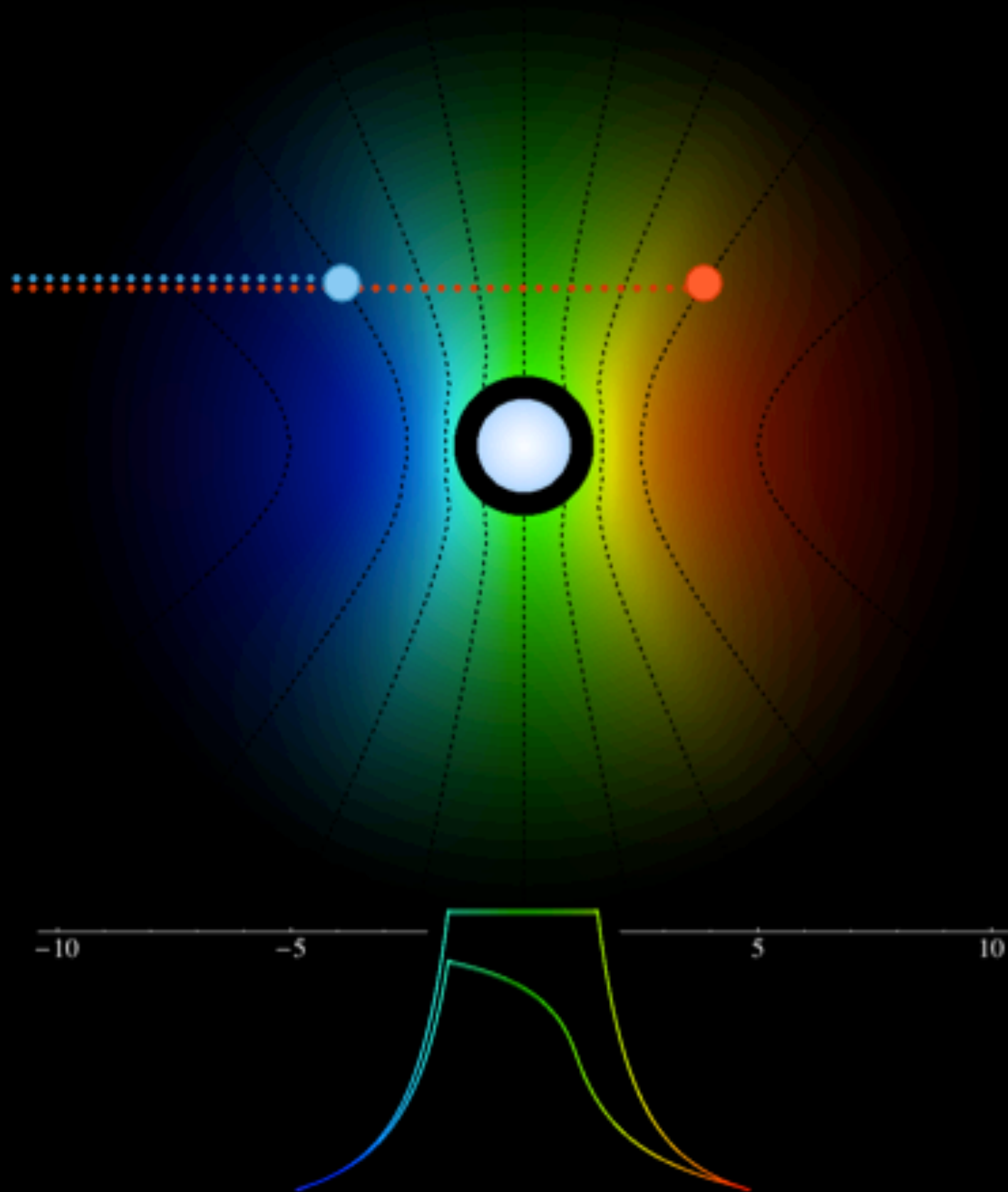
Line Asymmetry



Line Asymmetry

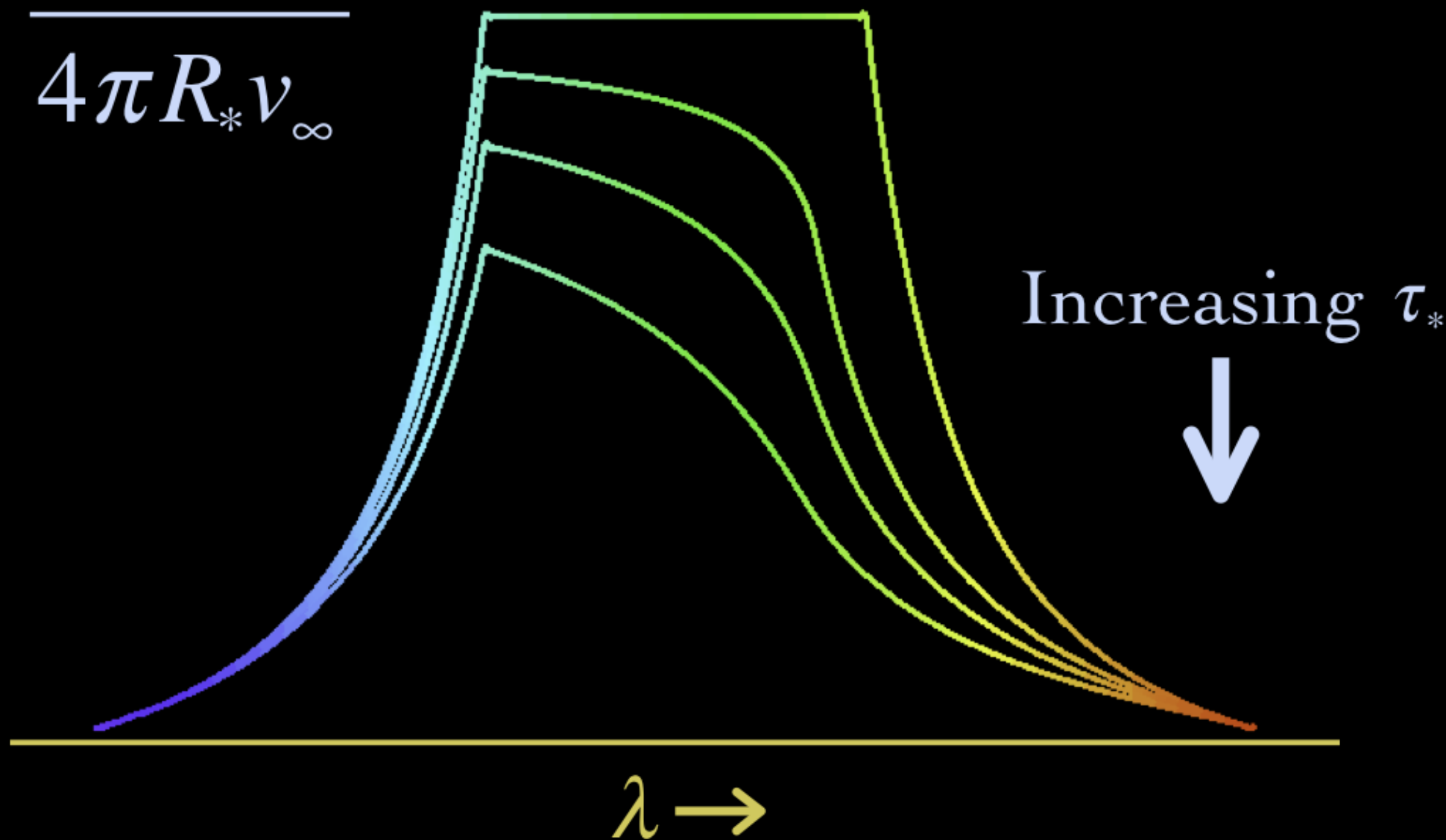
$$\tau = \tau_* \int_z^\infty \frac{R_* dz'}{r'^2 (1 - R_*/r')^\beta}$$

A

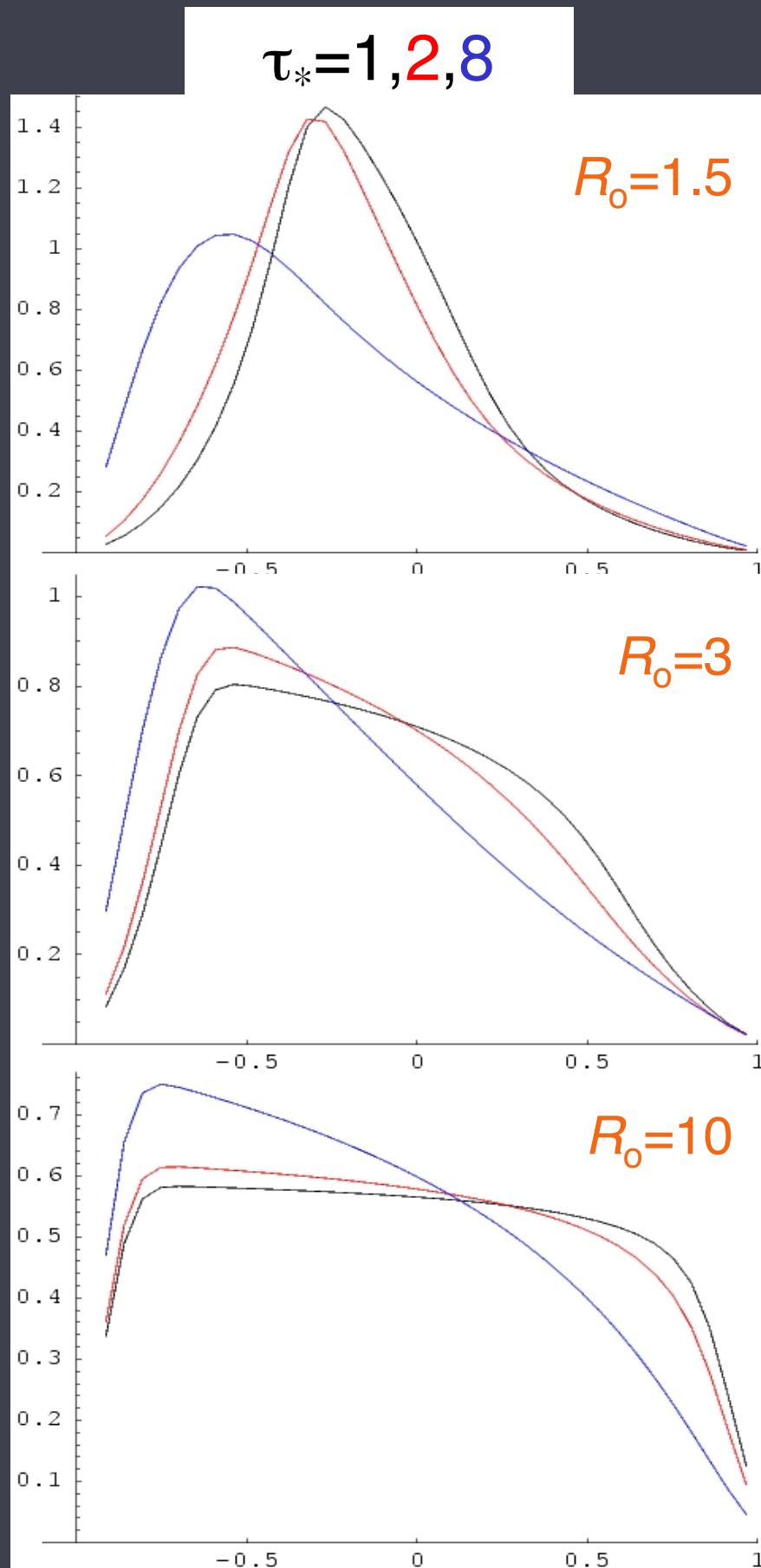
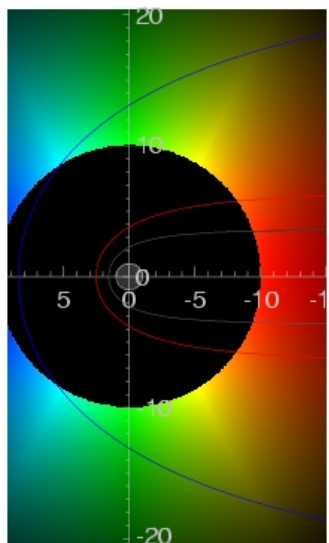
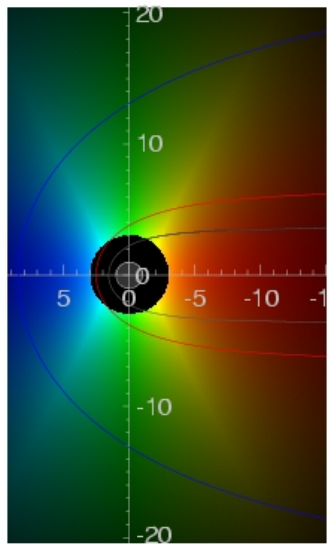
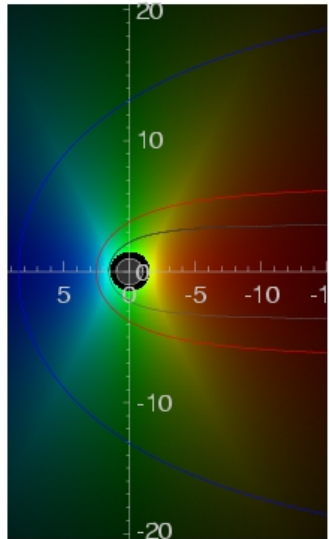


Wind Profile Model

$$\tau_* = \frac{\kappa \dot{M}}{4\pi R_* v_\infty}$$



Line profile shapes



key parameters: R_0 & τ_*

$$v = v_\infty (1 - r/R_*)^\beta$$

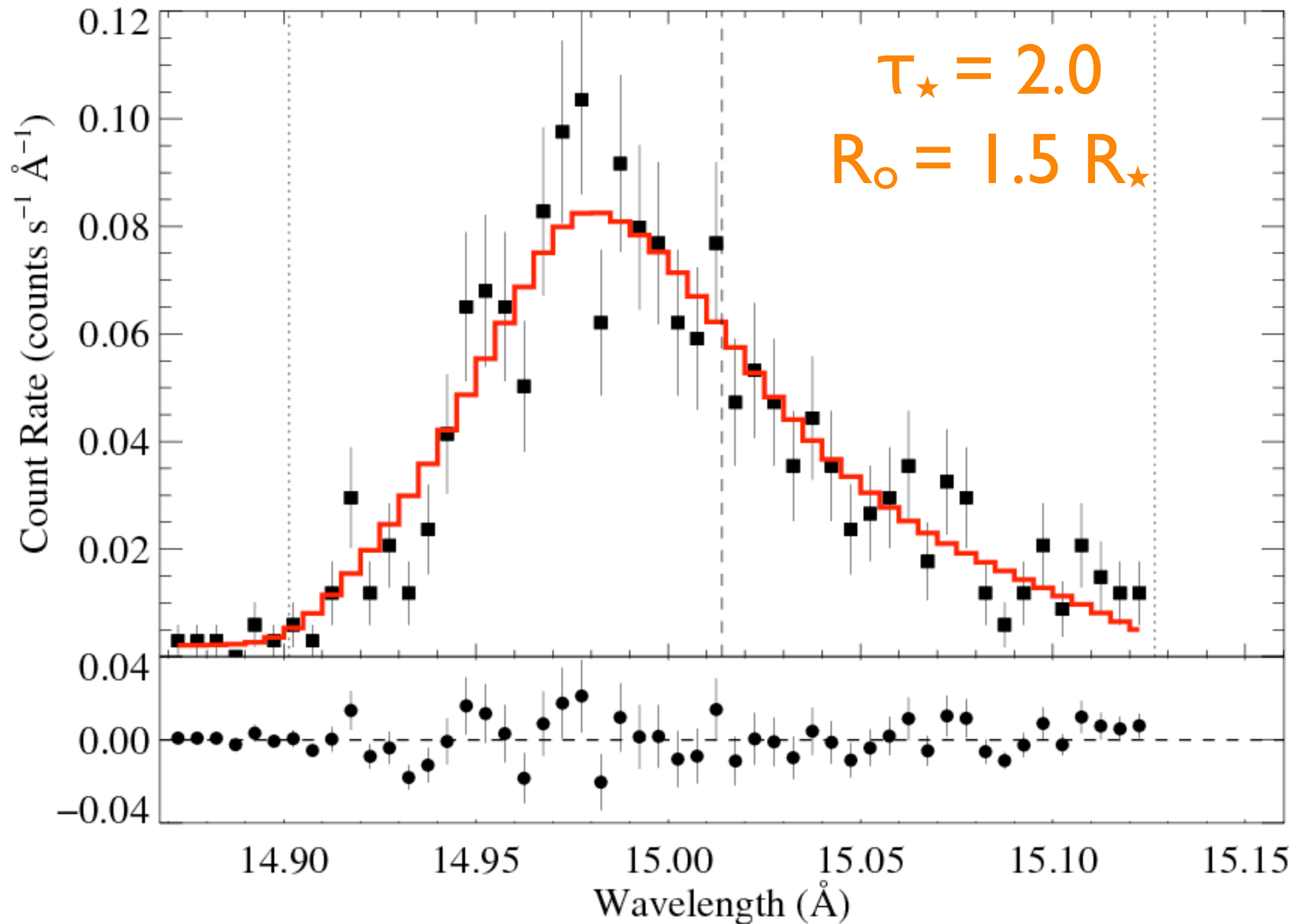
$$j \sim \rho^2 \text{ for } r/R_* > R_0, \\ = 0 \text{ otherwise}$$

$$\tau = \tau_* \int_z^\infty \frac{R_* dz'}{r'^2 (1 - R_*/r')^\beta}$$

$$\tau_* \equiv \frac{\kappa \dot{M}}{4\pi R_* v_\infty}$$

ζ Pup: *Chandra* MEG

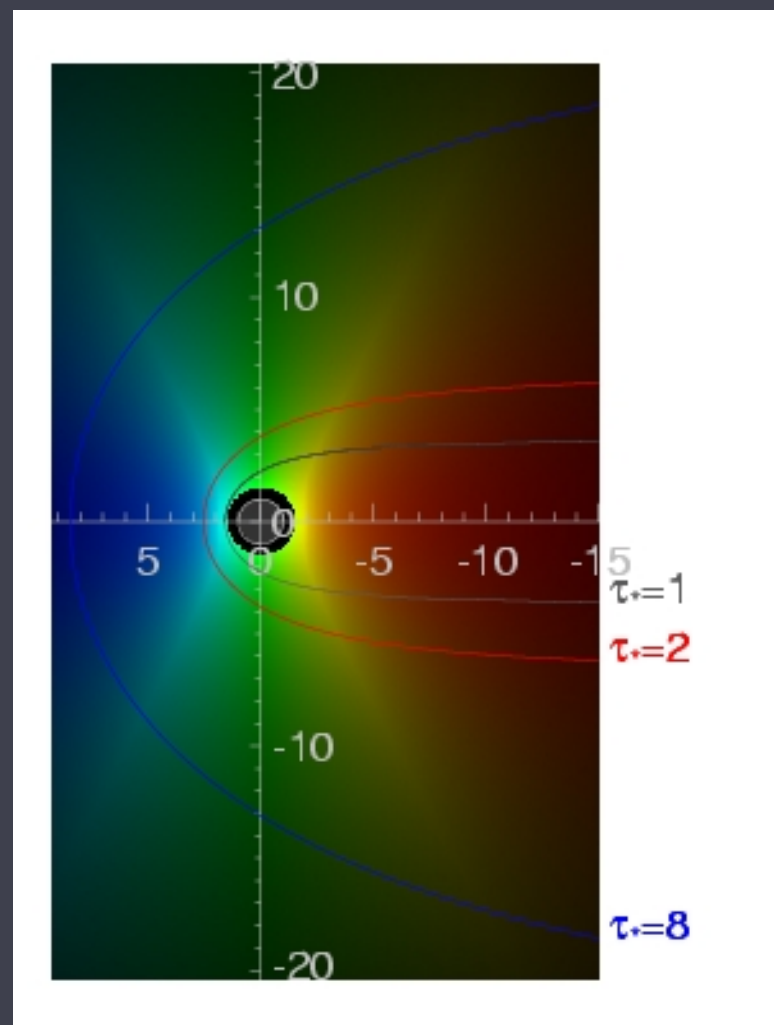
Fe XVII



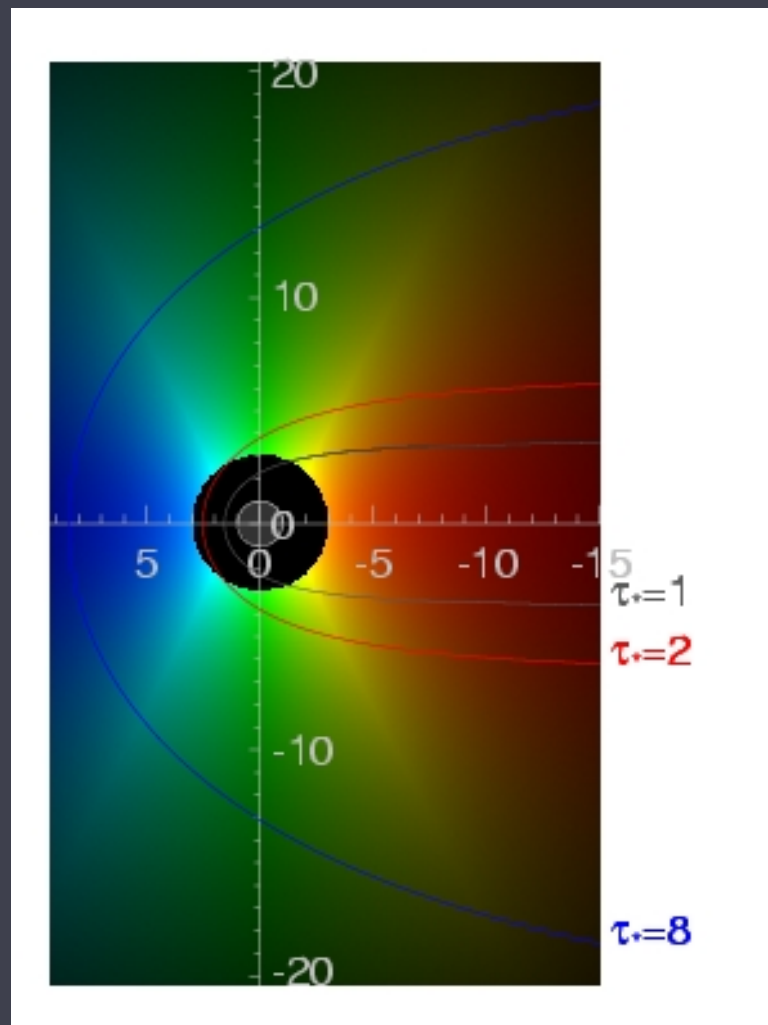
Hot plasma kinematics and location

R_o controls the line width via $v(r)$

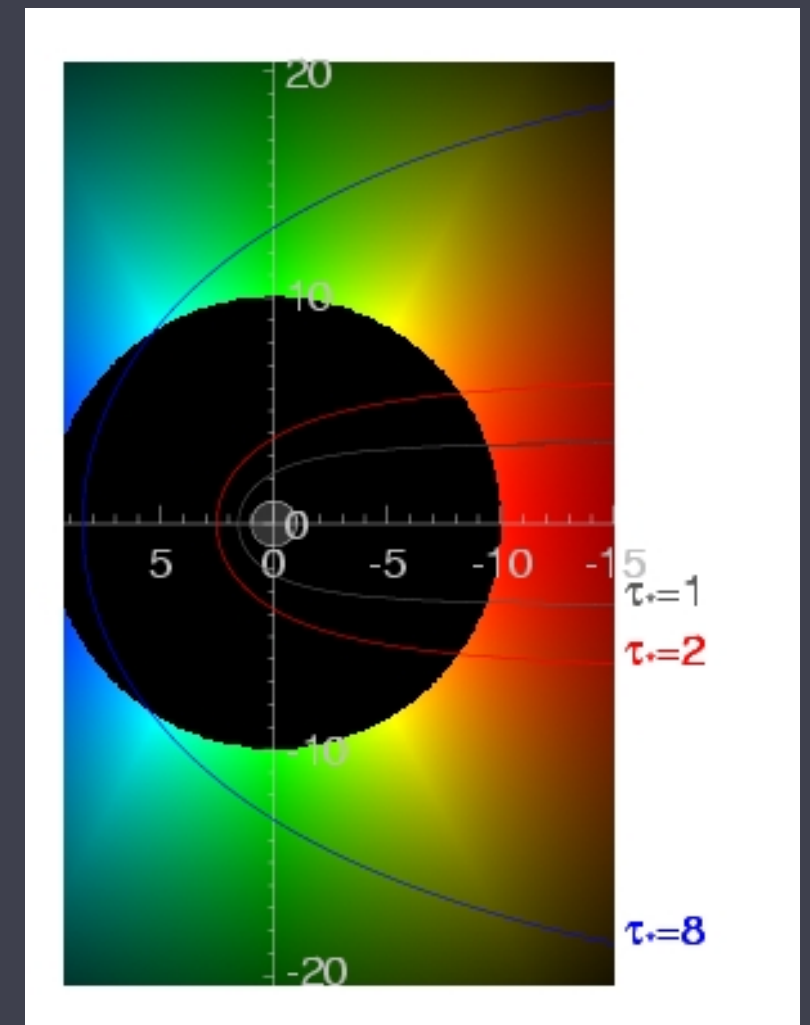
$R_o = 1.5 R_\star$



$R_o = 3 R_\star$

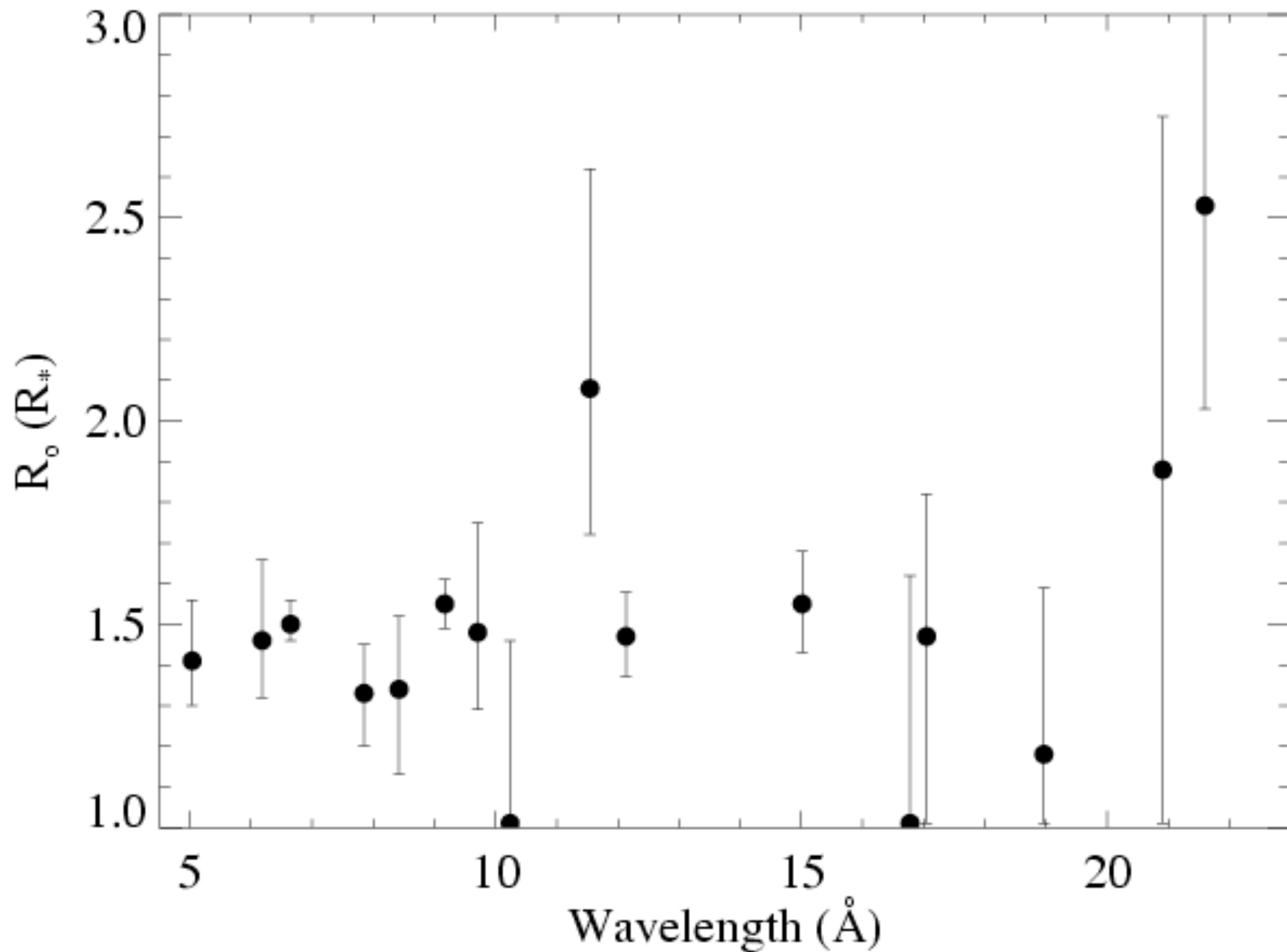


$R_o = 10 R_\star$

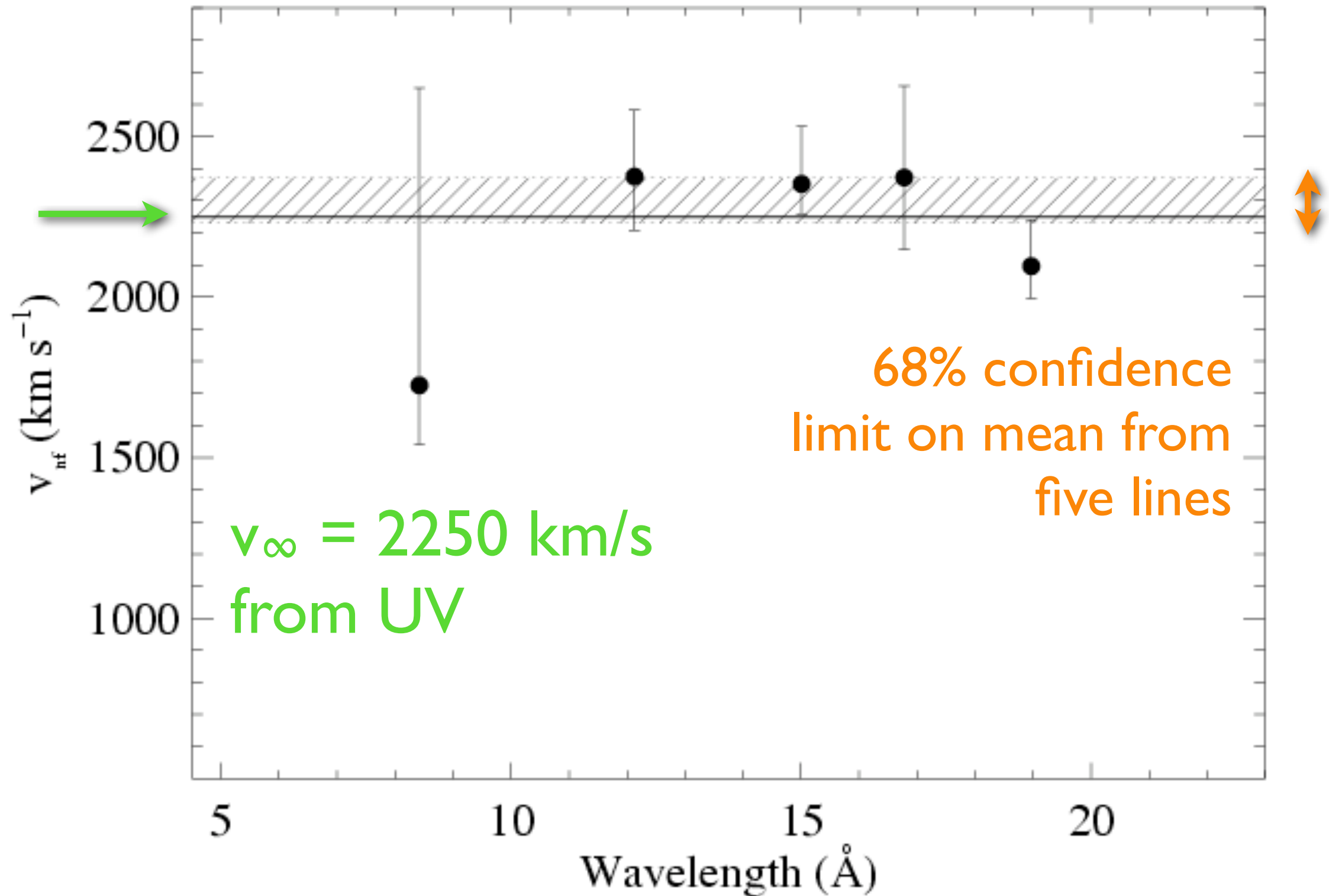


Distribution of R_o values for ζ Pup

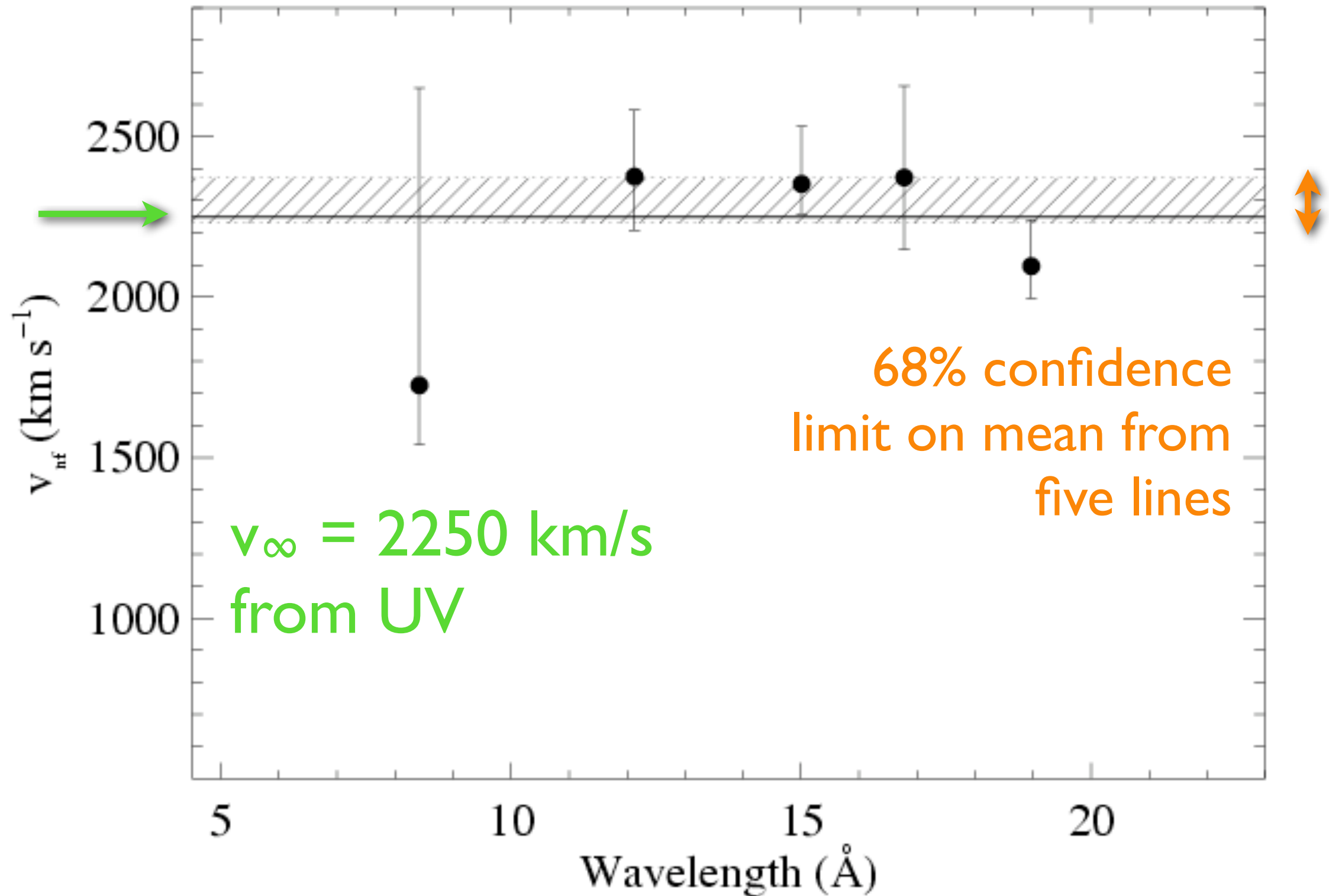
consistent with a global value of $R_o = 1.5 R_\star$



v_∞ can be constrained by the line fitting too



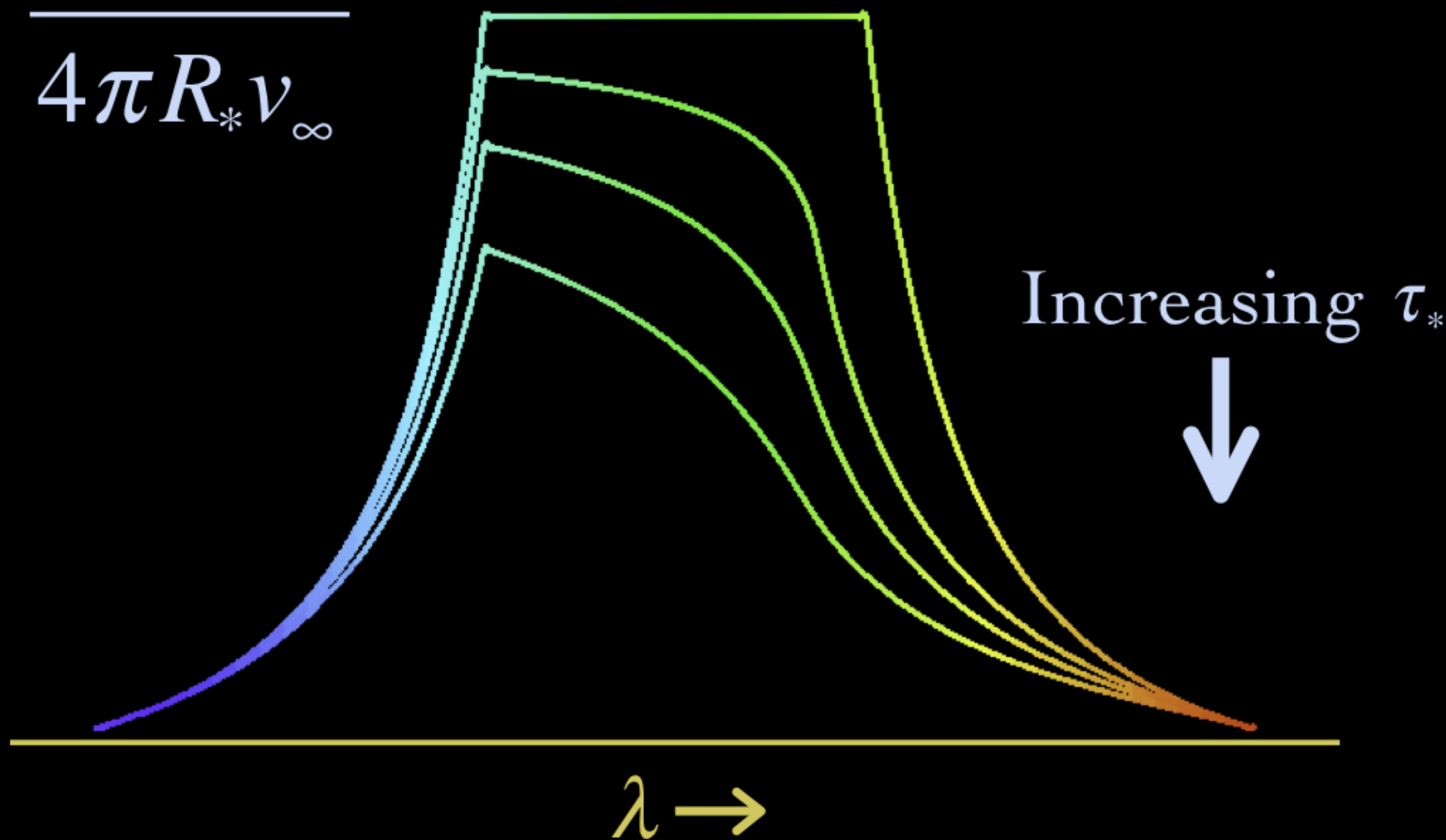
X-ray plasma and mean wind have same kinematics



The profiles also tell us about the level of
wind absorption

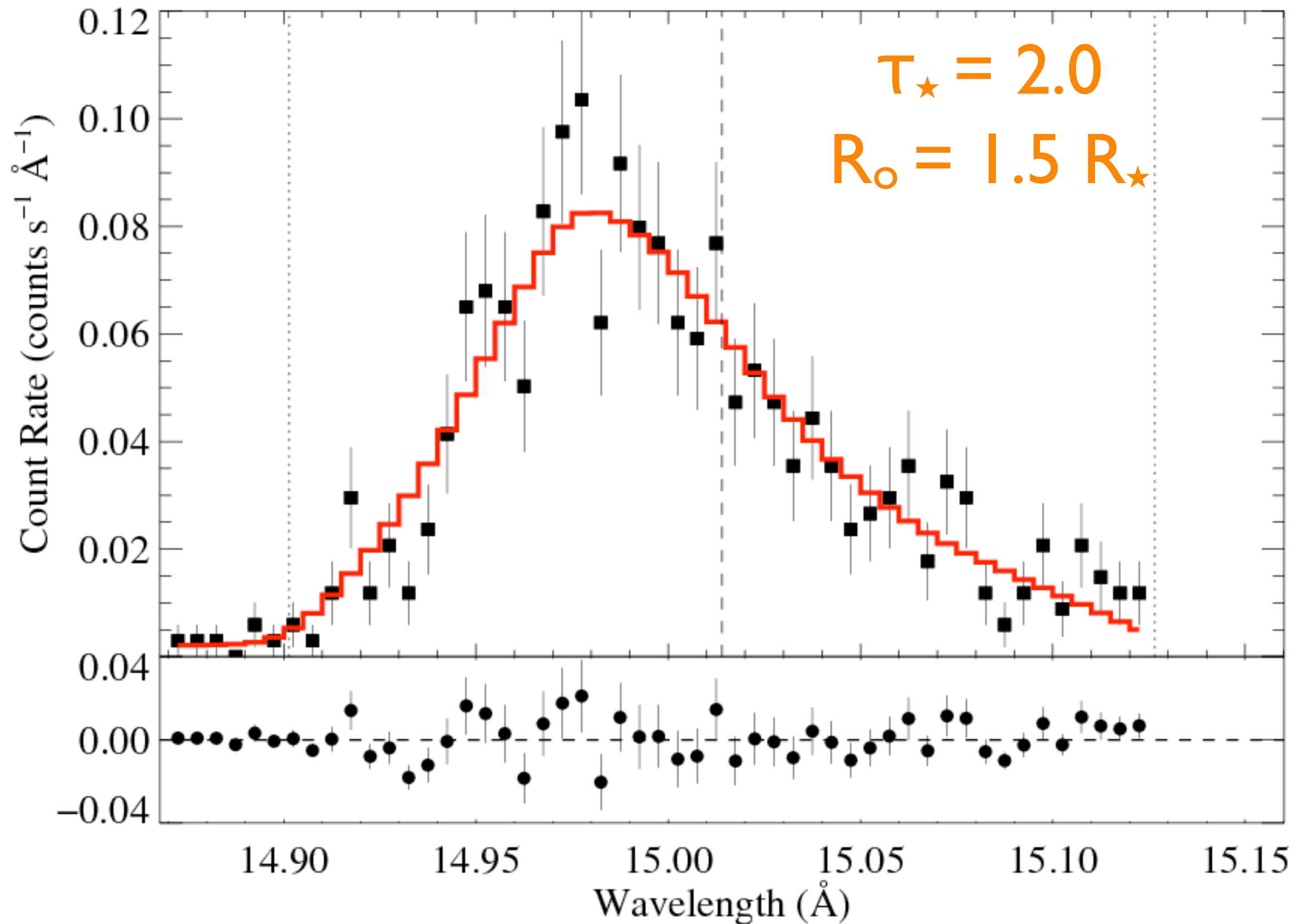
Wind Profile Model

$$\tau_* = \frac{\kappa \dot{M}}{4\pi R_* v_\infty}$$



ζ Pup: *Chandra* MEG

Fe XVII



Quantifying the wind optical depth

opacity of the **cold wind** component (due to bound-free transitions in C, N, O, Ne, Fe)

wind mass-loss rate

$$\dot{M} = 4\pi r^2 v \rho$$

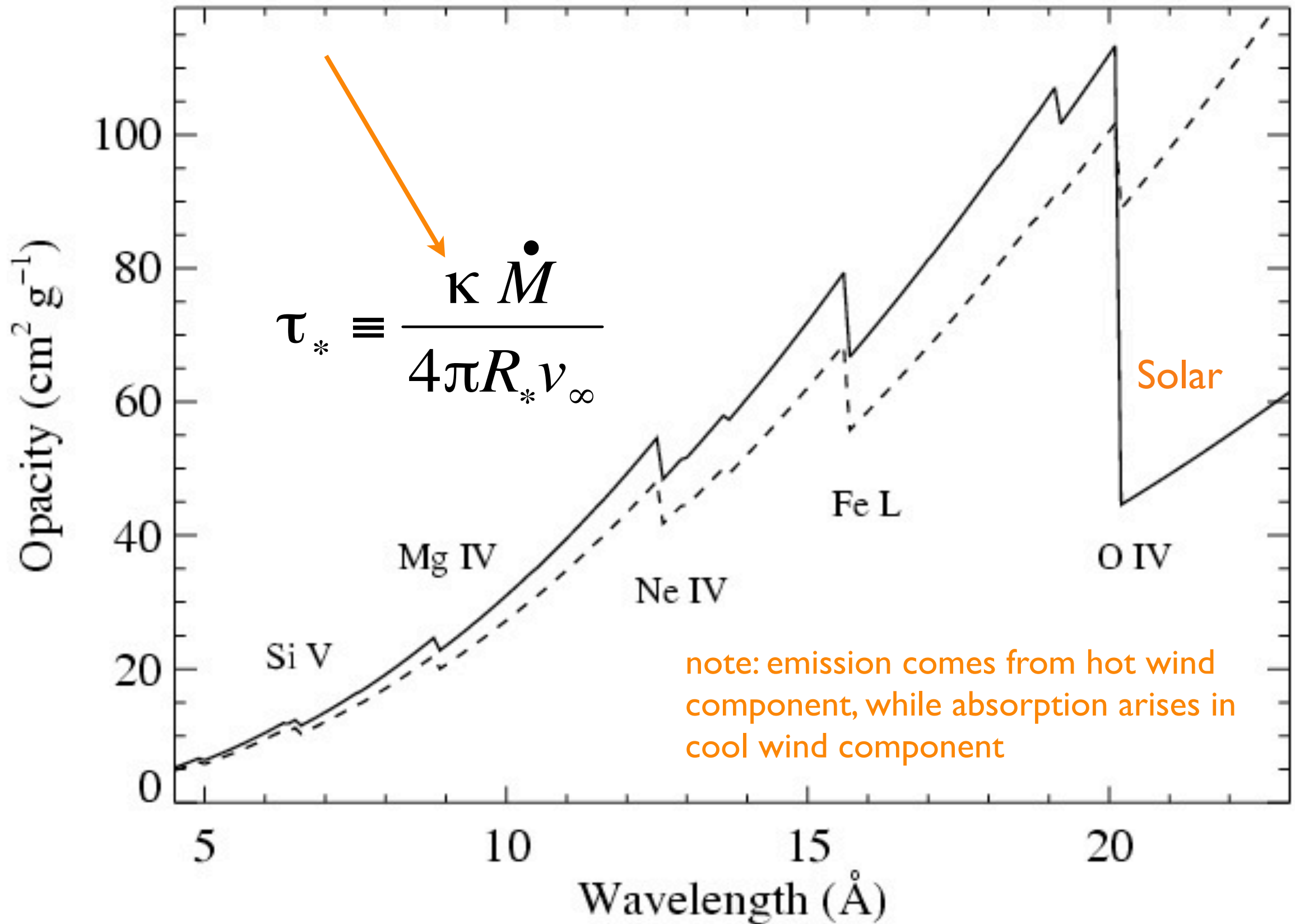
$$\tau_* \equiv \frac{\kappa \dot{M}}{4\pi R_* v_\infty}$$

stellar radius

wind terminal velocity

soft X-ray wind opacity

CNO processed

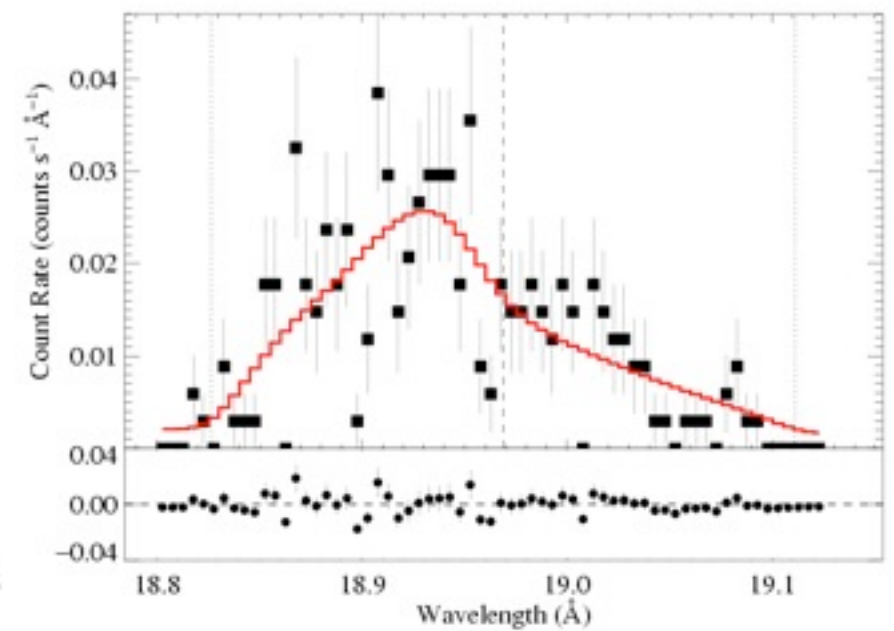
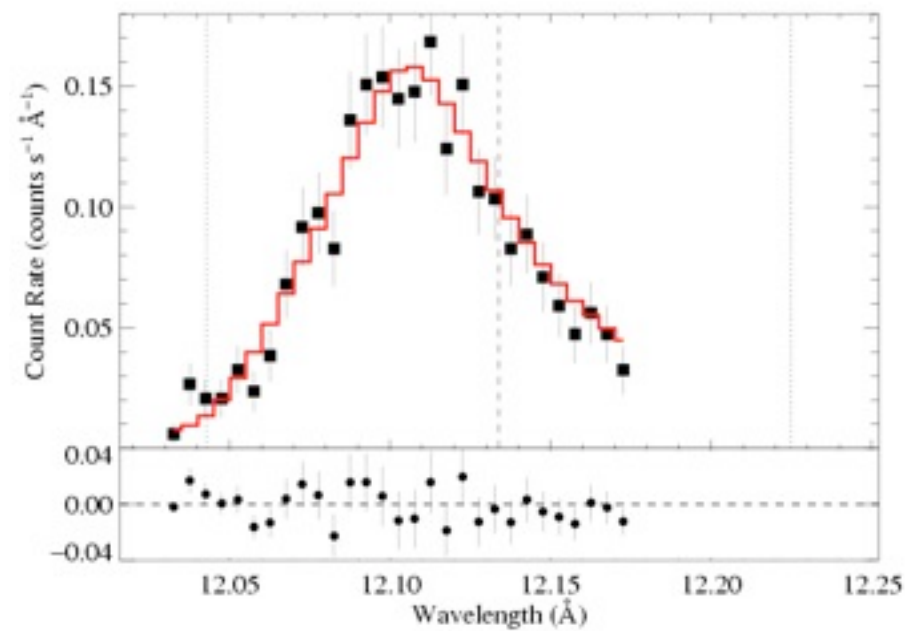
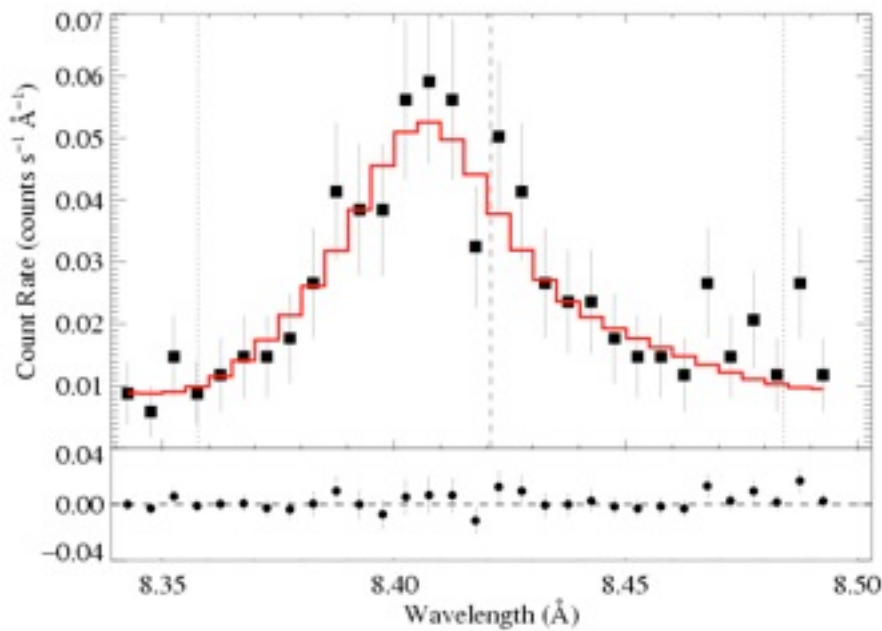


ζ Pup Chandra: three emission lines

Mg Ly α : 8.42 Å

Ne Ly α : 12.13 Å

O Ly α : 18.97 Å



$\tau_* \sim 1$

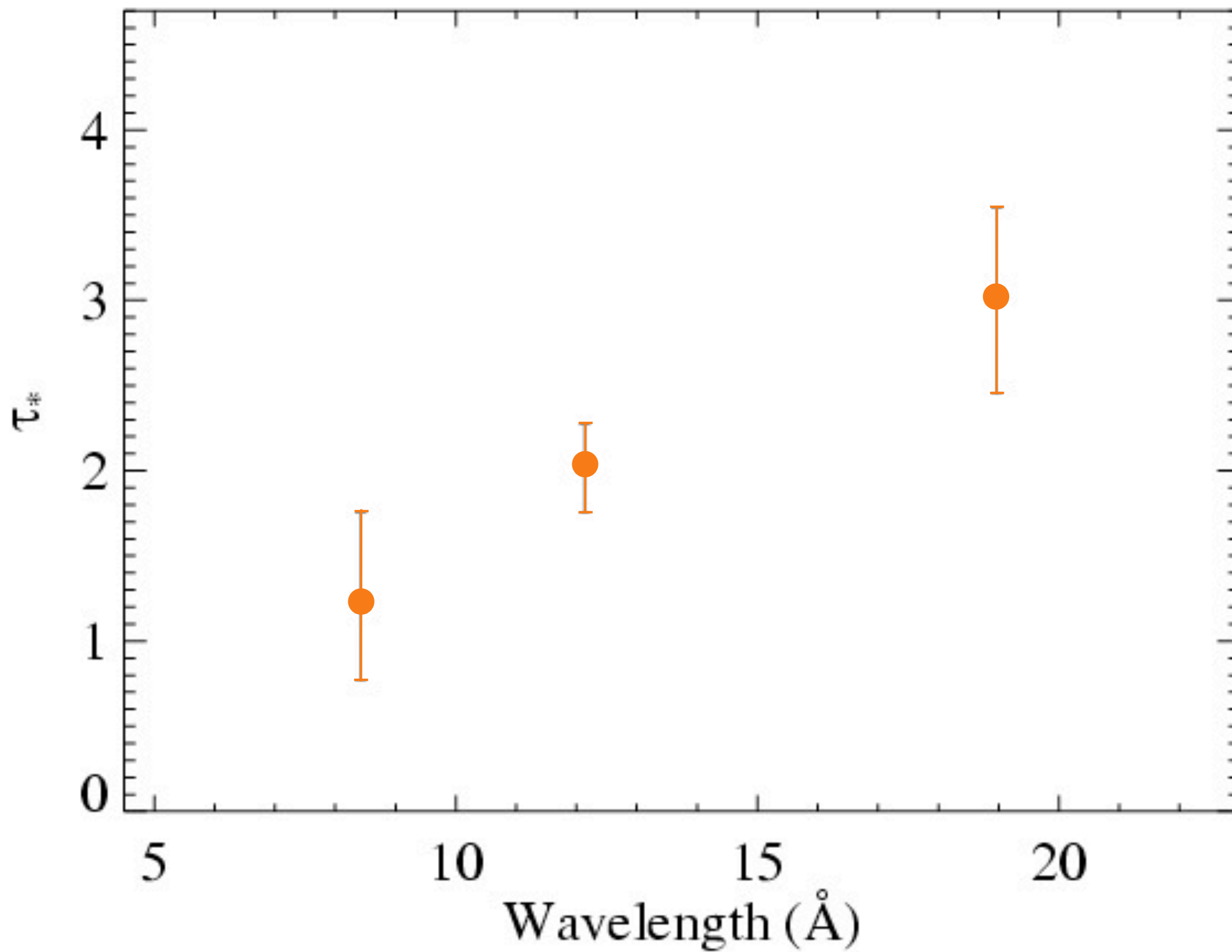
$\tau_* \sim 2$

$\tau_* \sim 3$

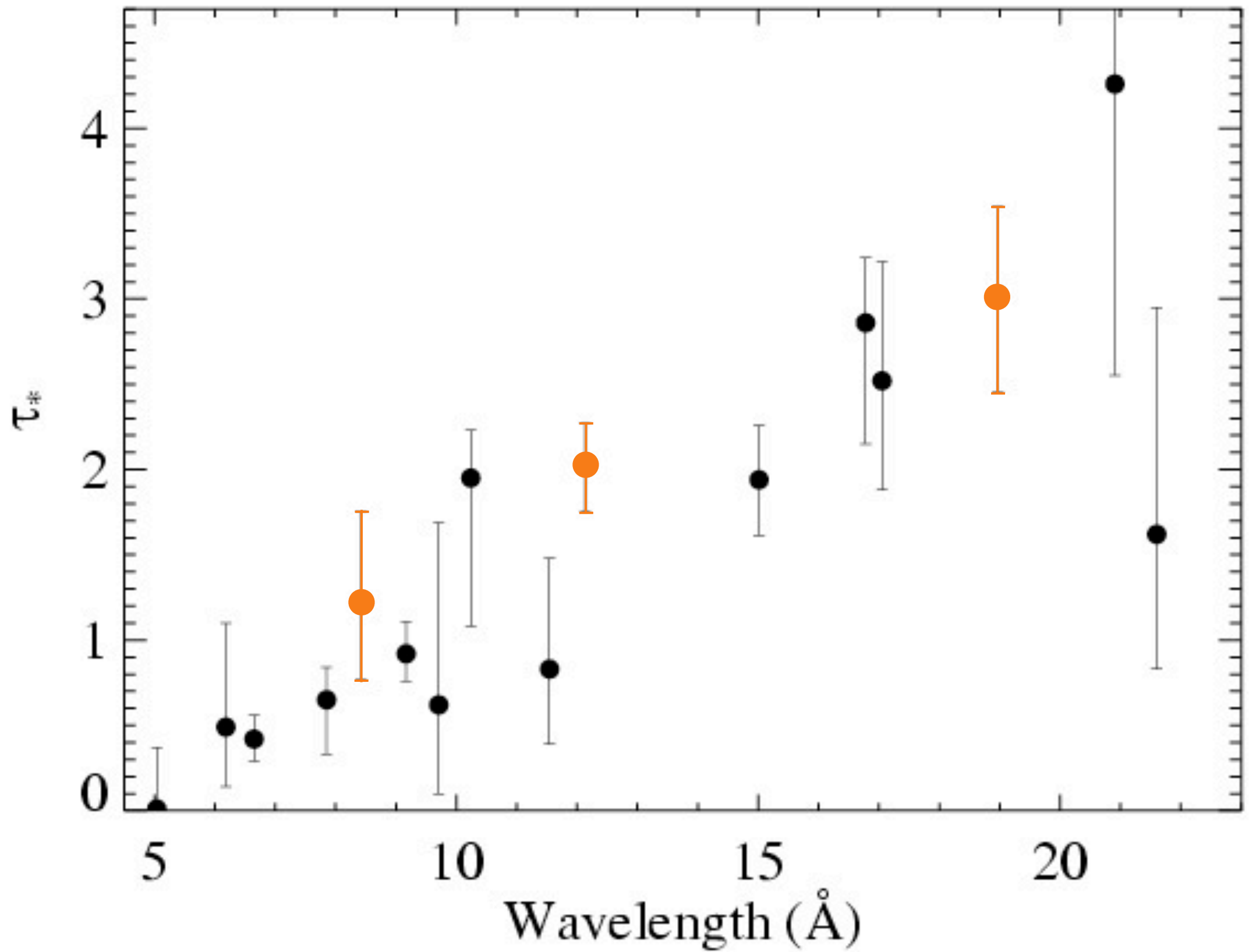
Recall:

$$\tau_* \equiv \frac{\kappa \dot{M}}{4\pi R_* v_\infty}$$

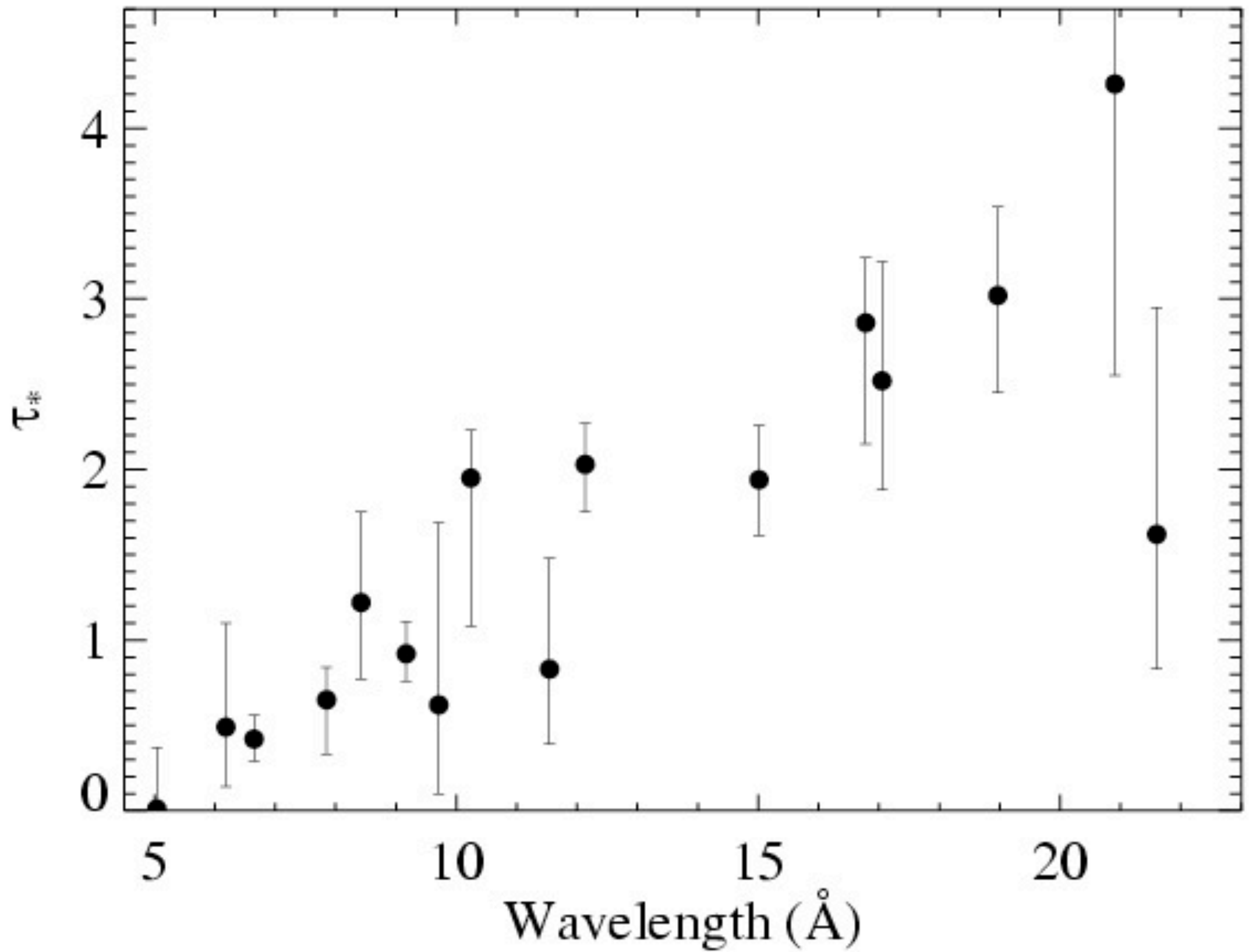
Results from the 3 line fits shown previously



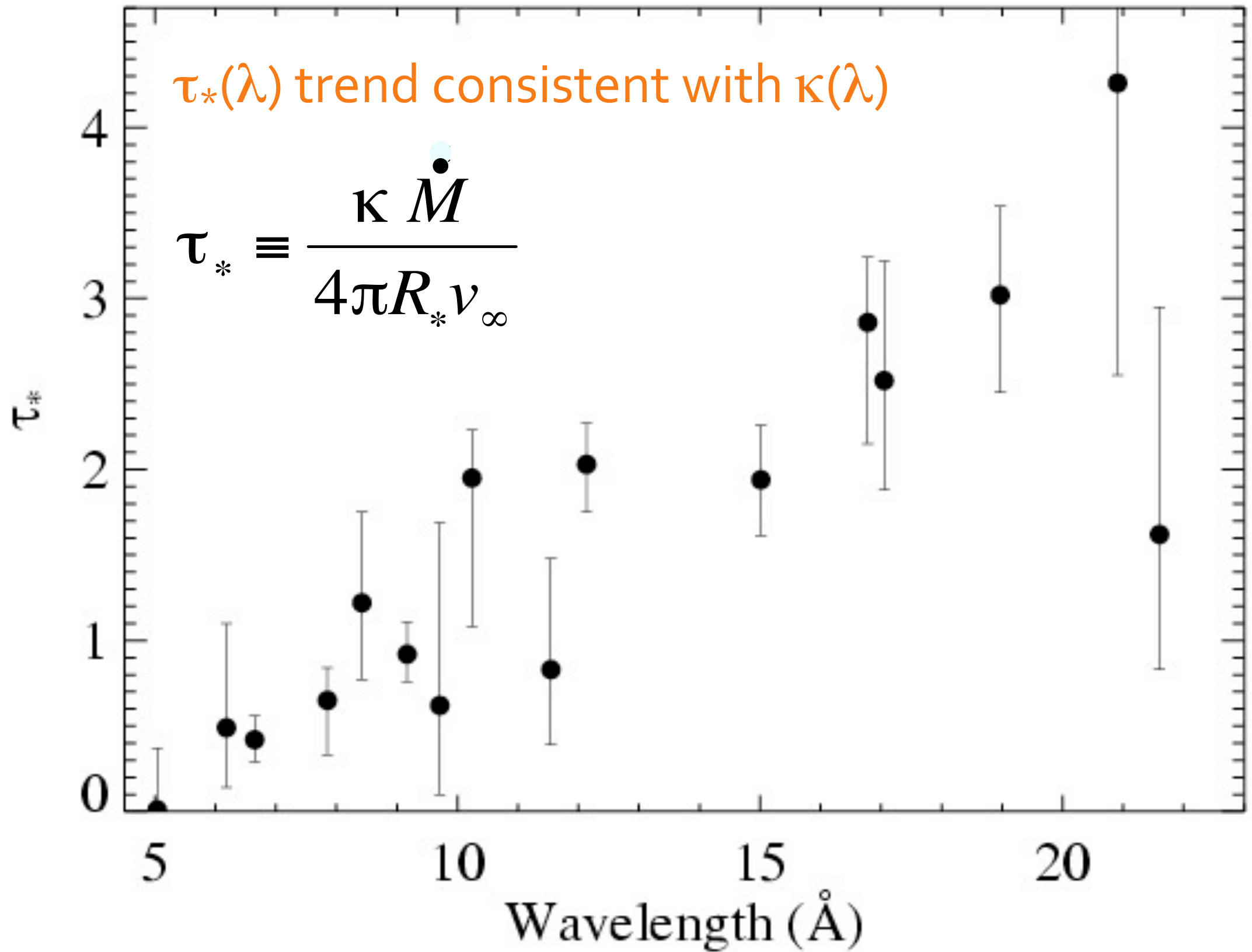
Fits to 16 lines in the *Chandra* spectrum of ζ Pup



Fits to 16 lines in the *Chandra* spectrum of ζ Pup

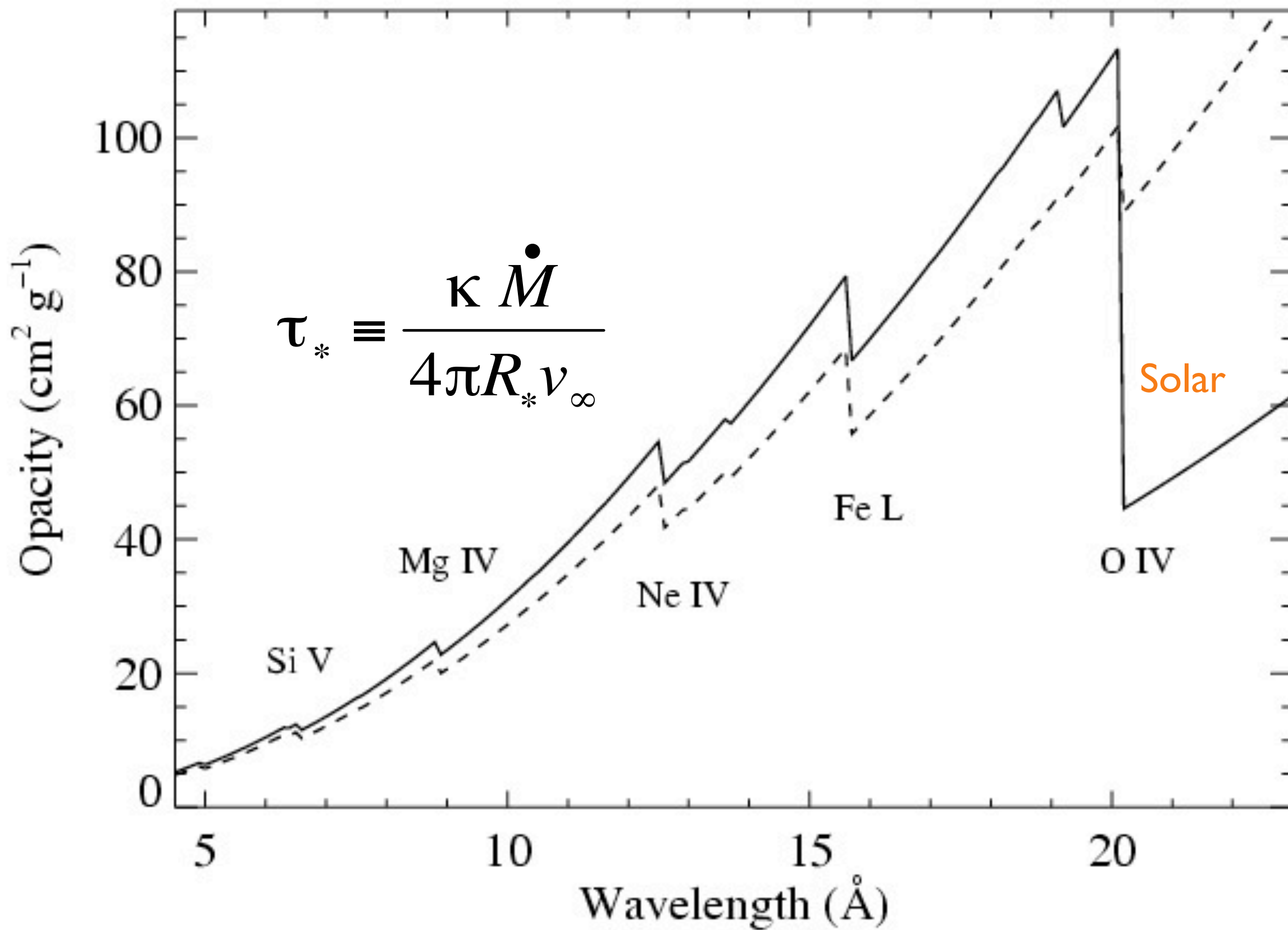


Fits to 16 lines in the *Chandra* spectrum of ζ Pup



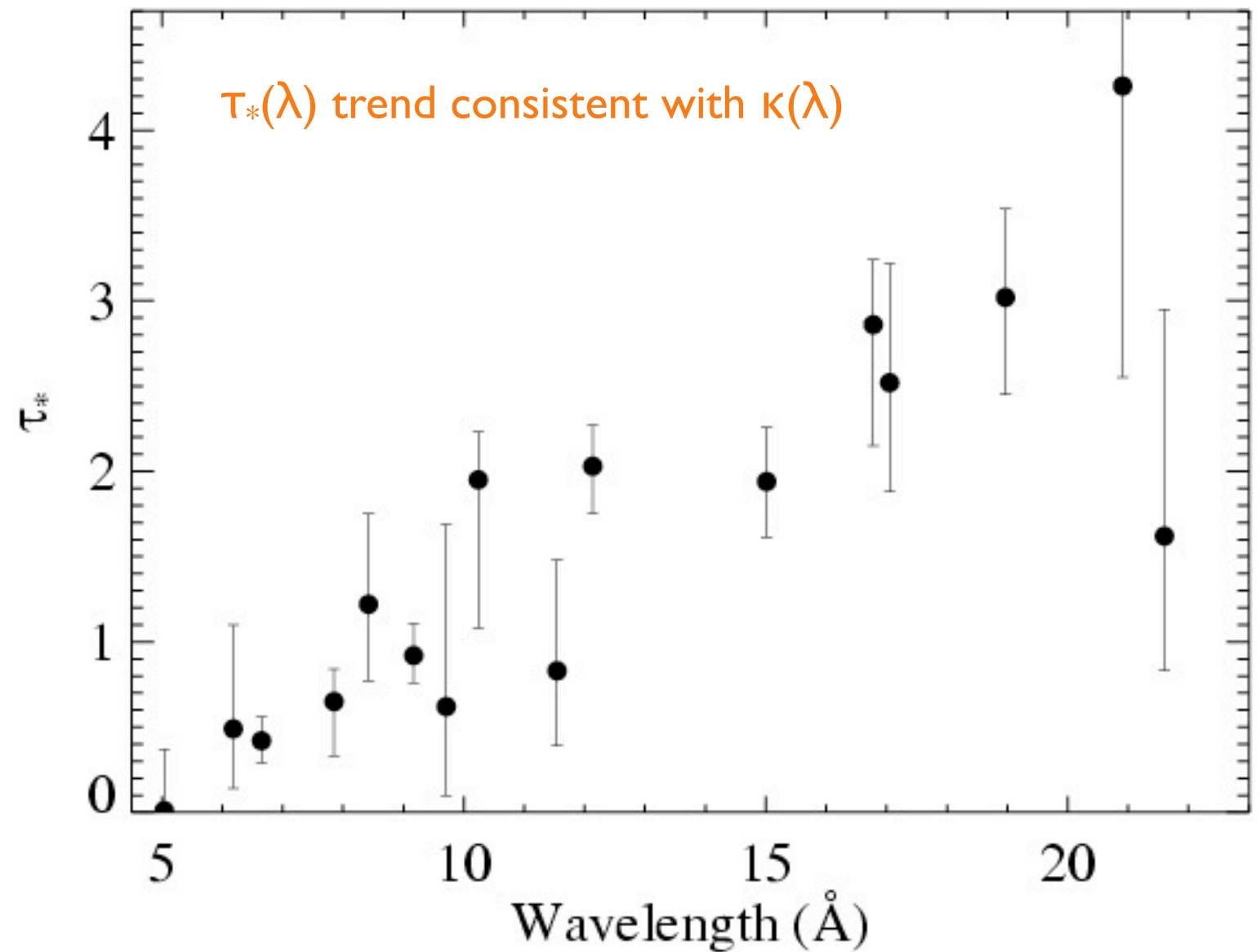
soft X-ray wind opacity

CNO processed



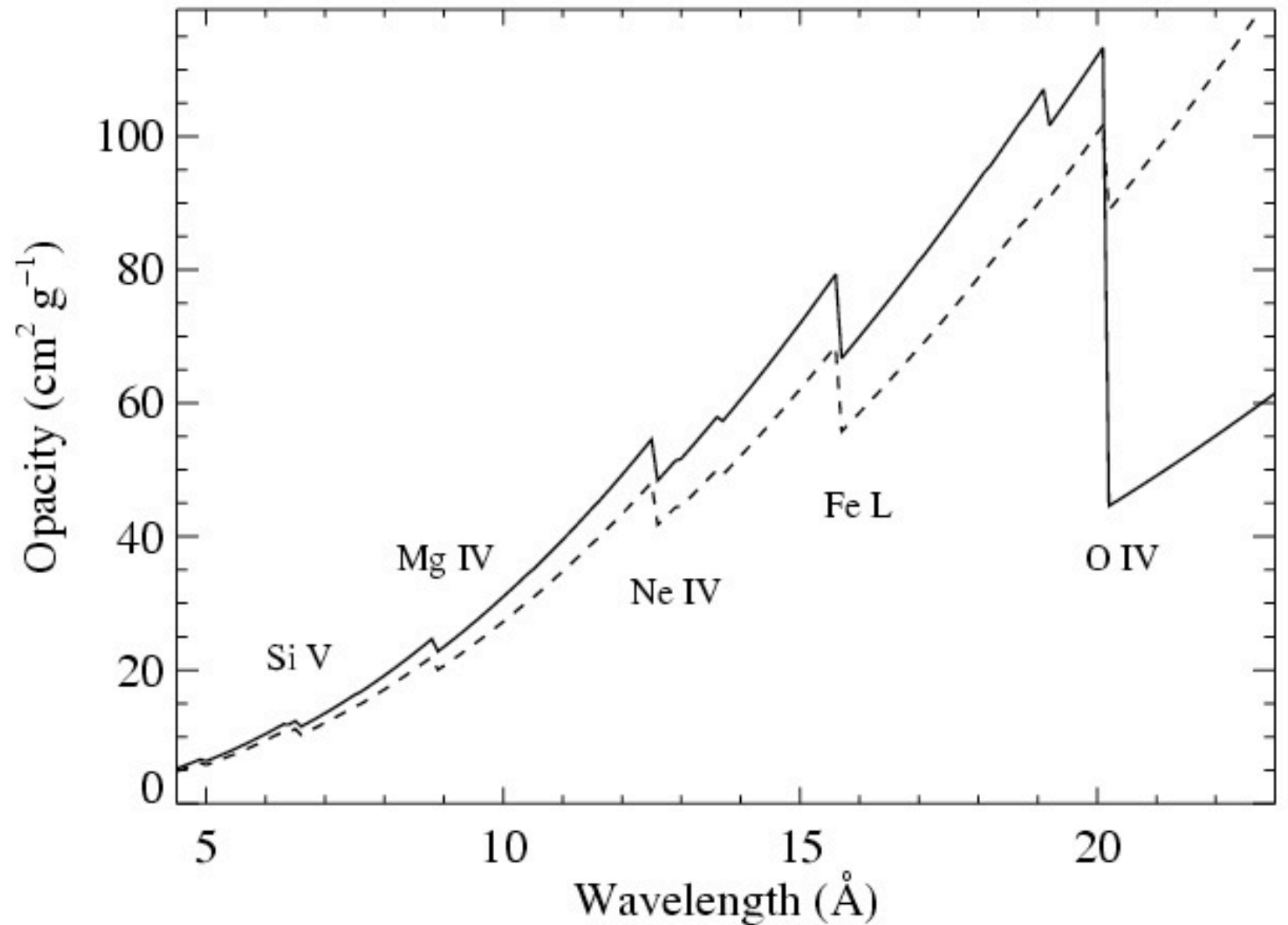
$$\tau_* \equiv \frac{\kappa \dot{M}}{4\pi R_* v_\infty}$$

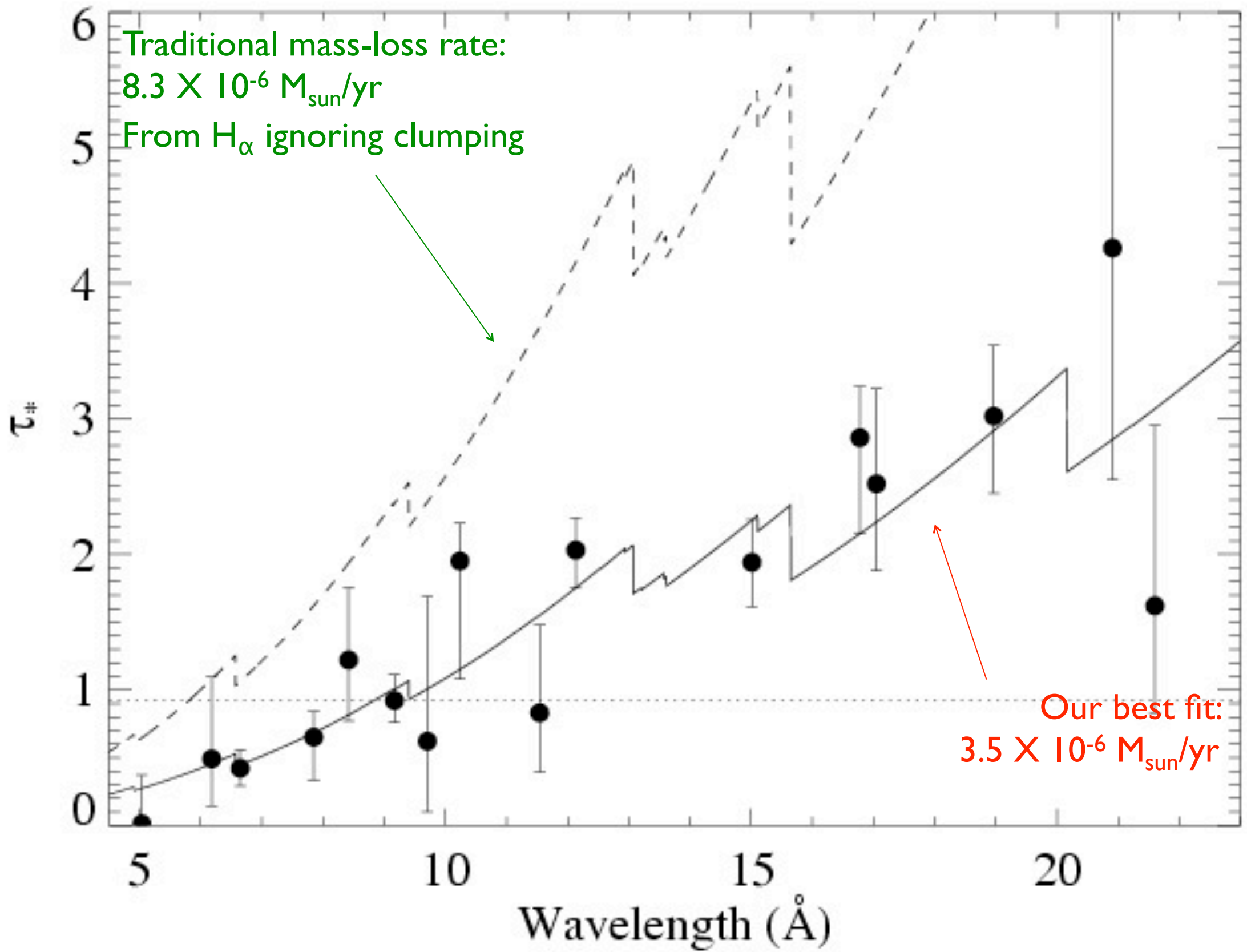
\dot{M} becomes the free parameter of the fit to the $\tau_*(\lambda)$ trend

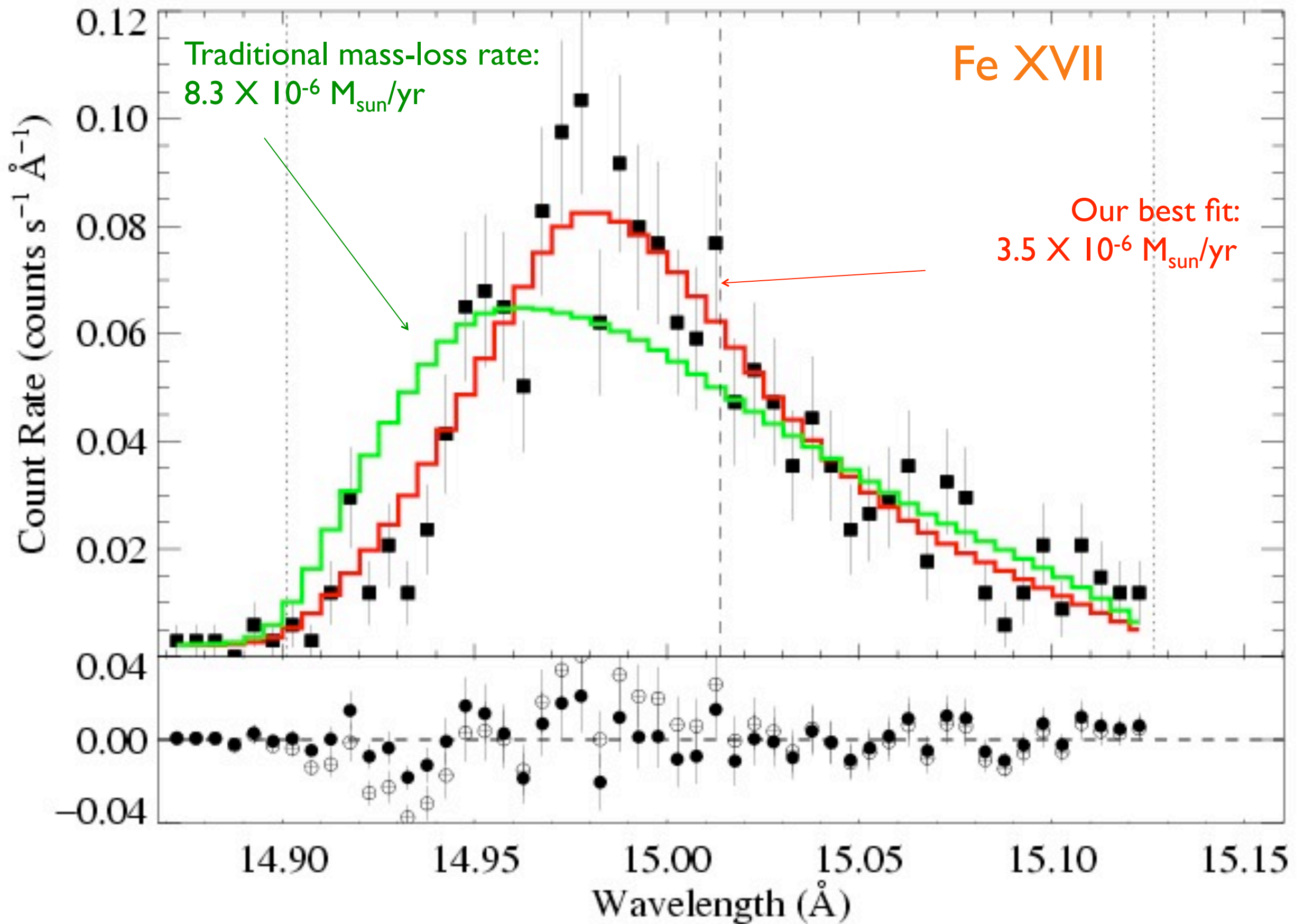


$$\tau_* \equiv \frac{\kappa \dot{M}}{4\pi R_* v_\infty}$$

\dot{M} becomes the free parameter of the fit to the $\tau_*(\lambda)$ trend







X-ray line profile based mass-loss rate: implications for clumping

basic definition: $f_{cl} \equiv \langle \rho^2 \rangle / \langle \rho \rangle^2$



clumping factor

X-ray line profile based mass-loss rate: implications for clumping

basic definition: $f_{cl} \equiv \langle \rho^2 \rangle / \langle \rho \rangle^2$

from density-squared
diagnostics like H α , IR
& radio free-free



from (column) density
diagnostic like τ_{\star} from
X-ray profiles



Bright OB stars in the Galaxy

III. Constraints on the radial stratification of the clumping factor in hot star winds from a combined H_{α} , IR and radio analysis[★]

J. Puls¹, N. Markova², S. Scuderi³, C. Stanghellini⁴, O. G. Taranova⁵, A. W. Burnley⁶ and I. D. Howarth⁶

¹ Universitäts-Sternwarte München, Scheinerstr. 1, D-81679 München, Germany, e-mail: uh101aw@usm.uni-muenchen.de

² Institute of Astronomy, Bulgarian National Astronomical Observatory, P.O. Box 136, 4700 Smoljan, Bulgaria, e-mail: nmarkova@astro.bas.bg

³ INAF - Osservatorio Astrofisico di Catania, Via S. Sofia 78, I-95123 Catania, Italy, e-mail: scuderi@oact.inaf.it

⁴ INAF - Istituto di Radioastronomia, Via P. Gobetti 101, I-40129 Bologna, Italy, e-mail: c.stanghellini@ira.inaf.it

⁵ Sternberg Astronomical Institute, Universitetski pr. 13, Moscow, 119992, Russia, e-mail: taranova@sai.msu.ru

⁶ Department of Physics and Astronomy, University College London, Gower Street, London WC1E 6BT, UK, e-mail: awzb@star.ucl.ac.uk, idh@star.ucl.ac.uk

Received; accepted

Abstract. Recent results strongly challenge the canonical picture of massive star winds: various evidence indicates that currently accepted mass-loss rates, \dot{M} , may need to be revised downwards, by factors extending to one magnitude or even more. This is because the most commonly used mass-loss diagnostics are affected by “clumping” (small-scale density inhomogeneities), influencing our interpretation of observed spectra and fluxes.

Such downward revisions would have dramatic consequences for the evolution of, and feedback from, massive stars, and thus robust determinations of the clumping properties and mass-loss rates are urgently needed. We present a first attempt concerning this objective, by means of constraining the radial stratification of the so-called clumping factor.

To this end, we have analyzed a sample of 19 Galactic O-type supergiants/giants, by combining our own and archival data for H_{α} , IR, mm and radio fluxes, and using approximate methods, calibrated to more sophisticated models. Clumping has been included into our analysis in the “conventional” way, by assuming the inter-clump matter to be void. Because (almost) all our diagnostics depends on the square of density, we cannot derive absolute clumping factors, but only factors normalized to a certain minimum.

This minimum was usually found to be located in the outermost, radio-emitting region, i.e., the radio mass-loss rates are the lowest ones, compared to \dot{M} derived from H_{α} and the IR. The radio rates agree well with those predicted by theory, but are only upper limits, due to unknown clumping in the outer wind. H_{α} turned out to be a useful tool to derive the clumping properties inside $r < 3..5 R_{*}$. Our most important result concerns a (physical) difference between denser and thinner winds: for denser winds, the innermost region is more strongly clumped than the outermost one (with a normalized clumping factor of 4.1 ± 1.4), whereas thinner winds have similar clumping properties in the inner and outer regions.

Our findings are compared with theoretical predictions, and the implications are discussed in detail, by assuming different scenarios regarding the still unknown clumping properties of the outer wind.

trade-off/degeneracy between clumping factor and mass-loss rate

$$\dot{M}_{\text{cl}} \equiv \dot{M}_{\text{smooth}} / f_{\text{cl}}^{0.5}$$

Puls et al. (2006) : relative clumping (vs. radius), but free scale factor

$$\zeta \text{ Pup mass-loss rate} < 4.2 \times 10^{-6} M_{\text{sun}}/\text{yr}$$

X-ray mass-loss rate breaks degeneracy and sets the scale factor

ζ Pup: radially varying clumping

for $\dot{M} = 3.5 \times 10^{-6} M_{\text{sun}}/\text{yr}$

$$f_{\text{cl}} \equiv \langle \rho^2 \rangle / \langle \rho \rangle^2$$

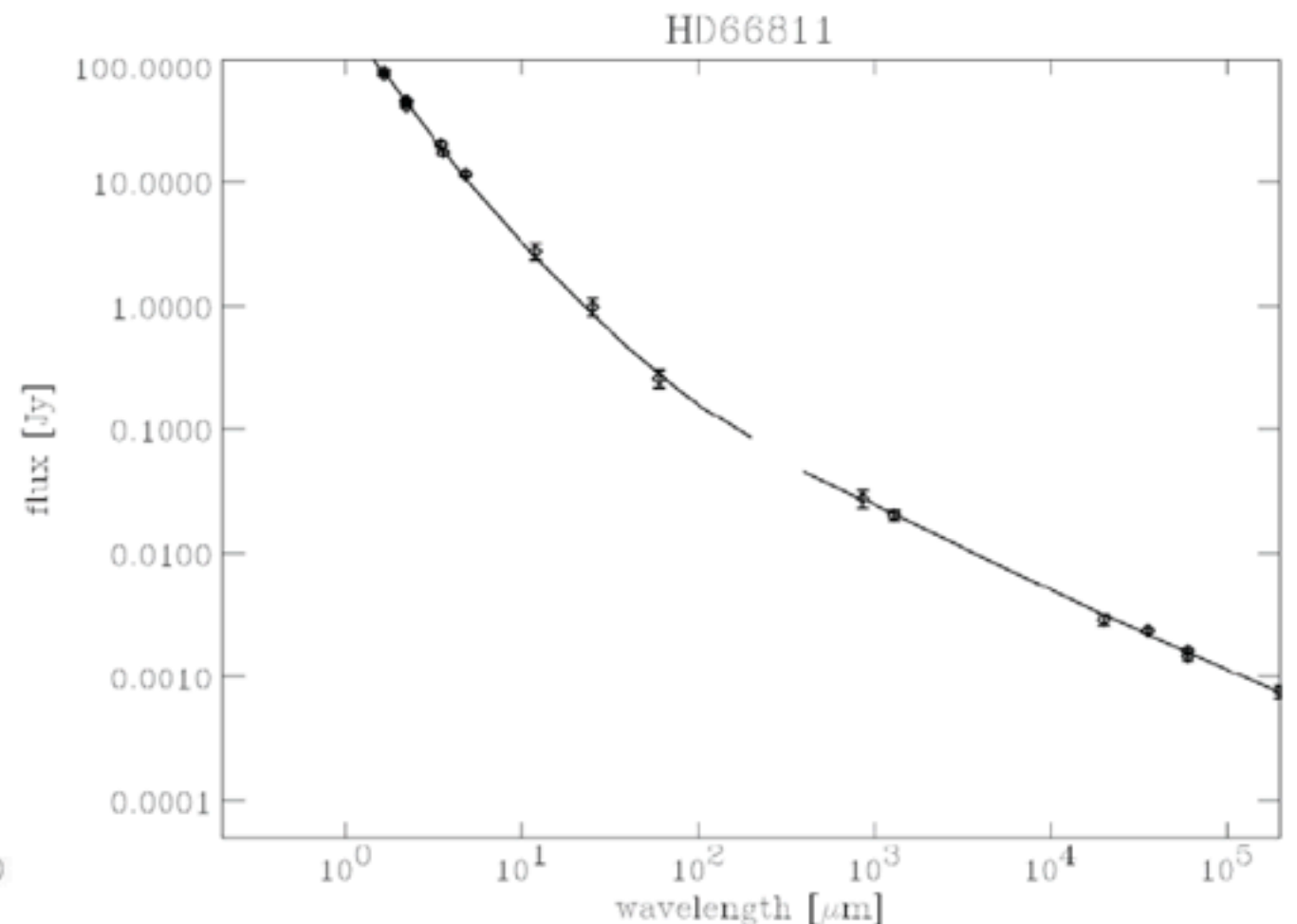
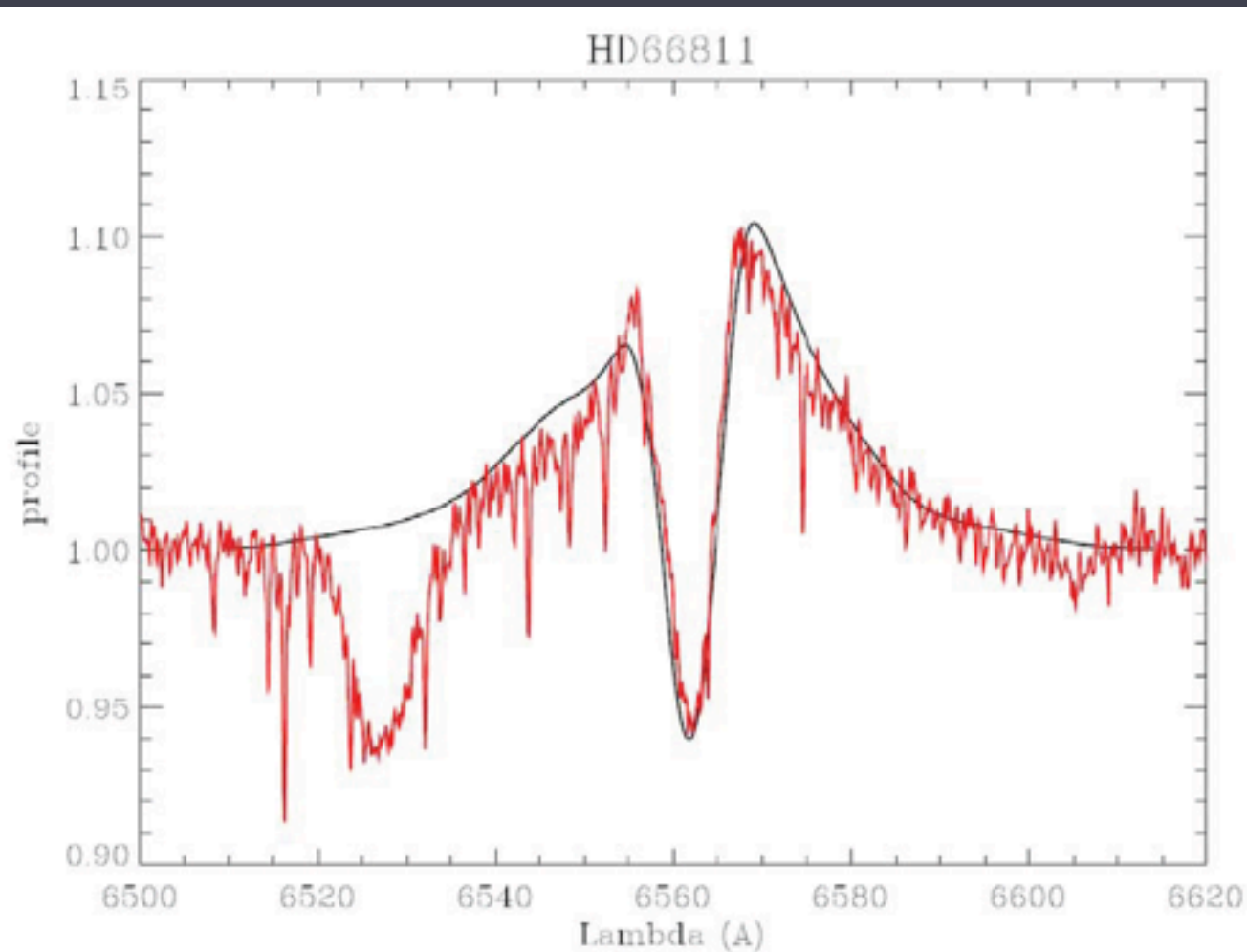
$$\dot{M}_{\text{cl}} \equiv \dot{M}_{\text{smooth}} / f_{\text{cl}}^{0.5}$$

$f_{\text{cl}} = 1.3$ @ $r < 1.12 R_*$ H α
 $f_{\text{cl}} = 6.0$ @ $1.12 < r < 1.5 R_*$ H α
 $f_{\text{cl}} = 3.7$ @ $1.5 < r < 2 R_*$ H α
 $f_{\text{cl}} = 2.6$ @ $2 < r < 15 R_*$ IR
 $f_{\text{cl}} = 1.3$ @ $r > 15 R_*$ radio

H α

IR

radio

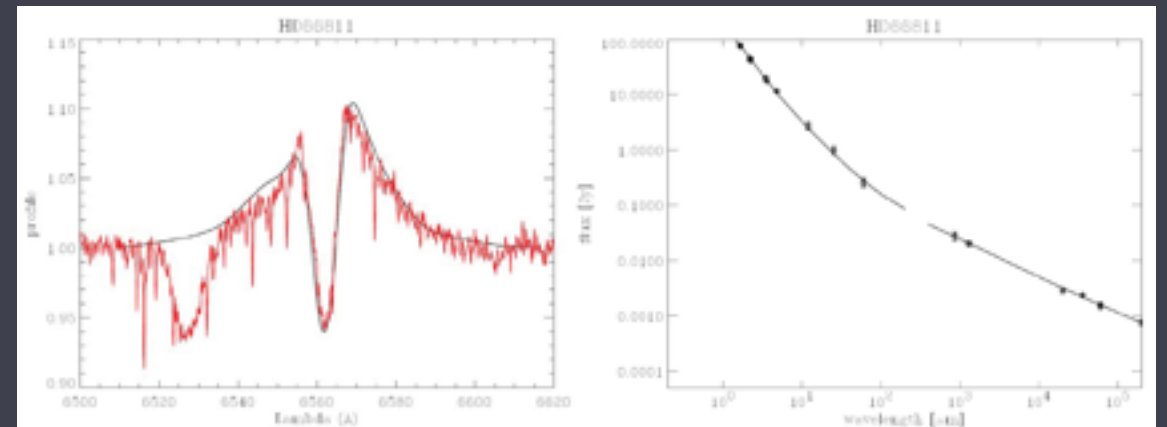
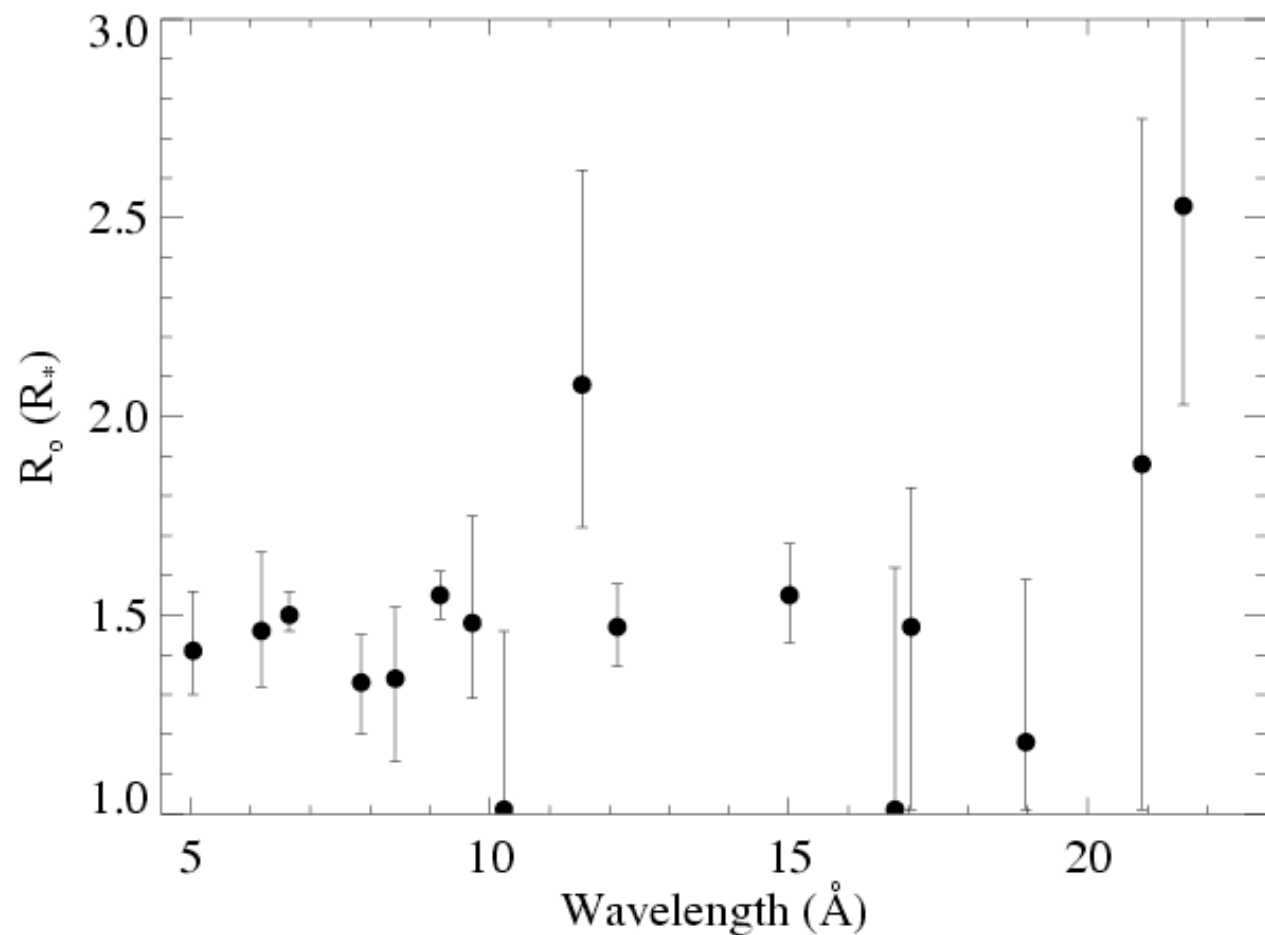


base of the wind ($r < 1.5 R_{\star}$)

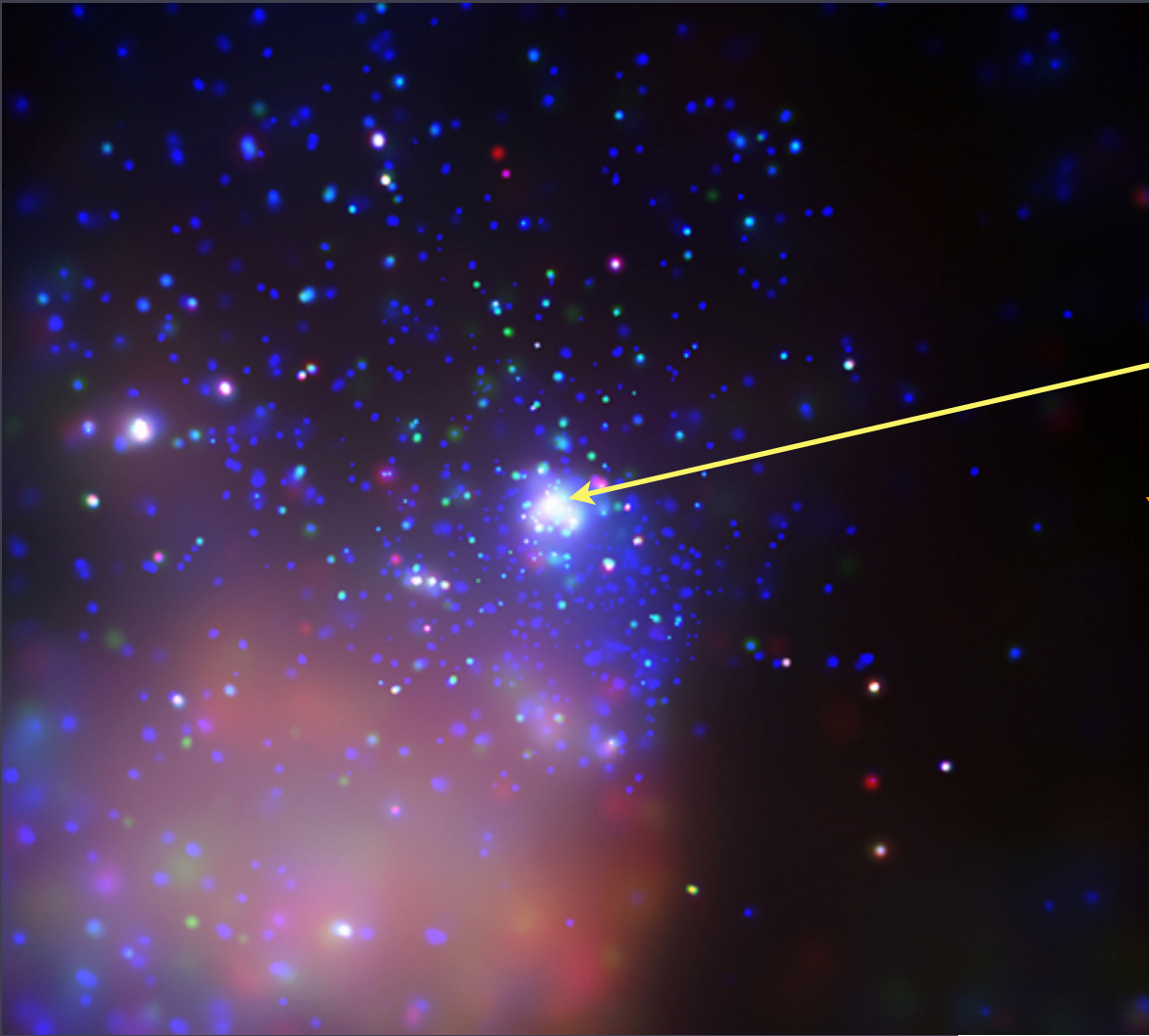
is clumped \rightarrow
...but...

recall: X-ray $R_o = 1.5 R_{\star}$

$f_{cl} = 1.3$ @ $r < 1.12 R_{\star}$ H α
 $f_{cl} = 6.0$ @ $1.12 < r < 1.5 R_{\star}$ H α
 $f_{cl} = 3.7$ @ $1.5 < r < 2 R_{\star}$ H α
 $f_{cl} = 2.6$ @ $2 < r < 15 R_{\star}$ IR
 $f_{cl} = 1.3$ @ $r > 15 R_{\star}$ radio

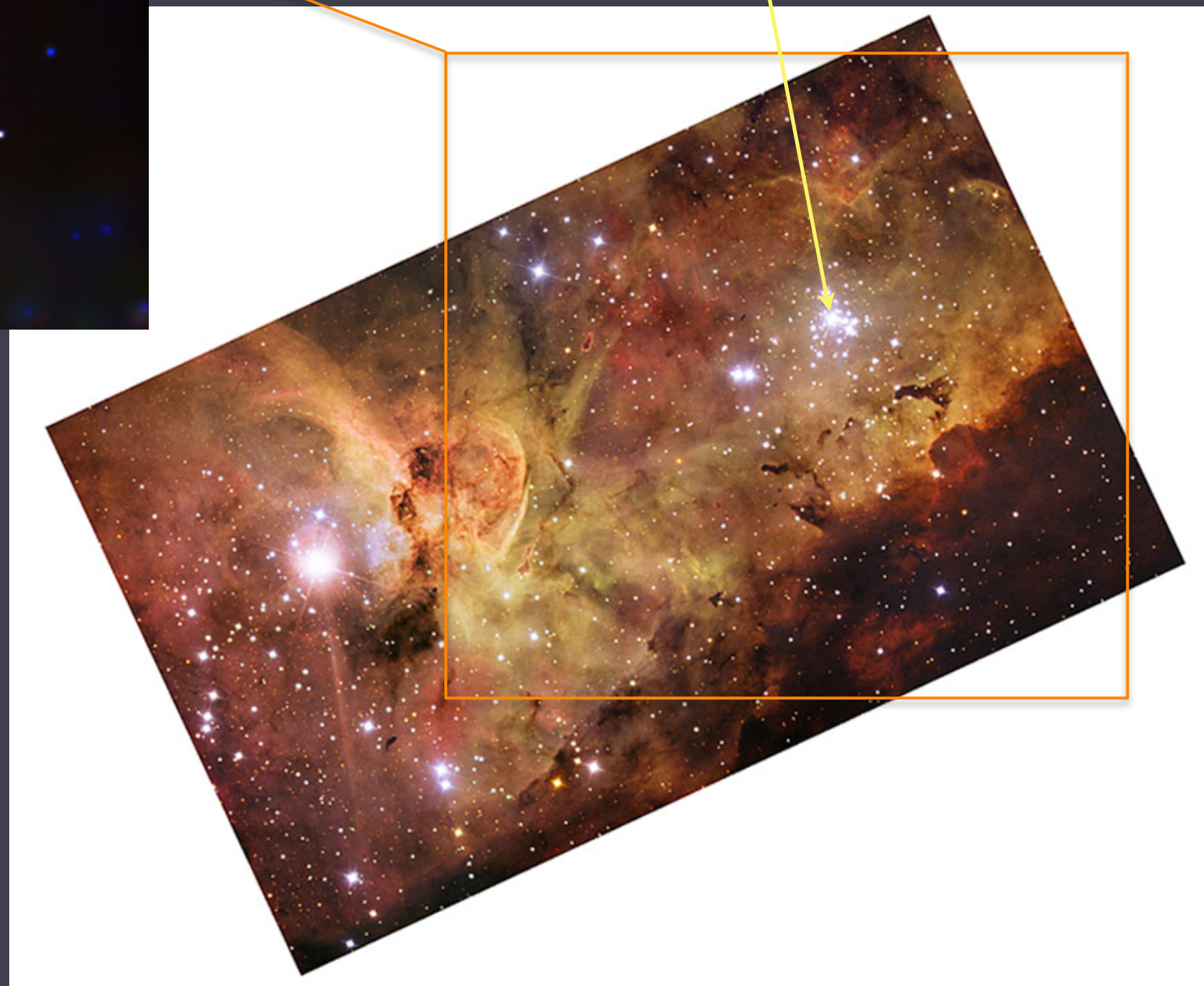


Other Stars?



Tr 14: Chandra

HD 93129A



Carina: ESO



HD 93129A

$$L_x \sim 7 \times 10^{32}$$

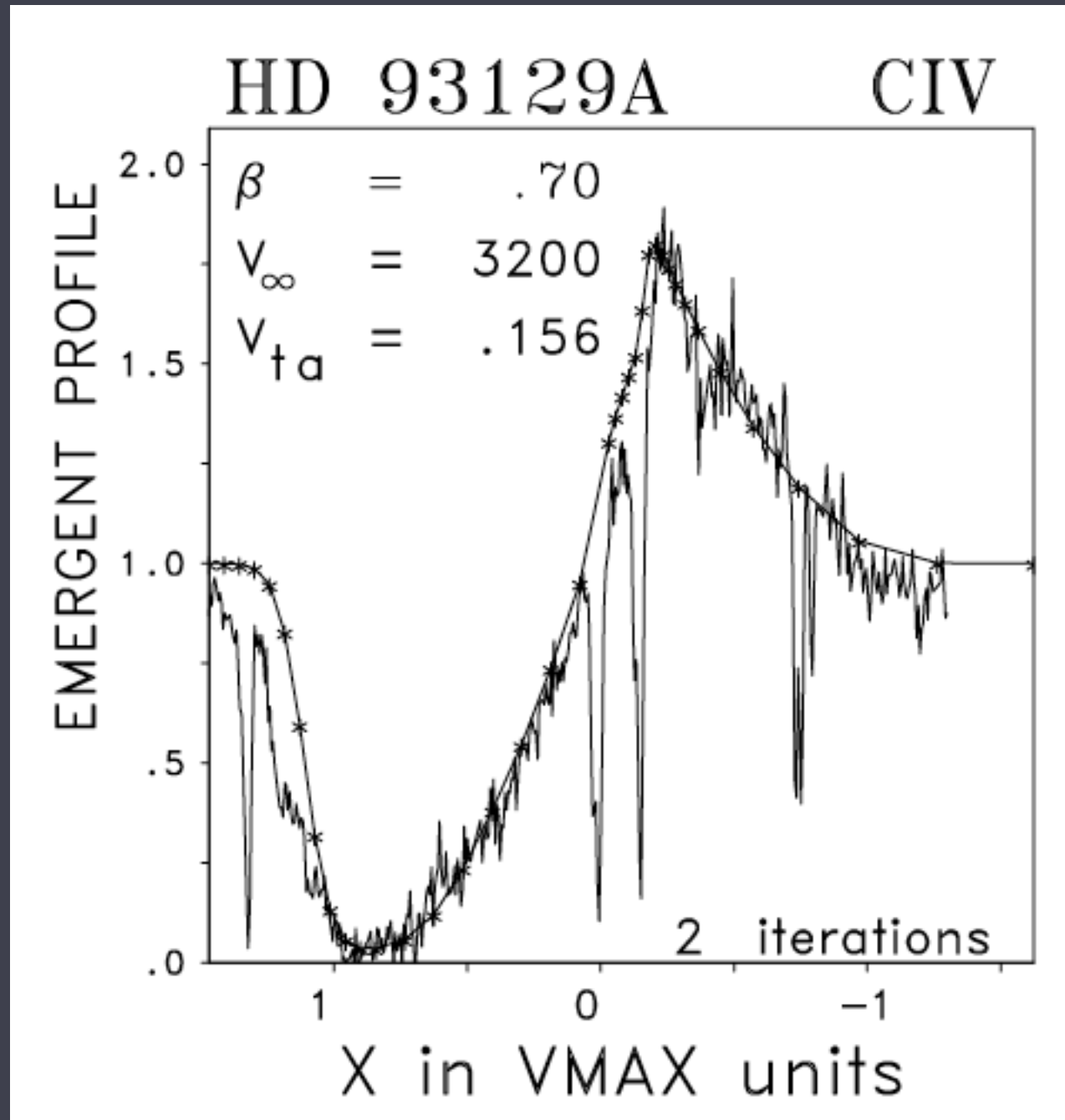
$$\langle h\nu \rangle \sim 1 \text{ keV}$$
$$: kT \sim 10^7 \text{ K}$$

Tr 14: Chandra

$$L_{\text{bol}} \sim 2 \times 10^6 L_{\text{sun}} \quad \text{so} \quad L_x/L_{\text{bol}} \sim 10^{-7}$$

Strong stellar winds: traditional diagnostics

UV



Taresch et al. (1997)

$$\dot{M} = 2 \times 10^{-5} M_{\text{sun}}/\text{yr}$$

$$v_{\infty} = 3200 \text{ km/s}$$

H α

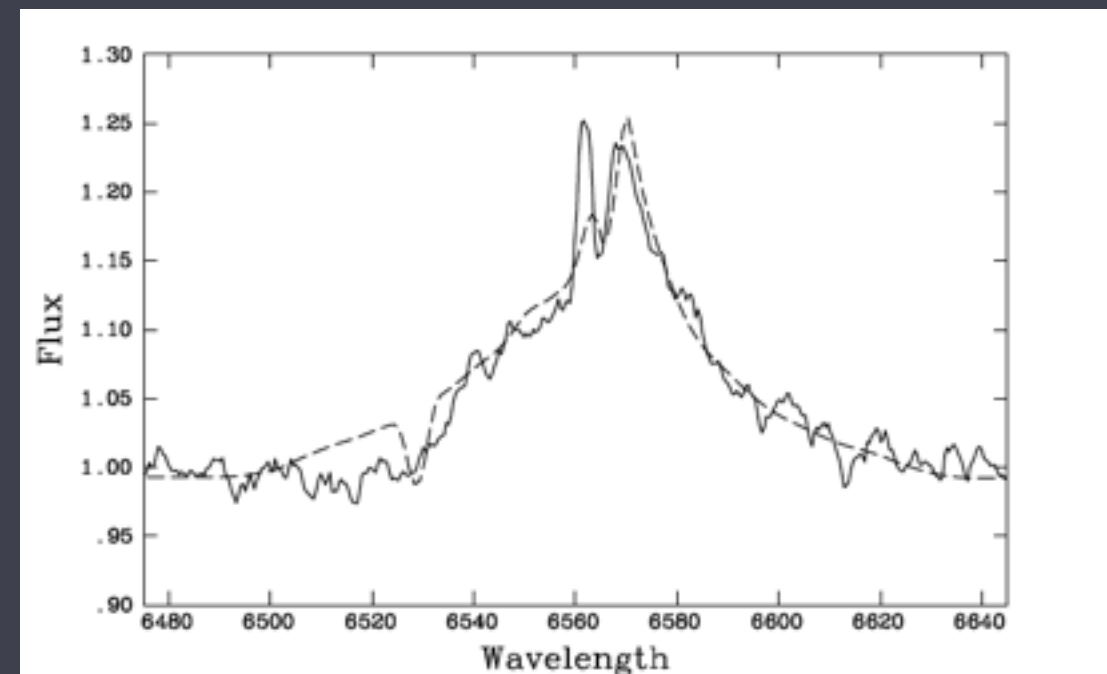


Fig. 13. Observed H α profile (solid) compared with the calculation assuming a mass loss of $18 \times 10^{-6} M_{\odot}/\text{yr}$ (dashed). Note that the blue narrow emission peak originates from the H II-region emission.

HD 93129A: strongest wind measured in an O star

H α

$$\dot{M} = 2 \times 10^{-5} M_{\text{sun}}/\text{yr}$$

assuming a *smooth* wind

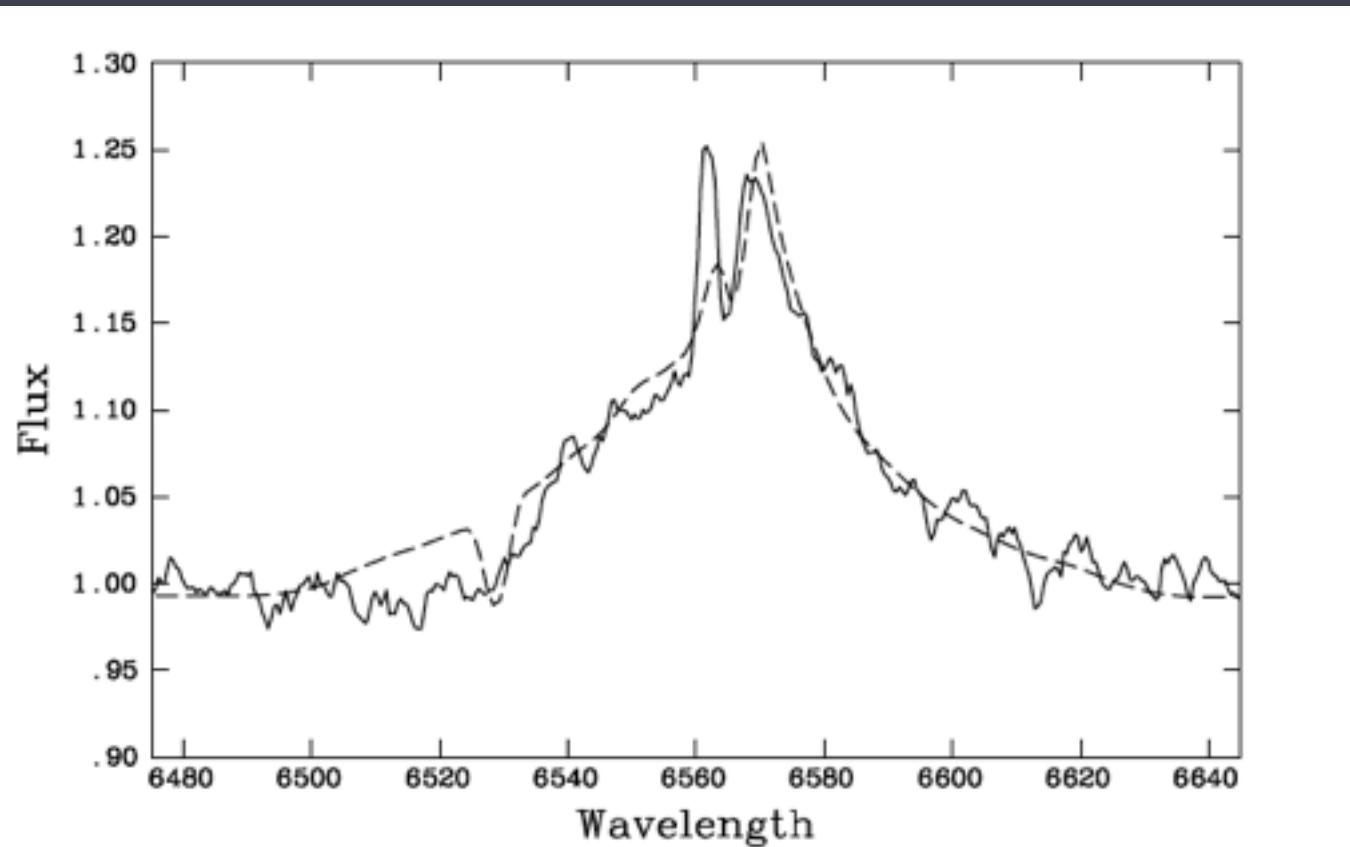


Fig. 13. Observed H α profile (solid) compared with the calculation assuming a mass loss of $18 \times 10^{-6} M_{\odot}/\text{yr}$ (dashed). Note that the blue narrow emission peak originates from the H II-region emission.

i.e. no clumping



HD 93129A

$$L_x \sim 7 \times 10^{32}$$

$$\langle h\nu \rangle \sim 1 \text{ keV}$$
$$: kT \sim 10^7 \text{ K}$$

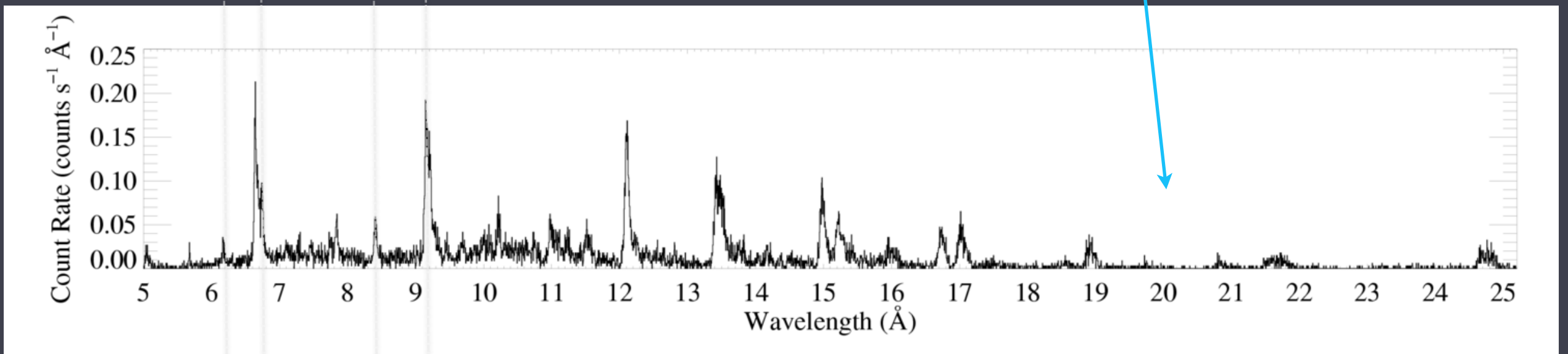
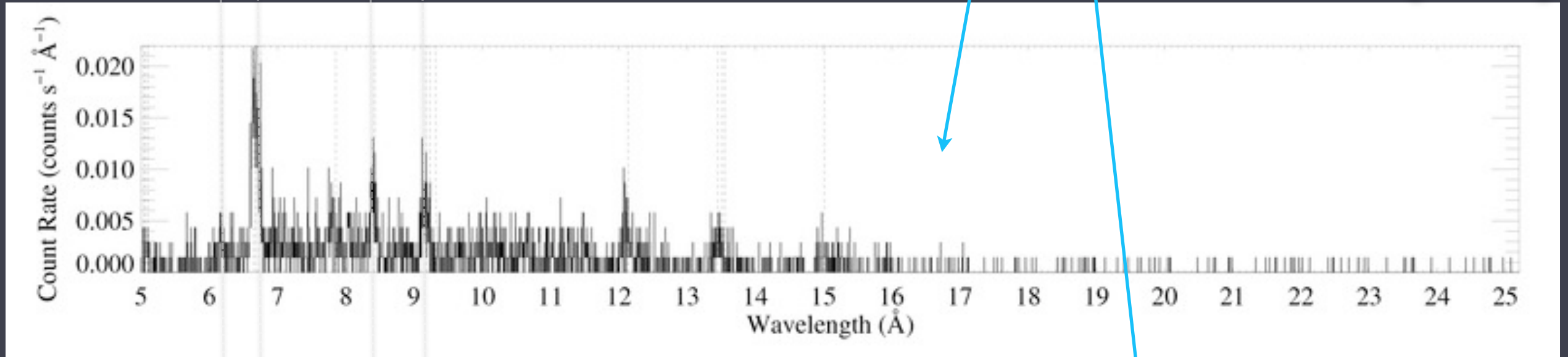
Tr 14: Chandra

$$L_{\text{bol}} \sim 2 \times 10^6 L_{\text{sun}} \quad \text{so} \quad L_x/L_{\text{bol}} \sim 10^{-7}$$

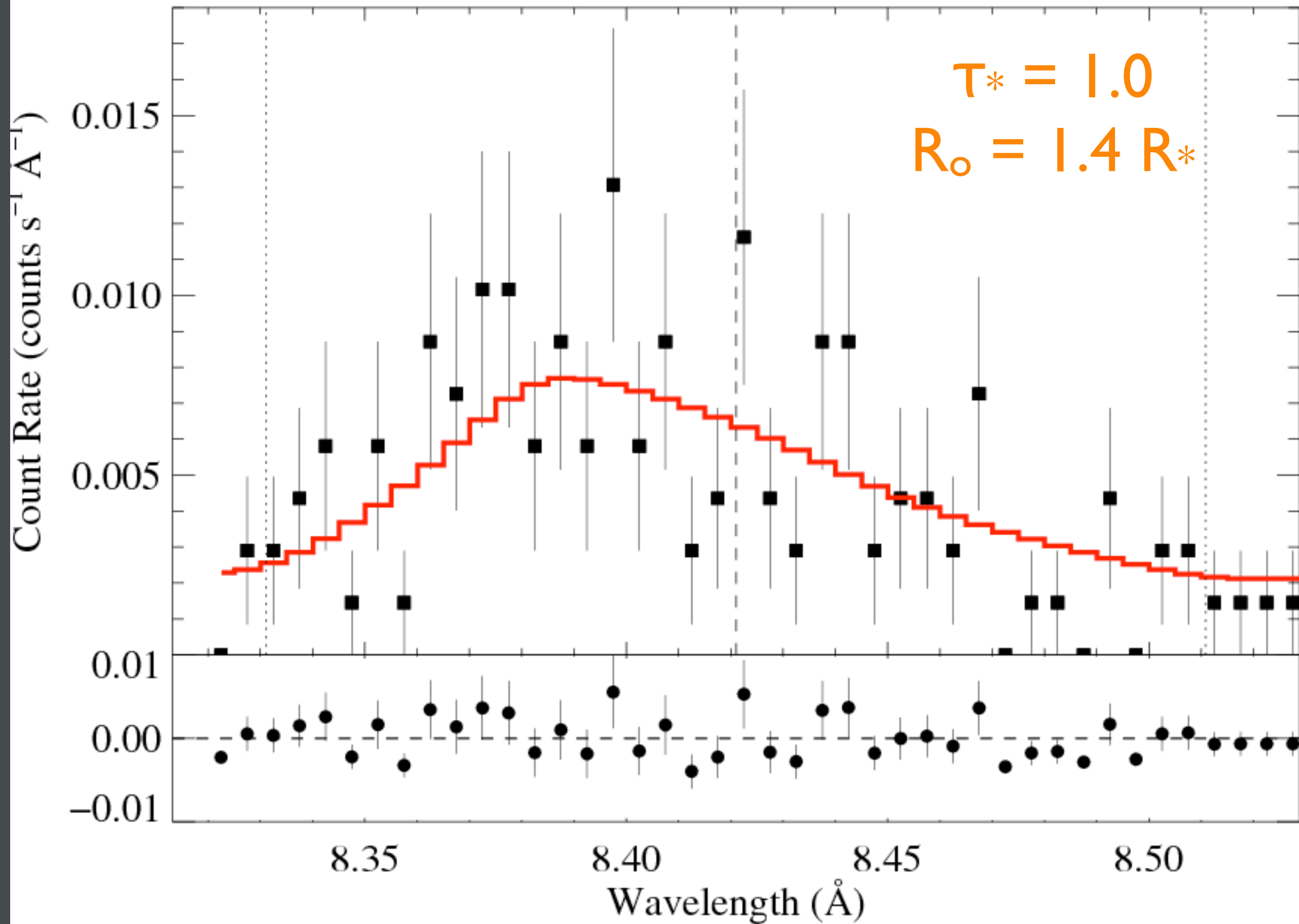
H-like vs. He-like soft emission absent: wind attenuation

Si XIII Mg XI
Si XIV Mg XII

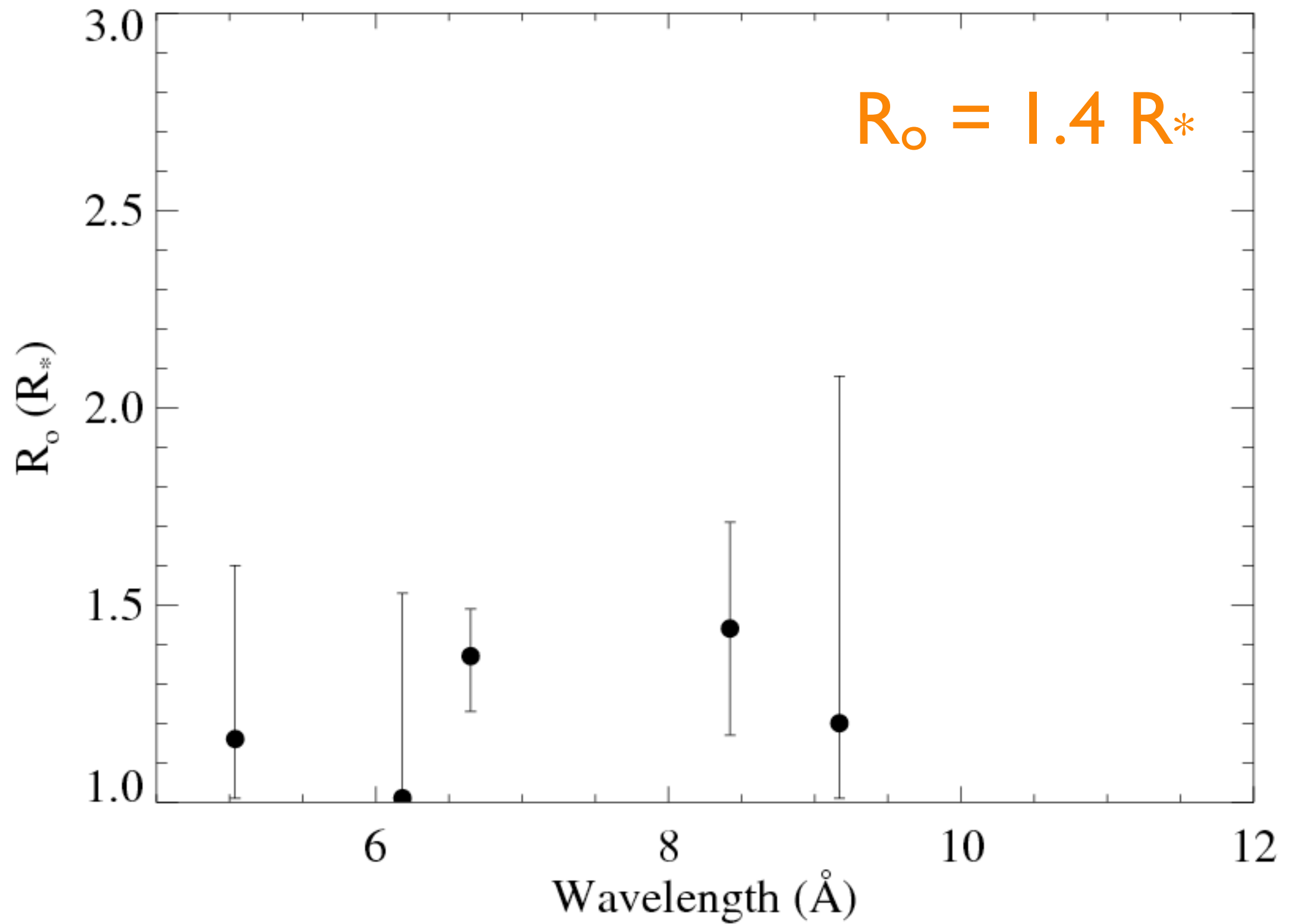
HD 93129A (O2 If*)

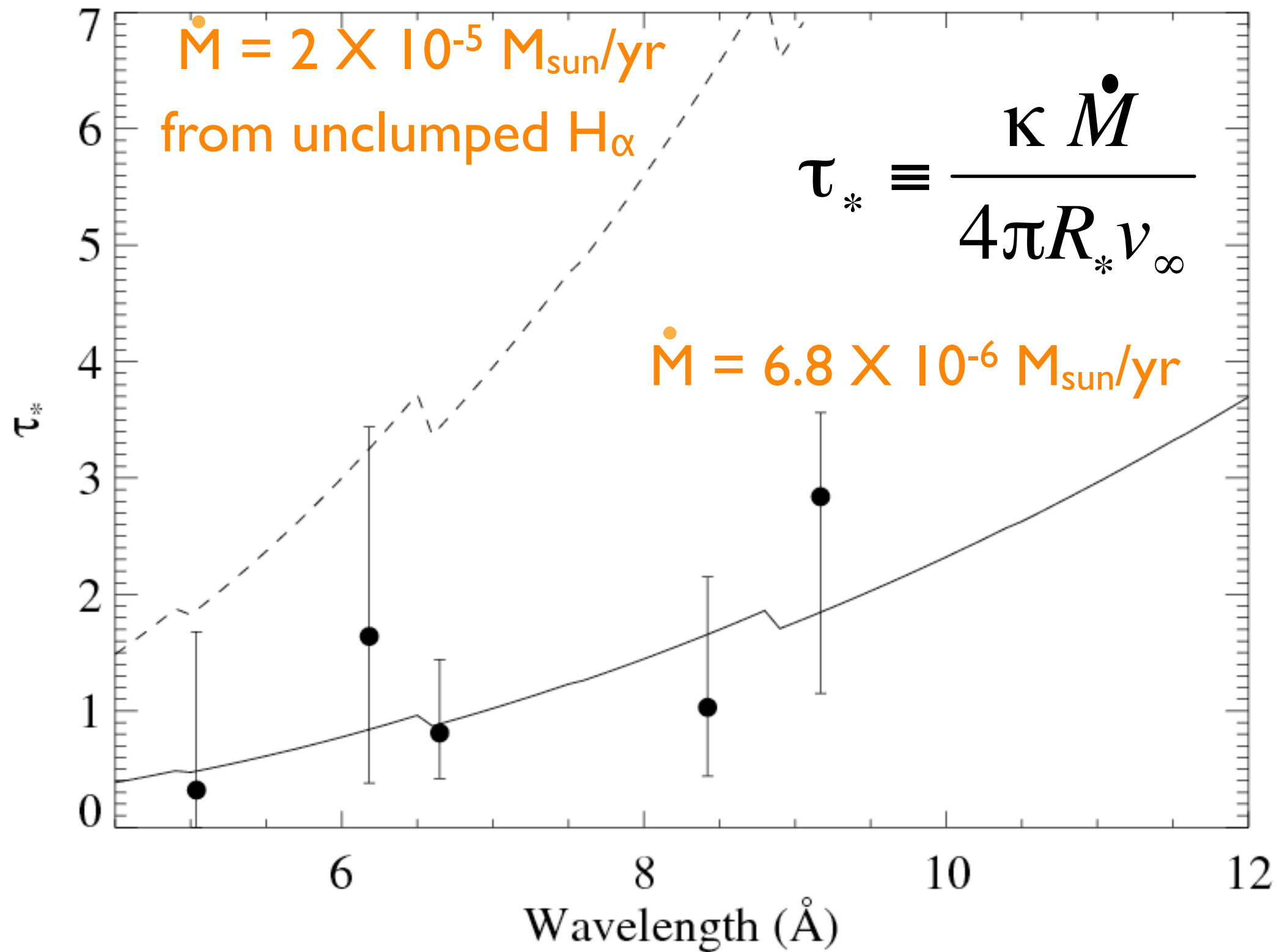


ζ Pup (O4 If)



R_o = onset radius of X-ray emission





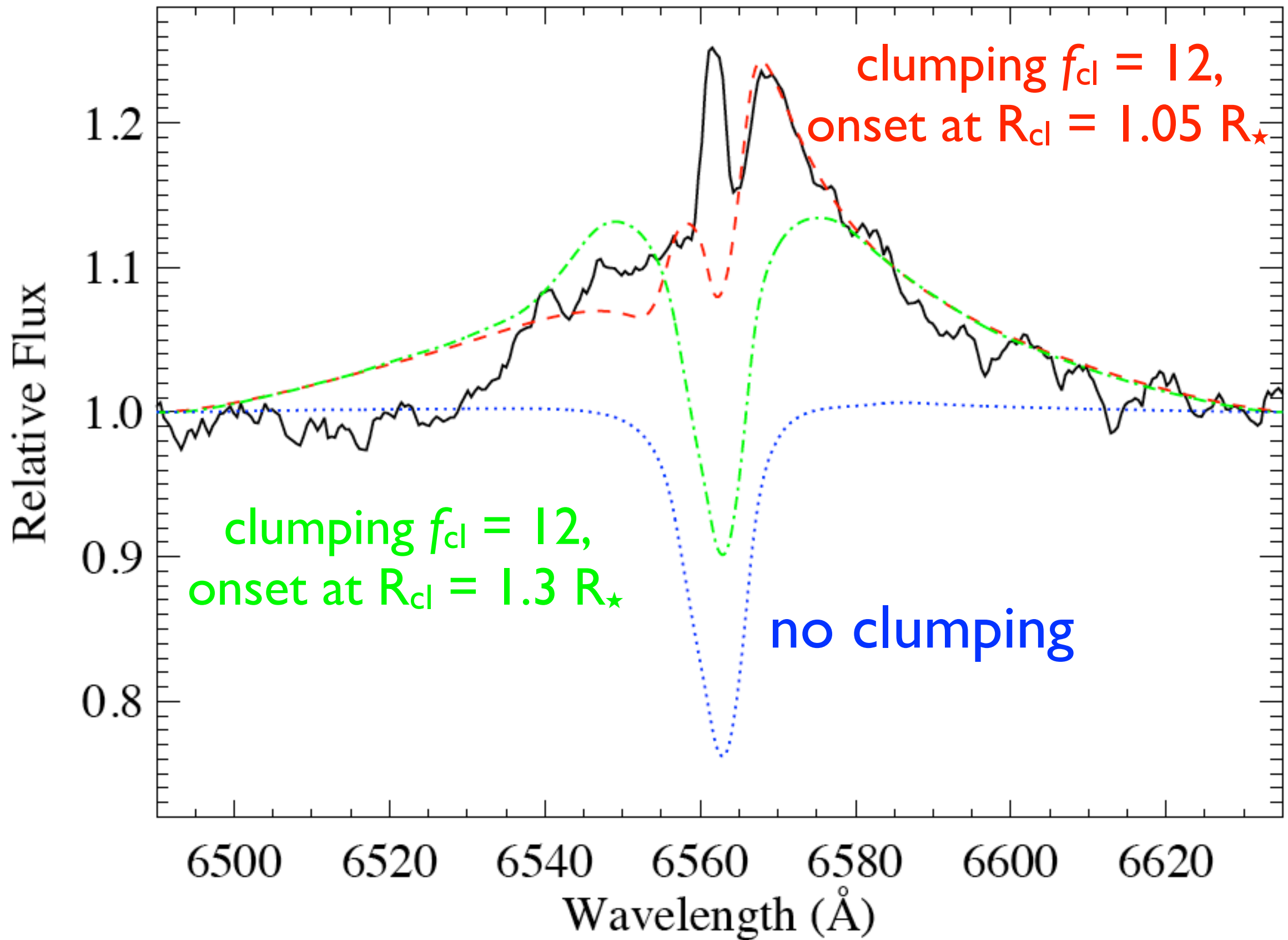
$$\tau_* = \kappa(\lambda) \dot{M} / 4\pi R_* v_{\infty}$$

Lower mass-loss rate: consistent with $H\alpha$?

Lower mass-loss rate: consistent with $H\alpha$?

Yes! With clump volume filling factor of $f_{cl} = 12$

$$\dot{M} = 7 \times 10^{-6} M_{\text{sun}}/\text{yr}$$



Conclusions

- X-ray emission is consistent with the LDI mechanism leading to shocks distributed throughout the wind
- Little or no X-ray emission at the base of the wind ($r < 1.5 R_{\star}$), though clumping extends lower
- Absorption signatures in line profiles enable a mass-loss rate measurement
- Mass-loss rates are lower (factor of 3 to 5) than traditionally thought
- This is consistent with clumping factors, $f_{cl} \sim 10$